Feedback control of atomic Fermi gases

Matthew L. Goh

A thesis submitted for the degree of
Bachelor of Philosophy with Honours in Physics, at
The Australian National University

October, 2019

Declaration

This report is an account of research undertaken predominantly between July 2019 and October 2019 at The Department of Quantum Science, Research School of Physics, The Australian National University, Canberra, Australia.

Except where acknowledged in the customary manner, the material presented in this thesis is, to the best of my knowledge, original and has not been submitted in whole or part for a degree at any university.

Matthew L. Goh

October, 2019

Acknowledgements

No thesis is written in a vacuum, least of all this one. I have only made it this far due to the wonderful support of supervisors, friends, family and mentors.

Stuart - you've been a truly amazing supervisor. Thanks for your excellent guidance and infinite patience throughout the year. And Joe - thank you for your support, wisdom, invaluable contributions to the world of teenage-boy-action-adventure literature [1], and for getting me started on this path to begin with. You may frequently claim to be great, but this has proven unnecessary as actions have spoken louder than words.

I would also like to extend my thanks to the rest of the group for providing such a welcoming and supportive environment and many good chats over burgers. Thank you to Simon, Angela, Ruvi and Alex for patiently fielding so many questions, and particularly to Zain for putting up with my stream of consciousness, light screaming and poor banter.

It's been said by some that the most important thing was not the physics we discovered, but the friends we made along the way. Thanks to my fellow Honours students for making this year what it was. And to my fellow Brucies who have been with me every step of the way, thank you for years of unending support and friendship. I wouldn't be half the person I am without all of you.

Finally, I'd like to thank my family for raising me and always valuing my education, even in the toughest of times.

Abstract

Ultracold atomic Fermi gases are the leading platform for analogue quantum simulation, and provide a promising avenue to study the origin of high-temperature superconductivity in cuprates. However, current experimental approaches to cooling Fermi gases use evaporative cooling, which is limited by poor thermalisation properties of fermions and is non-number-conserving. This prevents the creation of useful analogue simulators of many collective phenomena. This thesis is the first theoretical investigation into the use of continuous-measurement feedback control as an alternative means of cooling an atomic Fermi gas. Since tractable simulation of Fermi gas dynamics requires simplifications to the full quantum field theory, we derive and simulate a fermionic equivalent to the Gross-Pitaevskii equation, generalising a model of feedback-controlled BECs by Haine *et al.* [2] to multimode ultracold atomic Fermi gases. We demonstrate that in the absence of measurement effects, a suitable control can drive an interacting Fermi gas arbitrarily close to its ground state. However, although control schemes based upon damping spatial density fluctuations work well for single-spatial-mode BECs, we show that they perform poorly for Fermi gases with a large number of atoms due to counter-oscillation of multiple spatial modes, which must exist due to Pauli exclusion. We generalise a feedback-measurement model of BECs by Szigeti *et al.* [3, 4] to a multimode atomic Fermi gas, and perform stochastic simulations of measured, feedback-controlled fermions in the single-atom and many-atom mean-field limits. The effects of measurement backaction are an important consideration, since in a realistic experiment knowledge of the system state used for feedback must be obtained from measurement, leading to competition between measurement-induced heating and feedback cooling. We show that weaker and less precise measurements cool the system to a lower equilibrium excitation energy, but are unable to place practical lower bounds on measurement strength due to the lack of a system-filter separation. When measurement-induced heating is accounted for, we find that the equilibrium energy per particle scales superlinearly, suggesting that existing control schemes which work well for bosons would not be effective for fermions. In light of this, we propose several avenues of future investigation to overcome this limitation, leaving open the possibility of feedback control of atomic Fermi gases as a pathway to analogue quantum simulation.

Notational conventions

> By convention sweet is sweet, bitter is bitter, hot is hot, cold is cold, colour is colour; but in truth there are only atoms and the void.
>
> Democritus, c. 400 BC

This thesis largely follows established notational conventions, but here we clarify notation that may be ambiguous.

For a many-body system, operators with hats of the form $\hat{O}$ will always indicate an operator on the full many-body Fock space, and state kets of the form $|\psi\rangle$ indicate elements of this Fock space. When dealing with Hartree-Fock wavefunctions we will write expressions exclusively in the wavefunction formalism, and tildes (eg $\tilde{O}(\boldsymbol{x})$) indicate operators on $L^2(\mathbb{R}^n)$ which act on these wavefunctions. We will suppress tensor products, and write $|a\rangle\,|b\rangle \equiv |a\rangle \otimes |b\rangle$. We will frequently make use of commutators and anticommutators in Fock space, with the notation:

$$\left[\hat{A}, \hat{B}\right] \equiv \hat{A}\hat{B} - \hat{B}\hat{A}$$
$$\left\{\hat{A}, \hat{B}\right\} \equiv \hat{A}\hat{B} + \hat{B}\hat{A}.$$

Expectation values of the form $\langle \hat{O} \rangle$ will always indicate the usual quantum-mechanical expectation value $\mathrm{Tr}\{\hat{O}\hat{\rho}\}$ for some state $\hat{\rho}$. Stochastic expectation values will be written in the form $\mathbb{E}\{\cdot\}$.

We will write measures before our integrands in the form $\int dx f(x)$. We will often write sums and integrals without explicit limits; these should be assumed to be over the entire relevant domain. We will use the normalised angular frequency convention for the Fourier transform $\mathcal{F}\{\cdot\}$:

$$\mathcal{F}\Big\{f(x)\Big\}(k) = \frac{1}{\sqrt{2\pi}} \int dx f(x) e^{-ikx}$$
$$\mathcal{F}^{-1}\Big\{g(k)\Big\}(x) = \frac{1}{\sqrt{2\pi}} \int dx g(k) e^{ikx}.$$

Contents

List of Figures

Chapter 1

Introduction

In the 24 years since the first experimental realisations of Bose-Einstein condensates (BECs) in dilute atomic gases [5–7], ultracold atomic physics has matured rapidly. Cold atoms have shown great promise for applications in many fields of physics, emerging as a leading platform for precision sensing [8, 9] and quantum simulation [10–12]. With regard to the latter, there is a pressing need to produce large, extremely cold systems of fermionic atoms. However, standard techniques for producing ultracold atomic gases discard an overwhelming majority of atoms from the trap, and work very poorly for fermionic species [13]. It is for this reason that we seek to develop a new cooling technique for Fermi gases. In this thesis, we investigate *continuous-measurement feedback control* as an alternative method to overcome these limitations. This introduction outlines the context and motivation of this thesis: we outline the basics of quantum simulation (Sections 1.1 and 1.2), and the use and limitations of ultracold atoms for quantum simulation (Sections 1.3 and 1.4). With this motivation in mind, we review the state of the art in theory of feedback control of cold atoms (Section 1.5), and outline our approach and the structure of this thesis (Section 1.6).

1.1 The many-body problem is intractable

Quantum mechanics is *hard*. This simple fact is at the heart of both the rich results and tremendous difficulties in all branches of the study of quantum matter.

Early in our study of physics, we learn that the fundamentals of quantum mechanics are rather easy to state. Every quantum system is described by its state vector $|\psi\rangle$, itself an element of some system-dependent Hilbert space $\mathcal{H}$. This state vector is a complete description from which one may compute any observables and their projective measurement probabilities. The Hamiltonian $\hat{H}$ is a Hermitian linear operator which corresponds to the total energy, and is the generator of translations in time. This leads to the Schrödinger equation

$$i\hbar \frac{d}{dt} |\psi\rangle = \hat{H} |\psi\rangle , \tag{1.1}$$

which one can in principle integrate to determine the full dynamics of any system, given its Hamiltonian and an initial state. For a sufficiently low-dimensional system, this is eminently doable on a computer. In many branches of physics, it is trivial to write down the Hamiltonian for any system of interest.[1] Successfully simulating the resulting quantum

[1] For example, it is easy to write down a Hamiltonian for charged bodies interacting by a Coulomb force for quantum chemistry. Many exceptions exist - like nuclear physics, where nucleon-nucleon interactions

mechanical problems could resolve many open problems in quantum optics, atomic physics, condensed matter physics, quantum chemistry, nuclear physics, and related fields.

Most modern research problems in the quantum sciences involve many-body systems. Unfortunately, the dimensionality of quantum mechanics increases *exponentially* with the number of particles, putting anything beyond a small handful of interacting particles beyond our reach. Suppose we have N quantum systems,[2] with corresponding Hilbert spaces $\mathcal{H}_1$, $\mathcal{H}_2$, ..., $\mathcal{H}_N$. When we consider interaction between these systems, we must evolve a state vector in the *tensor product* $\mathcal{H}_{total}$ of these Hilbert spaces

$$\mathcal{H}_{total} = \mathcal{H}_1 \otimes \mathcal{H}_2 \otimes \ldots \otimes \mathcal{H}_N. \tag{1.2}$$

Consider the case where these systems are identical (the $\mathcal{H}_n$ are isomorphic) and have finite dimension D. Then $\mathcal{H}_{total}$ has dimension D^N, leading to the aforementioned exponential scaling with particle number. One should not underestimate how seriously limiting this is. Consider the interaction of N identical two-level systems. To even write down the state vector for $N = 70$ would require $\sim 10^{22}$ bytes of classical computer memory (more than a reasonable estimate of the combined storage space of all the computers on the planet), and to do so for $N = 300$ would require $\sim 10^{91}$ bytes (orders of magnitude more than the number of protons in the observable universe). Whether we wish to deal with tens of particles (nuclear physics and quantum chemistry) or orders of magnitude more (condensed matter physics), for most research-level problems we truly have no hope of directly solving the full quantum field theory on a classical computer.

The situation is even worse for fermionic systems.[3] Exchanging identical fermions results in a change of sign of a system's wavefunction. Thus, unless there are cancellations due to some symmetry, the evaluation of expectation values for strongly interacting fermionic systems involves highly oscillatory integrals that are extremely difficult to solve numerically [15], particularly in high-dimensional systems (that is, for a large number of particles). This is known as the *fermion sign problem*, and presents major challenges for condensed matter theory [16, 17], nuclear physics [18] and lattice quantum chromodynamics [19, 20].

Clearly, there are fundamental challenges in simulating the behaviour of quantum systems, particularly large or strongly interacting fermionic systems. Regardless, problems in the study of quantum matter must be solved, and we are motivated to seek alternatives.

1.2 The Hubbard model

Before we discuss alternative approaches to calculations in many-body quantum mechanics, it is pertinent to introduce an archetypal example of a many-body Hamiltonian: the *Hubbard model*. It describes particles localised to sites on a periodic lattice, which may 'hop' between sites, and interact with other particles at the same site (Figure 1.1). It is the simplest model that captures all the richness of many-body quantum mechanics, including the essential physics of competition between kinetic, potential and interaction energies [21]. The original version of the model was proposed by Hubbard[4] [24] as a model

are extremely complicated and cannot be written down in a simple form [14].

[2] These may be identical (e.g. the $\mathcal{H}_n$ are isomorphic) or nonidentical, and in the case of the former, distinguishable or indistinguishable - or any combination thereof.

[3] For a review of the basic properties of bosons and fermions, refer to Sections 2.1 and 2.2.

[4] The model was also independently conceived by Gutzwiller [22] and Kanamori [23] in the same year.

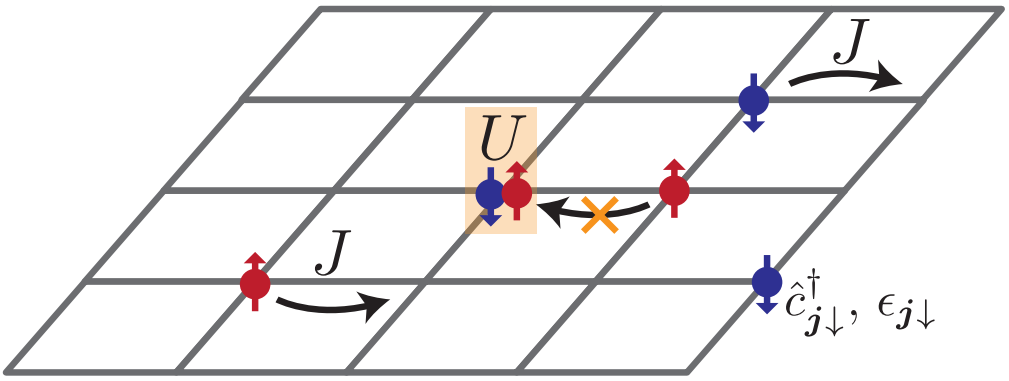

Figure 1.1: A diagram illustrating the 2D Fermi-Hubbard model. Fermions are created at site $\boldsymbol{j}$ with creation operator $\hat{c}^\dagger_{\boldsymbol{j}\sigma}$. They hop between sites with coupling strength J, but cannot hop to a site containing a fermion of the same spin due to the Pauli exclusion principle. If a spin-up and spin-down fermion exist at the same site, they interact with energy U.

for electrons in solid state materials - this is now sometimes known as the *Fermi-Hubbard model*, since its fields are fermionic. A variant describing interacting bosons on a lattice, known as the *Bose-Hubbard model*, was later introduced [25–27].[5] In modern notation, the Fermi-Hubbard Hamiltonian is

$$\hat{H} = \overbrace{-J \sum_{\langle \boldsymbol{j},\boldsymbol{k}\rangle\sigma} \left(\hat{c}^\dagger_{\boldsymbol{j}\sigma}\hat{c}_{\boldsymbol{k}\sigma} + \text{h.c.}\right)}^{\text{Hopping between lattice sites}} + \overbrace{U \sum_{\boldsymbol{j}} \hat{n}_{\boldsymbol{j}\uparrow}\hat{n}_{\boldsymbol{j}\downarrow}}^{\text{Local interactions}} + \overbrace{\sum_{\boldsymbol{j}\sigma} \epsilon_{\boldsymbol{j}\sigma}\hat{n}_{\boldsymbol{j}\sigma}}^{\text{Potential energy}} , \tag{1.3}$$

where the $\hat{c}^\dagger_{\boldsymbol{j}\sigma}$, $\hat{c}_{\boldsymbol{j}\sigma}$ are creation and annihilation operators[6] for lattice site $\boldsymbol{j}$ and spin $\sigma \in \{\uparrow,\downarrow\}\}$, $\hat{n}_{\boldsymbol{j}\sigma} = \hat{c}^\dagger_{\boldsymbol{j}\sigma}\hat{c}_{\boldsymbol{j}\sigma}$ is the corresponding density operator, the $\epsilon_{\boldsymbol{j}\sigma}$ are site-dependent potential energies, and the angular brackets $\langle \boldsymbol{j},\boldsymbol{k}\rangle$ denote summation over adjacent lattice sites only. The first term describes hopping between adjacent lattice sites, with coupling strength J. The second term describes the interaction of particles at the same lattice site, with corresponding energy U: these may be repulsive ($U > 0$) or attractive ($U < 0$), both of which lead to important physics. The final term describes potential energy, which may be site-dependent (in the case of detunings between lattice sites), and often includes a chemical potential μ to fix particle number.

Despite its conceptual simplicity, the Hubbard model is difficult to solve: the exponential scaling of complexity described in Section 1.1 applies, and in the case of the Fermi-Hubbard model, the fermion sign problem further complicates attempts at numerical simulation [15–17]. Numerically exact solutions only exist in very specific limits, such as half-filling, weak coupling, and carrier concentrations far from half-filling [30] - much interesting physics exists away from these limits, in parameter regimes that are extremely difficult to simulate.

[5] Throughout this thesis, the 'Hubbard model' will always be inclusive of both the Fermi-Hubbard and Bose-Hubbard models: we will refer specifically to the Fermi-Hubbard or Bose-Hubbard models when the quantum statistics are relevant.

[6] We have assumed familiarity with second-quantised notation for many-body quantum mechanics: a brief overview is presented in Section 2.2, and a comprehensive introduction can be found in Refs. [28, 29].

This complexity gives rise to rich physics, and the eigenstates of the Hubbard model tend to be complex and highly correlated [21].

The Hubbard model quickly outgrew its original purpose, later emerging as an important model in the study of superconductivity. Although some superconductors are well described by the BCS theory of superconductivity [31], it is inadequate to describe high-temperature superconductors ($T_c > 30$K) such as the cuprate superconductors. High-temperature superconductivity has perhaps the most promising engineering applications of any unresolved physics phenomenon, and thus significant research is currently devoted to understanding it. The Hubbard model has emerged as a leading model for the superconducting cuprates [32, 33], and it is believed by many (though not proven) that it captures the essential physics [13]. Quantum simulation of the Hubbard model is thus a promising route to understanding high-temperature superconductivity.

Beyond high-temperature superconductivity in cuprates, there are a number of other areas where simulating the Hubbard model could provide insight. The Hubbard model can be used to study analogues to quantum chromodynamics, and so could shed light on open problems in quantum field theory [34]. Its ability to simply model electron interactions also leads to uses in chemistry, where it has been applied to systems such as aromatic compounds [35–37], single-molecule magnets [38], and organic charge-transfer salts [39].

1.3 Cold atoms as a quantum simulator

If simulating quantum mechanics with a *classical* system is so hard, can we overcome these fundamental limitations by simulating it on a *quantum* system? This question was the root of Feynman's 1981 talk [40] which is generally credited with introducing the concepts of quantum computing and simulation. Subsequent research formalised the notion of a *universal quantum simulator* [41] - a quantum system that can simulate the dynamics of *any* Hamiltonian.[7] To realise this, significant research effort is currently focused towards the construction of universal quantum computers (see Ref. [42]) that can perform arbitrary unitary operations in Hilbert space. In principle, this would enable scalable simulation of the Hubbard model, and provide insight into problems discussed in Section 1.2 such as high-temperature superconductivity.

Current attempts to build universal quantum computers are hindered by short decoherence times (that is, quantum states are quickly destroyed by coupling to the environment) and difficulties in scaling to a large number of qubits [43]. Many consider it unlikely that such a device will be realised in a useful form in the near future, and significant further research is required. Despite the very recent claim of quantum supremacy [44], we are still very far from the circuit depths and fidelities required for quantum simulation on a digital quantum computer. However, a more immediately achievable realisation of Feynman's proposition can be achieved by constructing *analogue quantum simulators* (sometimes known as *quantum emulators*). Rather than build a quantum system that can simulate the behaviour of *any* quantum system as envisaged by Lloyd [41], we may instead construct a highly controllable device that replicates a *specific* Hamiltonian of interest, such as the Hubbard Hamiltonian. By performing experiments with such a device, we may study the dynamics of the original Hamiltonian by proxy; this is analogue quantum simulation. As an

[7] Lloyd [41] considered only local systems, but one could in principle simulate a Hamiltonian with nonlocal terms.

analogy, one may think of analogue quantum simulation as being the quantum equivalent of studying aerodynamics in a wind tunnel, as opposed to a computer simulation. A more detailed comparison of the advantages and disadvantages of these approaches to quantum simulation can be found in Ref. [45].

Ultracold atoms are well-suited to this 'impersonation' of a target Hamiltonian and study by proxy, and are therefore currently the leading platform for analogue quantum simulation [10–12]. They are pure,[8] free of unwanted thermal effects, and can easily be isolated from the environment. Furthermore, they can be easily controlled: they can be optically trapped [46], subjected to high-bandwidth, high-resolution arbitrary perturbing potentials [47], and their scattering properties can be controlled by manipulating them close to a Feshbach resonance, enabling a high degree of control over interatomic interaction strengths [48]. These methods of control may include time dependence, allowing experimental control over system dynamics. Both fermionic and bosonic Hamiltonians may be realised, since atomic species of both types exist.[9] A range of destructive [49–51] and non-destructive [49, 52–54] imaging techniques exist, enabling easy observation of experimental results. Ultimately, this provides a favourable environment to study our systems of interest. For example, studying Hubbard model dynamics in an ultracold atomic gas would be much easier than directly experimenting on superconducting cuprates, so long as we can realise the Hubbard Hamiltonian in such a system.

Fortunately, with periodic optical potentials and sufficiently low energy scales, ultracold atoms *do* realise the Hubbard model, a fact originally proven for bosonic atoms and the Bose-Hubbard model by Jaksch *et al.* [55] in 1998. Crucially for the purposes of this thesis, fermionic atoms also realise the Fermi-Hubbard model (see Appendix A.1 for a proof). They are therefore an ideal platform for the analogue quantum simulation of the Hubbard model, and experiments with ultracold fermions in optical lattices have been proposed that would provide critical insight into the origin of high-T_c superconductivity in cuprates [56].

We have thus far mostly focused on analogue quantum simulation of the Hubbard model as it is arguably the most promising application of ultracold Fermi gases, for which this thesis aims to develop new cooling techniques. However, ultracold atomic gases have many more diverse applications. Artificial gauge fields can be applied to such a system, opening the way to simulation of quantum Hall systems, topological insulators, and exotic strongly correlated topological phases [57]. Cold atoms are also a candidate for qubits in full-blown universal quantum computers [58], single-atom transistors [59], and analogue models of white dwarf stars [60]. Bosonic species are also ideal sources for atom interferometers, which enable state-of-the-art precision measurements [9]: these have diverse applications including inertial sensing [8] and precision measurement of fundamental physical constants [61, 62]. Future atom interferometers with improved sensitivity could be capable of improved tests of general relativity [63] and gravitational wave detection [64].

[8] They are produced in high vacuum, and the trapping methods are selective of not only particular atomic species, but even particular internal components. Thus, there are essentially no defects or dopants.

[9] Refer to Section 2.2.2 for an explanation of exchange statistics of neutral atoms.

1.4 Creating ultracold atomic gases

Presently, the main experimental approach for cooling atomic gases is a two-stage process: laser cooling followed by evaporative cooling. This approach was pioneered[10] to produce the world's first Bose-Einstein condensates in dilute atomic gases [5–7], and has subsequently been the leading method for cooling both fermionic and bosonic species [13]. The details of laser cooling are not relevant to the present work, but a detailed review may be found in Ref. [66] - it is sufficient to note that laser cooling is highly effective in cooling atoms from room temperature to the microkelvin regime, and is in principle number-conserving. A detailed review of progress and challenges for cooling cold atoms in optical lattice systems is presented in Ref. [13].

Evaporative cooling is based on preferential removal of high-energy atoms from a confined sample, followed by rethermalisation through scattering (Figure 1.2). Although it has been successfully employed to achieve quantum degeneracy in both bosonic [5–7] and fermionic[11] [67, 68] species, it has been suggested that it is unlikely to ever achieve sufficiently low entropy per particle to investigate phenomena such as d-wave superfluidity in an optical lattice [13]. Furthermore, it is limited in a much more general sense. Evaporative cooling is extremely non-number-conserving (almost all the atoms in the trap are lost over the evaporation process), which is a serious limitation for the study of collective phenomena like superconductivity, since we cannot reliably study collective phenomena with a small sample size. It is also species-dependent, as it relies upon scattering properties. This is particularly limiting for fermions, since they have minimal wavefunction overlap and thus small scattering cross-sections, leading to extremely poor thermalisation. In the low-energy regimes of interest, s-wave scattering dominates [69], and fermions of the same internal component do not scatter at all in this limit. Beyond these limitations, the details of evaporative cooling are not relevant, but a detailed review[12] may be found in Ref. [70].

This motivates the development of a new cooling technique. We wish to develop an alternative to evaporative cooling that is number-conserving, independent of scattering properties, and capable of achieving low temperatures and low entropy per particle.

1.5 Feedback cooling

In this thesis, we investigate *continuous-measurement feedback control* as a possible solution to the limitations of evaporative cooling. This involves continuously measuring a quantum system in order to gain partial information about the system state, then using this information to make active decisions about how to perturb the system in order to force it towards a desired state (feedback control). In our case, our desired state is the

[10] Evaporative cooling of atoms was first performed by Masuhara *et al.* [65], but this was without an initial laser cooling stage, and only achieved temperatures in the milikelvin regime: orders of magnitude hotter than the temperatures achieved by the first stage (laser cooling) of the approach introduced in Refs. [5–7]

[11] This is typically done by *sympathetic cooling* (e.g. Ref [67]). Bosonic and fermionic atoms are trapped in a spatially overlapping configuration, and the bosons are evaporated. The fermions exchange energy with the bosons via scattering (Pauli exclusion only applies to identical fermions, so the scattering properties are reasonable), and so the fermions are cooled by this process.

[12] Although this review is relatively old, little has changed in the techniques applied beyond the application of machine learning to optimise cooling curves (e.g. Ref. [54]).

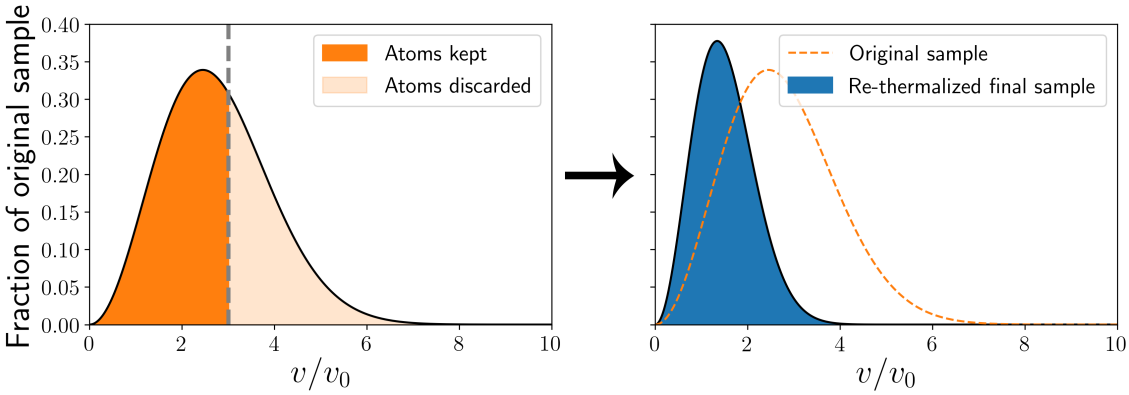

Figure 1.2: An example of evaporative cooling of a classical system. A thermal (Maxwell-Boltzmann) sample of temperature $T = 3\left(mv_0^2/2k_B\right)$ (for arbitrary velocity scale v_0) has all atoms with speed above $v/v_0 = 3$ removed (the fastest 39%), lowering its average energy per particle. After re-thermalisation, the system is in a thermal distribution with the same lower average energy, achieved at $T = 0.9\left(mv_0^2/2k_B\right)$. The temperature is reduced at the cost of discarding the highest-energy atoms.

many-body ground state of a quantum gas, and thus we will investigate *feedback cooling* - a type of feedback control in which we seek to bring a system as close to its ground state as possible. We will use the terms 'feedback cooling' and 'feedback control' interchangeably throughout this thesis as a result. Developing effective feedback control often involves optimising a trade-off between having enough information about the system state to control it well and *measurement backaction*, the unwanted changes in a system due to wavefunction collapse under measurement. In our case, measurement backaction will always take the form of a heating effect.

Feedback control of quantum systems is an extensive topic. We will only cover directly relevant aspects, but a comprehensive review of current theoretical and experimental progress can be found in Ref. [71]. Modelling of feedback control of cold atoms has thus far been entirely focused on BECs, with a particular goal of reducing the linewidth of outcoupled atom lasers. The first such studies were conducted by Wiseman and Thomsen [72, 73], with a single-mode model to reduce phase noise caused by interactions. The first investigation of spatial structure was performed by Haine *et al.* [2], who used a simple semiclassical mean-field model to investigate how effectively one could force a BEC to its ground state given perfect knowledge of the system state and control over time-dependent potentials. Their feedback scheme was later applied to a more realistic model of an atom laser including pumping, damping and outcoupling [74]. However, these semiclassical models did not include the important effect of measurement backaction. Drawing on previous work [75], Wilson *et al.* [76] derived a single-mode model for a single atom in a cavity including measurement effects. However, this assumed that the atom was confined to a region small relative to the wavelength of light in the cavity, an assumption that does not hold for a modestly sized BEC. Following on from this, Szigeti *et al.* developed a full-field model of a BEC under a measurement process more feasible for a BEC [3] and simulated it under a mean-field approximation [4]. Due to the mean-field approximation, this did not capture higher-order quantum field effects, and so the full-field model of Szigeti *et al.* [3, 4] was simulated by Hush *et al.* [77] using the number-phase Wigner (NPW) phase-space representation [78, 79] which does include correlation effects. Subsequent unpublished work

by Taylor *et al.* has further advanced the application of the NPW representation to the simulation of BECs under measurement and feedback control at finite temperature. We review in much greater detail the work of Haine *et al.* in Chapter 4, and the work of Szigeti *et al.* in Chapter 5.

Despite this extensive work in modelling feedback cooling of BECs, until now there have been no attempts to generalise these results to fermionic species, where the prospect of an alternative to evaporative cooling is most tantalising. In this thesis, we extend the results of Haine *et al.* [2] and Szigeti *et al.* [3, 4] to atomic Fermi gases, and thus take the very first steps towards achieving degeneracy in fermions with feedback cooling.

1.6 Outline of this thesis

The key goal of this thesis is to generalise existing quantum feedback control techniques for BECs to fermionic species. In particular, we aim to model techniques that can be used to bring an atomic Fermi gas close to its many-body ground state, in order to guide future experimental approaches to developing fermionic systems suitable for analogue quantum simulation. Roughly speaking, this thesis consists of alternating theory (Chapters 2, 3 and 5) and simulation (Chapters 4 and 6). We develop and simulate models of increasing complexity (fermionic equivalents of Refs. [2–4], respectively) in order to understand the roles of both measurement and control in the successful feedback control of an atomic Fermi gas.

A more detailed synposis of the thesis is as follows. In Chapter 2, we present useful background theory underlying our approach: discussing the fundamentals of bosons and fermions, quantum field theory, numerical simulation, and stochastic calculus. Chapter 3 is dedicated to the discussion of mean-field theory, and contains both background theory and new work - we review existing techniques for bosons, generalise these to fermions, and outline existing methods to calculate ground states for both. We then use these mean-field theory techniques in Chapter 4 to simulate feedback control of (predominantly fermionic) quantum gases in the absence of the measurement effects, exploring the important role of the control scheme in bringing a system to its ground state. However, these techniques do not account for the competing measurement-induced heating rate; in Chapter 5 we review tools to describe the dynamics of a quantum system undergoing continuous measurement and use these to generalise the mean-field theory of a BEC under measurement derived by Szigeti *et al.* [4] to a multimode fermionic system. This enables tractable simulation of feedback control of an atomic Fermi gas with measurement effects. In Chapter 6, we simulate our mean-field theory of fermions under measurement, examining parameter dependence of the model and the scaling of feedback control to large atom numbers. We find evidence to suggest that existing control schemes are ineffective for large numbers of fermionic atoms due to multimode effects, and so in Chapter 7 we review our findings and propose a number of future avenues of investigation to overcome these limitations.

Background theory

In this chapter, we present a selection of theory and tools that are used throughout this thesis. In Section 2.1, we review the basic properties of bosons and fermions from a statistical perspective. In Section 2.2, we discuss the fundamentals of quantum field theory and its application to the dynamics of cold atoms. Much of this thesis involves computer simulation of these dynamics, and so we discuss useful numerical techniques in Section 2.3. Finally, in Section 2.4, we describe the fundamentals of stochastic calculus, allowing us to model the dynamics of probabilistic processes like quantum measurement.

This chapter does not contain *all* of the background theory in this thesis. Mean-field theory is discussed in Chapter 3 and conditional quantum measurement theory is introduced in Chapter 5. Both Chapters 3 and 5 contain a combination of background theory and new work; this chapter is purely a review of existing techniques.

2.1 Bosons and fermions: a statistical perspective

In classical mechanics, particles are typically distinguishable. However, identical particles in quantum mechanics are indistinguishable; if their wavefunctions ever have any overlap, there is no experiment that could later determine which is which. Consider a two-level system with Hilbert space $\mathcal{H}$ and basis states $\{|\uparrow\rangle, |\downarrow\rangle\}$. The Hilbert space for two coupled two-level systems $\mathcal{H}_1 \otimes \mathcal{H}_2$ is spanned by $\{|\alpha\rangle, |\beta\rangle, |\gamma\rangle, |\delta\rangle\}$, where:

$$\begin{aligned} |\alpha\rangle &= |\uparrow\rangle_1 |\uparrow\rangle_2 , \qquad |\beta\rangle = |\uparrow\rangle_1 |\downarrow\rangle_2 , \\ |\gamma\rangle &= |\downarrow\rangle_1 |\uparrow\rangle_2 , \qquad |\delta\rangle = |\downarrow\rangle_1 |\downarrow\rangle_2 . \end{aligned} \tag{2.1}$$

Suppose now that the two-level systems are indistinguishable particles. Since no experiment can distinguish between the particles, exchanging them must preserve all observable quantities in the system, and can therefore result in at most a global phase rotation of the state vector. Consider a permutation operator $\hat{P}$ that performs this exchange:

$$\hat{P} |\psi\rangle_1 |\phi\rangle_2 = e^{i\theta} |\phi\rangle_1 |\psi\rangle_2 . \tag{2.2}$$

If we exchange the particles twice, we must end up with exactly the same state, so $\hat{P}^2 = \hat{1}$, and it follows that $\theta = n\pi$ for $n \in \mathbb{Z}$. Equation 2.2 thus reduces to

$$\hat{P} |\psi\rangle_1 |\phi\rangle_2 = \pm |\phi\rangle_1 |\psi\rangle_2 . \tag{2.3}$$

Thus, the state vector must be symmetric or antisymmetric under exchange of identical particles. This significantly constrains the allowable states. In the symmetric case (positive sign), the only allowable states (up to a global phase rotation) are $|\alpha\rangle$, $|\delta\rangle$ and $\frac{1}{\sqrt{2}}(|\beta\rangle + |\gamma\rangle)$. The particles may occupy the same state, so long as exchange symmetry is maintained. In the antisymmetric case (negative sign), the only allowable state is $\frac{1}{\sqrt{2}}(|\beta\rangle - |\gamma\rangle)$. There is no way of writing an antisymmetrised state for which the particles occupy the same state. These features generalise to an arbitrary number of particles (we will shortly discuss such a generalisation in Section 2.2), leading to two classes of identical particle:

- Identical *bosons* can occupy the same quantum state. A state vector is symmetric under the exchange of identical bosons.
- Identical *fermions* cannot occupy the same state. A state vector is antisymmetric under the exchange of identical fermions.

This simple difference in exchange (anti)symmetry leads to very different physics. By taking into account whether or not multiple particles may occupy the same state, and considering the most probable distribution at a given temperature, one can derive the mean occupancy of each energy state[1] at a given temperature without the use of quantum mechanics (see Chapter 8 of Huang [80] for a full derivation). For bosons, we obtain the Bose-Einstein distribution

$$\bar{n}_i = \frac{1}{e^{(\epsilon_i - \mu)/k_B T} - 1}, \tag{2.4}$$

and for fermions, we obtain the Fermi-Dirac distribution

$$\bar{n}_i = \frac{1}{e^{(\epsilon_i - \mu)/k_B T} + 1}, \tag{2.5}$$

where ϵ_i is the energy of the ith state, μ is the chemical potential, T is the temperature, and k_B is the Boltzmann constant. In the high-temperature limit ($T \gg \epsilon_i/k_B$), both (2.4) and (2.5) approach the Boltzmann distribution. In the low-temperature limit ($T \to 0$), they differ significantly. For the Bose-Einstein distribution, the occupation of the ground state grows without bound. In fact, below a critical temperature T_c, a macroscopic occupation of the ground state occurs. This is the phenomenon of Bose-Einstein condensation, in which a collection of bosons occupy a single spatial mode. It was predicted by Einstein in 1925 [81], and first observed in atomic gases many decades later in 1995 [5–7]. In stark contrast, multiple fermions cannot occupy the same mode: Equation 2.5 is bounded above by 1. This is the well-known *Pauli exclusion principle* and is largely responsible for the interesting behaviour of fermions. As $T \to 0$, Equation 2.5 tends towards a step function:

$$\Theta_i = \begin{cases} 1\,, & \text{if } \epsilon_i \leq \mu, \\ 0\,, & \text{if } \epsilon_i > \mu. \end{cases} \tag{2.6}$$

This is the *Fermi sea*: all states below the Fermi energy $\epsilon_F = \mu$ are filled with exactly one fermion, while all states above are completely empty. A comparison of the distributions is presented in Figure 2.1.

Many important behaviours of bosons and fermions can be qualitatively understood from

[1] For simplicity, we have assumed the energy states are nondegenerate; this is merely a sketch to provide intuition.

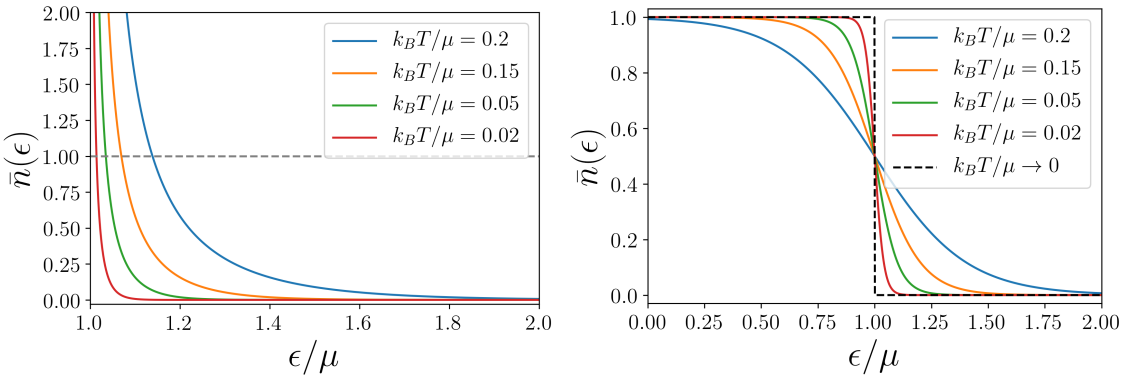

(a) The Bose-Einstein distribution.

(b) The Fermi-Dirac distribution.

Figure 2.1: The Bose-Einstein and Fermi-Dirac distributions across a continuous, nondegenerate energy spectrum for a range of temperatures. Note that the occupation of the ground state in the Bose-Einstein distribution grows without bound. For the Fermi-Dirac distribution, the occupation of each state is no greater than 1, and in the limit $T \to 0$, it approaches a step function, indicating a 'Fermi sea' in which all states below μ are filled with one particle, and all states above are empty.

this simple picture. The aforementioned prediction of Bose-Einstein condensation [81] was on similar statistical grounds to what we have discussed here. The properties of semiconductors can be understood in terms of particle-hole excitations to the Fermi sea, and the Fermi degeneracy pressure guiding the structure of neutron stars can be derived with little more than the distribution described here and basic tools of thermodynamics [80].

2.2 Quantum field theory

To move beyond a simple qualitative understanding, we require the tools of quantum field theory: the fundamental description of many-body quantum states and their dynamics. We will provide only a brief treatment of the essential tools here. Many of the texts cited elsewhere in this thesis serve as excellent introductions to the topic [29, 82–84], and the interested reader is strongly encouraged to consult these for further details.

2.2.1 Second quantisation and quantum field operators

Writing large many-body states in the (anti)symmetrised tensor product form described in Section 2.1 is unwieldy; fortunately, more convenient representations exist. Quantum field theory takes place in *Fock space*: a Hilbert space that supports N-particle states for arbitrary N.[2] Choose a discrete, orthonormal single-particle basis $\{|\phi_j\rangle\}$ and let the number of particles in state $|\phi_k\rangle$ be written as n_k. A state with a definite number of particles in each mode is called a *Fock state* and is written in occupation number notation as $|n_1, n_2, \ldots, n_k, \ldots\rangle$. We will write the *vacuum state* $|0, 0, \ldots, 0, \ldots\rangle$ as $|0\rangle$. Fock space

[2]The mathematical details of Fock space are not important for this thesis. It is sufficient to merely note that it is the Hilbert space spanned by the states we have described here. Full details are provided in the original paper by Fock [85].

is spanned by Fock states, and so a general many-body quantum state may be written as

$$|\Psi(t)\rangle = \sum_{n_1,n_2,\ldots,n_k,\cdots=0}^{\infty} c_{n_1,n_2,\ldots,n_k,\ldots}(t)\,|n_1,n_2,\ldots,n_k,\ldots\rangle\,. \tag{2.7}$$

In order to compute dynamics and represent operators, it is convenient to introduce *creation and annihilation operators* for each mode in the single-particle basis: this is known as *second quantisation*. For a given mode $|\phi_k\rangle$, we introduce the annihilation operator $\hat{c}_k$

$$\hat{c}_k\,|n_1,n_2,\ldots,n_k,\ldots\rangle = \sqrt{n_k}\,|n_1,n_2,\ldots,n_k-1,\ldots\rangle\,, \tag{2.8}$$

where $n_k \geq 1$,[3] and its adjoint, the creation operator $\hat{c}_k^\dagger$:

$$\hat{c}_k^\dagger\,|n_1,n_2,\ldots,n_k,\ldots\rangle = \sqrt{n_k+1}\,|n_1,n_2,\ldots,n_k+1,\ldots\rangle\,. \tag{2.9}$$

These are aptly named - we can see from the above that $\hat{c}_k$ and $\hat{c}_k^\dagger$ create and annihilate identical particles, respectively, in the mode $|\phi_k\rangle$. The action of the creation and annihilation operators is the same as the ladder operators for a harmonic oscillator, except they change the number of particles rather than energy quanta.

Exchange (anti)symmetry is encoded in the (anti)commutation relations of creation and annihilation operators. If the particles are bosons, the operators have the following commutation relations:

$$\left[\hat{a}_j,\hat{a}_k\right] = \left[\hat{a}_j^\dagger,\hat{a}_k^\dagger\right] = 0, \qquad \left[\hat{a}_j,\hat{a}_k^\dagger\right] = \delta_{jk}, \tag{2.10}$$

and if they are fermions, the operators have the following anticommutation relations:

$$\left\{\hat{a}_j,\hat{a}_k\right\} = \left\{\hat{a}_j^\dagger,\hat{a}_k^\dagger\right\} = 0, \qquad \left\{\hat{a}_j,\hat{a}_k^\dagger\right\} = \delta_{jk}. \tag{2.11}$$

It is easy to see the usual properties of bosons and fermions from these (anti)commutation properties. Consider a state containing one particle in the mode $|\phi_j\rangle$, and one in $|\phi_k\rangle$, which we may write in second-quantised notation as $\hat{c}_j^\dagger\hat{c}_k^\dagger\,|0\rangle$. Applying the (anti)commutation relations, we see that exchanging these particles is equivalent to exchanging the operators with an appropriate choice of sign

$$\hat{c}_j^\dagger\hat{c}_k^\dagger\,|0\rangle = \pm\hat{c}_k^\dagger\hat{c}_j^\dagger\,|0\rangle\,, \tag{2.12}$$

where we should have a positive sign for bosons, and a negative sign for fermions. Fortunately, Equation 2.12 holds trivially due to the (anti)commutation relations. The Pauli exclusion principle emerges naturally as a consequence of the anticommutation relations (2.11), since these imply that $\hat{c}_j^\dagger\hat{c}_j^\dagger = 0$ for fermionic operators;[4] thus two particles cannot be placed in the same state. For bosonic operators, $\hat{c}_j^\dagger\hat{c}_j^\dagger \neq 0$, allowing the creation of multiply-occupied modes.

We may easily transform creation and annihilation operators between single-particle bases. Consider a single-particle bases $\{\phi_j\}$ and $\{|\psi_\alpha\rangle\}$, with annihilation operators $\hat{c}_j$ and $\hat{d}_\alpha$,

[3] We cannot have a negative number of particles. If $n_k = 0$, then $\hat{c}_k\,|n_1,n_2,\ldots,n_k,\ldots\rangle = 0$.

[4] We have $\left\{\hat{c}_j^\dagger,\hat{c}_j^\dagger\right\} = 2\hat{c}_j^\dagger\hat{c}_j^\dagger = 0$, which implies that $\hat{c}_j^\dagger\hat{c}_j^\dagger = 0$.

respectively. The following transformations apply:

$$\hat{d}_\alpha = \sum_j \langle \psi_\alpha | \phi_j \rangle \, \hat{c}_j, \qquad \hat{d}_\alpha^\dagger = \sum_j \langle \phi_j | \psi_\alpha \rangle \, \hat{c}_j^\dagger. \tag{2.13}$$

This extends to continuous bases, such as position or momentum. In this case, we refer to the creation and annihilation operators as *field operators*. For example, the field operators $\hat{\psi}^\dagger(\boldsymbol{x})$, $\hat{\psi}(\boldsymbol{x})$ create and annihilate identical particles at position $\boldsymbol{x}$. For a discrete single-particle basis $\{|\phi_j\rangle\}$, they may be written

$$\hat{\psi}(\boldsymbol{x}) = \sum_j \phi_j(\boldsymbol{x}) \hat{c}_j, \qquad \hat{\psi}^\dagger(\boldsymbol{x}) = \sum_j \phi_j^*(\boldsymbol{x}) \hat{c}_j^\dagger, \tag{2.14}$$

where $\phi_j(x) = \langle \boldsymbol{x} | \phi_j \rangle$ is the spatial wavefunction for $|\phi_j\rangle$. This is simply a continuous generalisation of Equation 2.13. The inverse transform is:

$$\hat{c}_j = \int d\boldsymbol{x} \, \phi_j^*(\boldsymbol{x}) \hat{\psi}(x), \qquad \hat{c}_j^\dagger = \int d\boldsymbol{x} \, \phi_j(\boldsymbol{x}) \hat{\psi}^\dagger(x). \tag{2.15}$$

For field operators, the (anti)commutation relations are essentially the same, but with Dirac delta functions rather than Kronecker delta functions, since the variables are continuous. For bosons, we have

$$\left[\hat{\psi}(\boldsymbol{x}), \hat{\psi}(\boldsymbol{y})\right] = \left[\hat{\psi}^\dagger(\boldsymbol{x}), \hat{\psi}^\dagger(\boldsymbol{y})\right] = 0, \qquad \left[\hat{\psi}(\boldsymbol{x}), \hat{\psi}^\dagger(\boldsymbol{y})\right] = \delta(\boldsymbol{x} - \boldsymbol{y}), \tag{2.16}$$

and for fermions

$$\left\{\hat{\psi}(\boldsymbol{x}), \hat{\psi}(\boldsymbol{y})\right\} = \left\{\hat{\psi}^\dagger(\boldsymbol{x}), \hat{\psi}^\dagger(\boldsymbol{y})\right\} = 0, \qquad \left\{\hat{\psi}(\boldsymbol{x}), \hat{\psi}^\dagger(\boldsymbol{y})\right\} = \delta(\boldsymbol{x} - \boldsymbol{y}). \tag{2.17}$$

Second-quantised notation allows a convenient representation of observables. For example, to promote the 1D position operator $\hat{x} = \int dx \, |x\rangle \, x \, \langle x|$ from first to second quantisation, we make the transformation

$$\int dx \, |x\rangle \, x \, \langle x| \to \int dx \hat{\psi}^\dagger(x) x \hat{\psi}(x). \tag{2.18}$$

Hamiltonians are also typically written in second-quantised notation. We have already encountered the Fermi-Hubbard Hamiltonian (1.3), written in terms of creation and annihilation operators for each discrete lattice site. It is common to construct Hamiltonians out of field operators in the position basis; we will present such an example in the following section.

2.2.2 Quantum field theory of cold atoms

The systems under consideration throughout this thesis are ultracold atomic gases. A deep knowledge of atomic physics is not required to read this thesis - however, for a comprehensive introduction, we encourage the reader to consult Ref. [86].

As discussed in Section 2.1, exchanging two identical fermions results in a sign change in the system's state vector. However, exchanging two *pairs* of fermions results in two sign changes, and thus no change overall. Therefore, pairs of fermions can be considered bosonic, and they have the same exchange symmetry properties of lone bosons. Neutral

atoms are composed of fermions: protons, neutrons[5] and electrons. At sufficiently cold temperatures (energy scales well below an atom's first ionisation energy), an atom will remain bound as a single unit, and can therefore be treated as a single particle. If the atom contains an odd number of fermions, exchanging two identical atoms will result in a sign change of the state vector, and the atom will itself be fermionic. In the case of an even number of fermions, exchanging two identical atoms results in the exchange of an integer number of pairs of fermions, and so the sign changes cancel out, making the atom itself a boson. In fact, since a neutral atom contains an equal number of protons and electrons, we can simply note that at these energy scales, atoms with an even number of neutrons are bosonic, and atoms with an odd number of neutrons are fermionic.

We note that we may treat an atom as a single particle in this regime and that atoms may have an internal spin component[6] σ. Consequently, throughout this thesis, we will use field operators $\hat{\psi}_\sigma(\boldsymbol{x})$, $\hat{\psi}^\dagger_\sigma(\boldsymbol{x})$ for atoms, which may be bosonic (even neutron number) or fermionic (odd neutron number). We will model them with the non-relativistic Hamiltonian:

$$\hat{H} = \overbrace{\sum_\sigma \int d\boldsymbol{x} \hat{\psi}^\dagger_\sigma(\boldsymbol{x}) \left(-\frac{\hbar^2}{2m} \boldsymbol{\nabla}^2_{\boldsymbol{x}} + V(\boldsymbol{x}, t) \right) \hat{\psi}_\sigma(\boldsymbol{x})}^{\text{Single-particle potential and kinetic energy}} + \underbrace{\sum_{\sigma\sigma'} \int d\boldsymbol{x} \int d\boldsymbol{y} U_{\sigma\sigma'}(\boldsymbol{x} - \boldsymbol{y}) \hat{\psi}^\dagger_\sigma(\boldsymbol{x}) \hat{\psi}^\dagger_{\sigma'}(\boldsymbol{y}) \hat{\psi}_{\sigma'}(\boldsymbol{y}) \hat{\psi}_\sigma(\boldsymbol{x})}_{\text{Pair interaction (scattering)}} . \quad (2.19)$$

The particles have kinetic energy, and are subjected to a potential $V(\boldsymbol{x}, t)$, which may include both time-independent trapping terms and time-dependent control terms. They also interact by scattering, represented in (2.19) by a quartic pair interaction $U_{\sigma\sigma'}(\boldsymbol{x} - \boldsymbol{y})$. Throughout this thesis, we will exclusively consider atomic gases with one or two spin components, and so we will not need to consider spin-dependence of the pair interaction. Furthermore, at low energy scales in dilute atomic gases, scattering beyond s-wave is negligible (see Chapter 5 of Pethick and Smith [69] for a detailed discussion of this approximation). Consequently, the pair interaction simplifies to

$$U_{\sigma\sigma'}(\boldsymbol{x} - \boldsymbol{y}) = \frac{U_0}{2} \delta(\boldsymbol{x} - \boldsymbol{y}), \quad (2.20)$$

where

$$U_0 = \frac{4\pi\hbar^2 a}{m}, \quad (2.21)$$

for characteristic scattering length a and atoms of mass m. The scattering length a varies in the vicinity of a Fano-Feshbach resonance [87, 88], and it is commonplace in cold atom laboratories to tune it precisely by exploiting this [48]. Thus, we will generally assume that U_0 can be arbitrarily varied in our models. Nonetheless, it is still important to model the effect of interatomic scattering, since in a realistic experiment we cannot completely

[5] Protons and neutrons are composite particles composed of three quarks (elementary fermions), but since they have an odd number of fermions, they are fermionic by the same principle we have applied to the atom.

[6] This can be any internal component, and it is common to use two hyperfine states. However, the description remains the same.

remove interactions, only minimise them by manipulating the atoms near a Fano-Feshbach resonance. Applying the approximation in Equation 2.20, the Hamiltonian (2.19) reduces to:

$$\hat{H} = \sum_{\sigma} \int d\boldsymbol{x} \hat{\psi}_{\sigma}^{\dagger}(\boldsymbol{x}) \left(-\frac{\hbar^2}{2m} \boldsymbol{\nabla}_{\boldsymbol{x}}^2 + V(\boldsymbol{x}, t) \right) \hat{\psi}_{\sigma}(\boldsymbol{x}) + \frac{U_0}{2} \sum_{\sigma\sigma'} \int d\boldsymbol{x} \hat{\psi}_{\sigma}^{\dagger}(\boldsymbol{x}) \hat{\psi}_{\sigma'}^{\dagger}(\boldsymbol{x}) \hat{\psi}_{\sigma'}(\boldsymbol{x}) \hat{\psi}_{\sigma}(\boldsymbol{x}). \tag{2.22}$$

We will frequently use this Hamiltonian to model cold atomic gases throughout this thesis. U_0 can be negative (attractive interactions) or positive (repulsive interactions). The semiclassical methods applied in this thesis are not suitable to describe attractive interactions in fermions, and so we will always have $U_0 \geq 0$. Future approaches to overcome this limitation are described in Section 7.1.2.

In cold-atom experiments, it is common to confine the system tightly in one or two dimensions, by applying optical and/or magnetic traps of greater strength along these axes. By separability,[7] the system's state will be a product of states along each axis. If the trapping frequency is sufficiently high along the tightly-confined axes, then the system will be in its ground state along these axes,[8] and only the loosely confined axes will have non-trivial dynamics. For example, $\omega_x = \omega_y \ll \omega_z$ leads to a 'pancake' system that is comparatively thin and has no dynamics in the z direction, and thus is an effective 2D system in the x and y directions. For two tightly-confined axes ($\omega_x \ll \omega_y = \omega_z$), we obtain a 'cigar' shape that is comparatively thin and has no dynamics in the y and z directions, and is therefore an effective 1D system in the x direction. Both types have been experimentally realised for both bosonic [89, 90] and fermionic [91, 92] species, and much of this thesis will study feedback control of effective 1D systems.

2.2.3 Dynamics in quantum field theory: the Heisenberg picture

Expectation values of a quantum system evolve with time, and so some mathematical objects used in their computation must also evolve with time. A common approach is to view the observable operators as being static, and the state vectors themselves evolving: this is the *Schrödinger picture*. Many calculations in this thesis are significantly easier in the *Heisenberg picture*, which views the state vectors as being static, and the operators as evolving. Consider a system with initial state vector $|\Psi\rangle$ and initial observable operator $\hat{O}$ at time t_0. Then the expectation value will evolve as

$$\langle \hat{O} \rangle(t) = \langle \Psi | \overbrace{\hat{U}^{\dagger}(t, t_0) \hat{O} \underbrace{\hat{U}(t, t_0) | \Psi \rangle}}^{\text{Heisenberg picture: } \hat{O}(t) = \hat{U}^{\dagger}(t, t_0) \hat{O} \hat{U}(t, t_0)} , \tag{2.23}$$

$$\text{Schrödinger picture: } |\Psi(t)\rangle = \hat{U}(t, t_0) |\Psi\rangle$$

where $\hat{U}(t, t_0)$ is the time evolution operator from time t_0 to t. Only the observables matter: we will obtain equivalent dynamics regardless of what object we choose to group the time evolution with. Grouping the time evolution operators with the states by defining $|\Psi(t)\rangle = \hat{U}(t, t_0) |\Psi\rangle$ leads to the Schrödinger picture, and grouping them with the operators by defining $\hat{O}(t) = \hat{U}^{\dagger}(t, t_0) \hat{O} \hat{U}(t, t_0)$ leads to the Heisenberg picture.

[7] Assuming a trap of the form $V(\boldsymbol{x}) = \frac{1}{2} m \left(\omega_x^2 x^2 + \omega_y^2 y^2 + \omega_z^2 z^2 \right)$.

[8] A large trapping frequency will lead to a large excitation energy along these axes. At sufficiently low energy scales, the system therefore cannot become excited except along the loosely-confined axes.

We may solve for this time evolution of operators using the *Heisenberg equation of motion* [28], even for a time-dependent Hamiltonian $\hat{H}(t)$:[9]

$$i\hbar\frac{d\hat{O}}{dt} = \left[\hat{O}(t), \hat{H}(t)\right] + i\hbar\frac{\partial\hat{O}}{\partial t}. \tag{2.24}$$

Throughout this thesis, we will only consider the evolution of operators that lack explicit time dependence, and so the second term will always be zero. Our observables and Hamiltonians will always be written in terms of second-quantised field operators, and so this enables us to compute quantum dynamics entirely in terms of the field operator algebra described in this section.

Operators in Fock space are enormous mathematical objects, and it is impractical to directly represent them on a computer and integrate Equation 2.24 to compute a system's dynamics. A class of approximations known as *mean-field theories* can be used to make equations of motion tractable, at the cost of neglecting certain quantum effects. Chapter 3 is dedicated to this topic.

2.3 Numerical techniques and basis choice

Many of the simulations in this thesis are computationally expensive, and it is crucial to optimise by choosing a sensible basis. In this section, we describe techniques for efficient and accurate computation in mixed bases.

2.3.1 The harmonic oscillator

Throughout this thesis, we consider models built upon the harmonic oscillator. Recall that the single-particle, 1D harmonic oscillator obeys the following Schrödinger equation:

$$i\hbar\frac{d\psi_(x)}{dt} = \left(-\frac{\hbar^2}{2m}\frac{\partial^2}{\partial x^2} + \frac{1}{2}m\omega^2x^2\right)\psi(x). \tag{2.25}$$

It is common to non-dimensionalise this by defining time in units of $t_0 = \omega^{-1}$ and position in units of $x_0 = \sqrt{\hbar/m\omega}$, yielding:

$$i\frac{d\psi(x)}{dt} = \left(-\frac{1}{2}\frac{\partial^2}{\partial x^2} + \frac{1}{2}x^2\right)\psi(x). \tag{2.26}$$

This removes all parameters without loss of generality, which is extremely helpful for numerical simulations. When we introduce extra terms, it will also reduce the dimensionful parameters of our models to a smaller number of dimensionless ones, allowing greater insight with simulations of fewer parameter combinations. With this non-dimensionalised length scale, the stationary states of Equation 2.26 are given by [93]:

$$\phi_n(x) = \frac{\pi^{-1/4}}{\sqrt{2^n n!}}H_n(x)e^{-x^2/2}, \tag{2.27}$$

[9] This is crucial, since we will always include time-dependent control terms.

where $H_n(x)$ is the nth Hermite polynomial[10] and $\xi = x/x_0$ is a dimensionless position variable. These span $L^2(\mathbb{R})$ and are known as the *Hermite-Gauss basis*.

2.3.2 Diagonalisation of evolution terms

The approximated unitary dynamics in this thesis[11] involve nonlinear Schrödinger-like equations with an analytically solvable harmonic oscillator component, plus perturbing components that are diagonal in the position basis (and may depend on time). These may be written in the form:

$$i\hbar\frac{d\psi_n(x)}{dt} = \underbrace{\overbrace{-\frac{\hbar^2}{2m}\frac{\partial^2\psi_n(x)}{\partial x^2}}^{\text{Diagonal in } k\text{-space}} + \overbrace{\frac{1}{2}m\omega^2x^2\psi_n(x)}^{\text{Diagonal in } x\text{-space}}}_{\text{Diagonal in Hermite-Gauss basis}} + \underbrace{f(x,t)\psi_n(x)}_{\text{Diagonal in } x\text{-space}}. \tag{2.28}$$

Finite differencing is imprecise, so for accurate computation it is preferable to transform nonlocal terms into a basis where they are diagonalised - such as computing the kinetic energy term in k-space. Noting the diagonalisation properties of Equation 2.28, we have two options:

1. **Store the wavefunction(s) in x-space**, and transform to k-space every time step in order to compute the kinetic energy term. For D grid points, this is $\mathcal{O}(D\log D)$ since we can use a fast Fourier transform (FFT) for the basis transformation. We refer to this as the *spectral method*.

2. **Store the wavefunction(s) in the Hermite-Gauss basis** (that is, store the c_n in the expansion $|\Psi\rangle = \sum_n c_n|\phi_n\rangle$, where the $|\phi_n\rangle$ are the harmonic oscillator eigenstates), and project onto x-space every time step to compute the perturbing terms. There is no known accelerated algorithm for the Hermite-Gauss transform, so this is $\mathcal{O}(D^2)$, but significantly less coefficients need to be stored for an accurate state representation. We refer to this as the *Hermite-Gauss method*.

In practice, the spectral method is the easiest to implement and construct desired initial states in. However, it is inappropriate for very high-energy states and/or states with many fermions. In the former case, the wavefunctions tend to be extremely narrow at points due to high kinetic energy, and in the latter case the wavefunctions are highly oscillatory to preserve Pauli exclusion; both require a prohibitively large number of grid points. In comparison, we typically only need a basis size on the order of the number of particles to accurately represent states in the Hermite-Gauss basis.

2.3.3 Harmonic oscillator field products with Hermite-Gaussian quadrature

As stated previously, the spectral method relies on reversible FFTs, which are easy to implement exactly on a computer. In the case of the Hermite-Gauss method, we must be more careful. The basis transform may not be exactly reversible and requires computation

[10] Two main conventions exist for Hermite polynomials, roughly corresponding to their use in physics and probability. We will always use the physicists' convention, corresponding to $\alpha^2 = 1$ in Equation 7.8.5 of Ref. [94]

[11] Specifically, this refers to the GPE (3.1) for bosons, and the FGPE (3.33) for fermions.

of the coefficients via the following integral:

$$c_{j,n} = \int dx \phi_j(x) \psi_n(x), \tag{2.29}$$

where the $\phi_j(x)$ are the Hermite-Gauss modes (harmonic oscillator eigenfunctions, Equation 2.27). However, the higher-order Hermite-Gauss modes are highly oscillatory, and cannot be accurately integrated over on an evenly-spaced grid of tractable size. We now describe a method by which they can be *exactly* integrated with a modest number of grid points. Although this method is outlined elsewhere [95], we choose to explain it in full in this thesis as existing explanations are difficult to follow.

The discretisation and numerical approximation of an integral is known as *quadrature*. For a single-variable function $f(x)$, we typically evaluate an integral $\int_a^b dx f(x)$ by choosing quadrature weights w_j and quadrature points $x_j \in [a, b]$, then summing over them to approximate the integral

$$\int_a^b dx f(x) = \sum_j w_j f(x_j) + \epsilon\left(f, \{x_j\}, \{w_j\}\right), \tag{2.30}$$

where $\epsilon\left(f, \{x_j\}, \{w_j\}\right)$ is an error term that we hope to minimise. Often, the weights and points are chosen geometrically: we could choose the x_j to be N equally spaced points with step size δ_x, leading to the Riemann-sum-like integral approximation

$$\int_a^b dx f(x) = \delta_x \sum_{j=0}^{N-1} f(a + j\delta_x) + \epsilon\left(f, \delta_x\}\right), \tag{2.31}$$

where $\epsilon(f, \delta_x) \to 0$ as $\delta_x \to 0$ for a well-behaved function. For finite step size, there will almost always be a finite error, and the use of equally-spaced quadrature points is particularly ineffective for highly oscillatory functions, such as high-order Hermite-Gauss modes (harmonic oscillator wavefunctions, Equation 2.27).

The quadrature weights and points need not be chosen geometrically. *Gaussian quadrature* refers to a class of methods for selecting the w_j and x_j such that the error is *zero* for certain types of functions. A variant known as *Hermite-Gaussian* quadrature allows us to calculate integrals over Hermite polynomials with Gaussian weighting functions exactly. Choose some $D \in \mathbb{N}$: this determines the order of Hermite polynomials up to which we will be able to integrate exactly. We write the jth Hermite polynomial as $H_j(x)$. If we choose our quadrature points such that x_j is the jth root of $H_D(x)$, and choose the quadrature weights

$$w_j = -\frac{2^D (D-1)! \sqrt{\pi}}{H'_D(x_j) H_{D-1}(x_j)}, \tag{2.32}$$

then the error for the integral $\int_{-\infty}^{\infty} dx f(x) e^{-x^2}$ is given by [94]:

$$\epsilon\left(f\right) = \frac{D! \sqrt{\pi}}{2^D (2D)!} f^{(2D)}(\eta), \tag{2.33}$$

where $f^{(2D)}(x)$ is the $2D$th derivative of f, and $\eta \in \mathbb{R}$ is unknown. If $f(x)$ is a polynomial of order $2D-1$ or less, then trivially the error (2.33) is exactly zero, and the quadrature will be exact to machine precision. Fortunately, this is often true for integrals over wavefunctions

constructed from the Hermite-Gauss basis. Suppose now that we have two wavefunctions $\psi_1(x)$, $\psi_2(x)$ written in the energy eigenbasis truncated at D dimensions, such that

$$\psi_1(x) = \sum_{j=0}^{D-1} c_j \phi_j(x), \qquad \psi_2(x) = \sum_{j=0}^{D-1} d_j \phi_j(x), \tag{2.34}$$

where the $\phi_j(x)$ are harmonic oscillator eigenfunctions (2.27). We wish to evaluate the integral

$$\int_{-\infty}^{\infty} dx \psi_1^*(x)\psi_2(x) = \sum_{j,k=0}^{D-1} c_j d_k \int_{-\infty}^{\infty} dx \phi_j^*(x)\phi_k(x). \tag{2.35}$$

Noting the functional form of the Hermite-Gauss modes (2.27), we may write the integral on the right-hand side of Equation 2.35 as $\int_{-\infty}^{\infty} dx f(x) e^{-x^2}$, where $f(x)$ is a polynomial of degree $2D-2$ or less. By Equation 2.33, it follows that the error will be exactly zero for the given weights and points, and thus the quadrature will be exact.

We refer to Equation 2.35 as an integral over a *two-field product*, since the integrand contains two wavefunctions constructed from the Hermite-Gauss basis. By an essentially identical argument to the above, we may compute an N-field product exactly by using $ND - N$ quadrature points. An N-field product requires the transformed quadrature points[12] $x'_j = 2x_j/N$, where x_j is the jth root of the appropriate Hermite polynomial. For example, in Chapter 4, we will frequently need to calculate nonlinear interatomic scattering terms in the Hermite-Gauss basis. To do so, we must evaluate integrals of the form:

$$\mathcal{I} = \int dx \, |\psi_1(x)|^2 \, \psi_2(x)\phi_n(x), \tag{2.36}$$

where the $\psi_j(x)$ are in the form of Equation 2.34 and $\phi_n(x)$ is some arbitrary Hermite-Gauss mode (2.27) for $n < D$. This is a *four-field product*, and can be computed exactly with $4D-4$ quadrature points, chosen as $x'_j = x_j/2$.

Using this technique, when simulating Schrödinger-like equations in the Hermite-Gauss basis, we can exactly compute any perturbing term that is diagonal in the position basis with only modest computational effort. This is why the Hermite-Gauss method is so effective for fast, precise calculations in systems based on the harmonic oscillator.

2.4 Stochastic calculus and Wiener processes

In order to model probabilistic dynamical process like quantum measurement, we must introducess randomness to calculus, leading to an area of mathematics broadly known as *stochastic calculus*. Detailed pedagogical treatments of the topic in a physical sciences context can be found in Refs. [96, 97].

Chiefly, we will consider *stochastic differential equations* (SDEs) that are driven by *white noise* - a noise process with zero mean that is completely uncorrelated at different times. For our purposes, this is best represented[13] in terms of the *Wiener increment* $dW(t)$,

[12] This transformation is required to preserve the exponent of the Gaussian weighting function.

[13] One can directly formulate stochastic calculus in terms of the white noise itself, but this is a far more convenient representation. The Wiener increment can be derived directly from white noise [97].

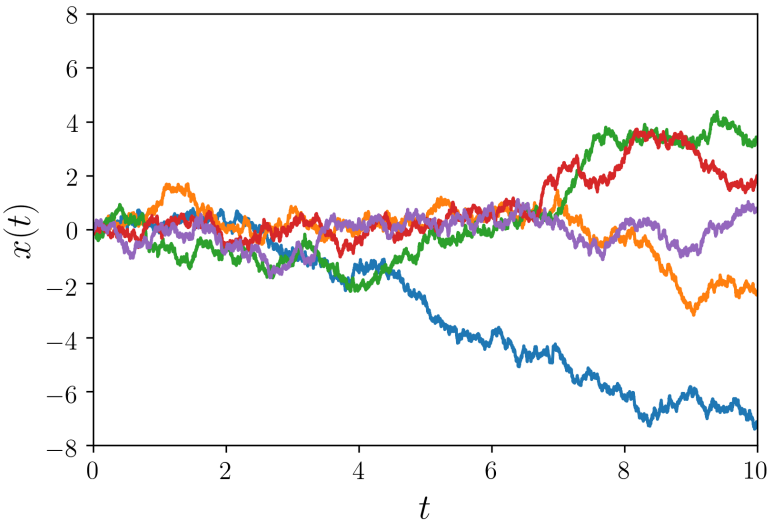

Figure 2.2: Five example trajectories of the SDE $dx = \circ dW(t)$, integrated with the Stratonovich integral using the XMDS2 package [98]. Since the evolution is conditioned on random noise, the dynamics are not deterministic.

which has the properties:[14]

$$\begin{aligned} \mathbb{E}\left\{dW(t)\right\} &= 0, \\ \mathbb{E}\left\{dW(t)^2\right\} &= dt, \\ \mathbb{E}\left\{dW(t)dW(t')\right\} &= dtdt'\delta(t-t'), \end{aligned} \tag{2.37}$$

where $\mathbb{E}\{\cdot\}$ denotes a *stochastic average* - an average over all possible choices of random white noise. It can be shown that the Wiener increment is sampled from a Gaussian distribution [96], with probability density:[15]

$$P(dW) = \frac{\exp\left((-dW^2)(2dt)\right)}{\sqrt{2\pi dt}}. \tag{2.38}$$

Consider a first-order differential equation for some physical variable x varying with time t. In the absence of any random processes, we have a *deterministic* equation of motion

$$dx = f(x,t)dt. \tag{2.39}$$

Introducing a Wiener increment $dW(t)$, we may construct an SDE

$$dx = \underbrace{f(x,t)dt}_{\text{Deterministic}} + \underbrace{g(x,t)dW(t)}_{\text{Random}}. \tag{2.40}$$

This can be used to describe a physical process, with deterministic ($f(x,t)$) and random ($g(x,t)dW(t)$) driving terms in its evolution. Since Equation 2.40 depends on a random noise process, it is not deterministic. There are now infinite *trajectories* (possible outcomes

[14] We have assumed use of the Itô integral in Equation 2.37, which we introduce later in this section.

[15] Strictly speaking, this is only true for discrete increments Δt and ΔW. However, this is of little consequence since any computer implementation will integrate in discrete steps. Consequently, many texts present the distribution in this form (e.g. Ref [96]).

of the system), conditioned on the outcomes of the random noise process - a simple example is depicted in Figure 2.2. One can think of the stochastic average $\mathbb{E}\{\cdot\}$ as an average over these trajectories. To time-evolve this system, we integrate over equation 2.40:

$$x(t) = x(t_0) + \int_{t_0}^{t} dt' f(x(t'), t') + \int_{t_0}^{t} dt' g(x(t'), t') dW(t'). \tag{2.41}$$

However, there is an ambiguity in the stochastic term $\int_{t_0}^{t} dt' g(x(t'), t') dW(t')$ - different elementary definitions of the integral yield different results. Recall that one can define integration as a limit of a sum (the *Riemann-Stieltjes integral*). Consider a definite integral over a single-variable function

$$\mathcal{I} = \int_{t_0}^{t} dt' f(t'). \tag{2.42}$$

Recall from elementary calculus that we divide up the interval $[t_0, t]$ into n partitioning points $t_0 \leq t_1 \leq \ldots \leq t_{n-1} \leq t$. We define the intermediate points τ_j such that $t_{j-1} \leq \tau_j \leq t_j$, and compute the sum

$$S_n = \sum_{j=1}^{n} f(\tau_j) (\tau_j - \tau_{j-1}). \tag{2.43}$$

For a well-behaved function $f(t)$, in the limit of infinite partitioning points we have the convergence $S_n \to \mathcal{I}$, *regardless of the choice of intermediate points* τ_j. The situation is more complicated for a stochastic integral. If we were to similarly define our stochastic term in Equation 2.41 as the limit[16] of a Riemann-Stieltjes-like integral, we would find that its limit actually depends on how we choose our intermediate points τ_j. We will provide only a heuristic treatment here - for the full mathematical details, we refer the interested reader to Chapter 4 of Ref. [97].

The choice $\tau_j = t_{j-1}$ leads to the *Itô integral*. When describing quantum noise, the Itô integral is a convenient choice for analytics, and so the stochastic master equations in previous works [3, 4, 72, 73, 76, 77] and this thesis are formulated using the Itô integral. This integral also has a different chain rule and product rule, with the latter given by

$$d(xy) = x\,(dy) + (dx)\,y + (dx)\,(dy). \tag{2.44}$$

An alternative definition of the stochastic integral is given by the *Stratonovich integral*, which corresponds to the choice of the midpoint $\tau_j = (t_{j-1} + t_j)/2$. This integral actually has the standard chain rule from deterministic calculus. Throughout this thesis, we will always denote the Wiener increement for an SDE in the Stratonovich formulation as $\circ dW(t)$, and in the Itô formulation as $dW(t)$.

Since the randomness in the models of this thesis is quantum in origin, our master equations will always be in Itô form for the reasons stated previously. However, for numerical simulations, we prefer the Stratonovich form. We implement all stochastic simulations in this thesis in the open-source software package XMDS2 [98], which only has efficient routines for the Stratonovich integral. Fortunately, there is a simple expression that can be used to cast between the two formulations. An Itô SDE in the form of equation 2.40

[16] In practice, this is actually a *mean-square limit*. Details are provided in Chapter 2 of Ref. [97].

can be cast to Stratonovich form by the following equation:

$$dx = \underbrace{f(x,t)dt}_{\text{Deterministic}} - \underbrace{\frac{1}{2}g(x,t)\cdot\nabla g(x,t)}_{\text{Stratonovich correction}} + \underbrace{g(x,t)\circ dW(t)}_{\text{Stochastic noise}}, \tag{2.45}$$

where we have moved from the Itô to Stratonovich integral and corrected by a deterministic term known as the *Stratonovich correction*. We will often consider coupled SDEs of the Itô form

$$dx_j = A_j dt + \sum_k B_{jk} dW_k(t), \tag{2.46}$$

where the x_j are separate variables,[17] and the dW_j are corresponding independent Wiener processes. This may be cast to the following Stratonovich form:

$$dx_j = \underbrace{A_j dt}_{\text{Deterministic}} - \underbrace{\frac{1}{2}\sum_{kl} B_{kl}\partial_l B_{jk} dt}_{\text{Stratonovich correction}} + \underbrace{\sum_k B_{jk}\circ dW_k(t)}_{\text{Stochastic noise}}. \tag{2.47}$$

We now have the mathematical tools to model stochastic processes. We will apply these tools in Chapter 5 to model quantum measurement of cold atoms, and simulate these models numerically in Chapter 6.

[17] Although we have written this as a set of discrete variables, this may be a discretised continuous variable, like a grid in position space.

Chapter 3

The art of mean-field theory

As outlined in Section 1.1, full quantum field theoretic calculations for our systems are computationally intractable due to exponential scaling of the Hilbert space. We thus seek low-dimensional dynamical approximations that enable a simpler description. By making assumptions about the form of our quantum state, we may be able to reduce the full many-body dynamics to that of a simpler *order parameter*. This is an approach broadly known as *mean-field theory*, where the full quantum field theory can be approximated by a simpler, lower-dimensional 'mean field'.

Mean-field theory discards significant information about the system. All mean-field theories used in this thesis ignore the effect of quantum correlations, which are a crucial aspect of phenomena like superconductivity. They are therefore incapable of describing the richest behaviour of many-body quantum mechanics that inspired the development of quantum simulators to begin with. Nonetheless, mean-field theory is often sufficient to capture the bulk or average behaviour of a system, and is therefore a reasonable choice to model cooling processes. Previous studies of feedback cooling in bosonic systems have mostly used mean-field theory [2–4], with the notable exception of Ref. [77].

This chapter contains both a review of existing background and new work. In Section 3.1, we review existing methods for BECs: we discuss the well-known Gross-Pitaevskii equation and how it can be derived from two different uncorrelated state approximations. In Section 3.2, we derive a multimode fermionic equivalent using the Hartree-Fock approximation, which we call the fermion GPE (FGPE). This is a first step towards extending the results of Refs. [2–4] to fermions. In Section 3.3, we review ground state finding algorithms: imaginary time evolution for bosons, and the Hartree-Fock self-consistent field method for fermions. This enables us to calculate ground states for all systems simulated in Chapters 4 and 6, allowing us to quantify how close a quantum gas is to its ground state in our simulations.

3.1 Mean-field theory of BECs

We have thus far been intentionally vague about the details of mean-field theory, since there are many types of approximation that fall under this banner. We now illustrate the key concepts by deriving a mean-field theory for bosons at zero temperature,[1] which will later be used to simulate feedback control of a BEC (as was originally done by Haine *et*

[1] This is a 'zero-temperature' formalism since we consider pure states only. A thermal state at finite temperature must be a mixed ensemble.

al. [2]).

We will derive the Gross-Pitaevskii equation (GPE):

$$i\hbar\frac{d\phi(\boldsymbol{x})}{dt} = \left(-\frac{\hbar^2}{2m}\boldsymbol{\nabla}_{\boldsymbol{x}}^2 + V(\boldsymbol{x},t) + U_0\left|\phi(\boldsymbol{x})\right|^2\right)\phi(\boldsymbol{x}), \tag{3.1}$$

originally proposed by Gross [99, 100] and Pitaevskii [101]. This equation describes the evolution of a wavefunction-like object with a single set of spatial coordinates, and is therefore much simpler than the full quantum field theory.

3.1.1 Approximation by an order parameter

Consider a system of identical bosons of mass m in a trapping potential $V_0(\boldsymbol{x})$ with time-varying controls $V_C(\boldsymbol{x},t)$, interacting by a pair interaction of the form $U(\boldsymbol{x}-\boldsymbol{y})$. The bosons are created and annihilated at position $\boldsymbol{x}$ by bosonic field operators $\hat{\psi}^\dagger(\boldsymbol{x})$ and $\hat{\psi}(\boldsymbol{x})$, respectively. We assume that the system is in a coherent state of a single mode, and therefore the state $|\Psi\rangle$ of the system may be written as a tensor product of coherent states in the spatial basis (see Appendix A.2 for a proof of this property):

$$|\Psi\rangle = \bigotimes_{\boldsymbol{x}'}\left|\phi(\boldsymbol{x}')\right\rangle, \tag{3.2}$$

and thus the state is an eigenstate of the field annihilation operator for any position:

$$\hat{\psi}(\boldsymbol{x})\left|\Psi\right\rangle = \phi(\boldsymbol{x})\left|\Psi\right\rangle. \tag{3.3}$$

Since all observables may be written in terms of field operators, we may calculate any property of the system from the order parameter alone. Expectation values of all observables of interest may be written in the form:

$$\langle\hat{O}\rangle = \int d\boldsymbol{x}\left\langle\left(\hat{\psi}^\dagger(\boldsymbol{x})\right)^n\tilde{O}(\boldsymbol{x})\left(\hat{\psi}(\boldsymbol{x})\right)^m\right\rangle, \tag{3.4}$$

which, applying Equation 3.3, yields:

$$\langle\hat{O}\rangle = \int d\boldsymbol{x}\left(\phi^*(\boldsymbol{x})\right)^n\tilde{O}(\boldsymbol{x})\left(\phi(\boldsymbol{x})\right)^m. \tag{3.5}$$

Thus, all observables can be calculated in terms of $\phi(\boldsymbol{x})$, which is the *order parameter* of our mean-field theory: a mathematical object that fully describes the approximate system state, and is far less complicated than the full state vector. If we can compute its evolution, we can describe the full many-body dynamics entirely in terms of an object with the dimensionality of a single-particle wavefunction.

3.1.2 Dynamics: the Gross-Pitaevskii equation

Since the approximate system state is completely described by $\phi(\boldsymbol{x})$, we wish to find its equation of motion. We consider the cold-atom Hamiltonian (Equation 2.22) in the

bosonic, single-spin-component case:

$$\hat{H} = \int d\boldsymbol{x}\, \hat{\psi}^\dagger \left(-\frac{\hbar^2}{2m}\boldsymbol{\nabla}_{\boldsymbol{x}}^2 + V(\boldsymbol{x},t) \right) \hat{\psi}(\boldsymbol{x}) + \frac{U_0}{2} \int d\boldsymbol{x}\, \hat{\psi}^\dagger(\boldsymbol{x})\hat{\psi}^\dagger(\boldsymbol{x})\hat{\psi}(\boldsymbol{x})\hat{\psi}(\boldsymbol{x}), \tag{3.6}$$

where the field operators have bosonic commutation relations. The time-evolution of a field operator is determined from the Heisenberg equation of motion (Equation 2.24). Applying expectation values, we find:

$$\begin{aligned} i\hbar\frac{d\phi(\boldsymbol{x})}{dt} = i\hbar\frac{d\left\langle\hat{\psi}(\boldsymbol{x})\right\rangle}{dt} &= \left\langle\left[\hat{\psi}(\boldsymbol{x}), \hat{H}\right]\right\rangle \\ &= \left\langle -\frac{\hbar^2}{2m}\boldsymbol{\nabla}_{\boldsymbol{x}}^2\hat{\psi}(\boldsymbol{x}) + V(\boldsymbol{x},t)\hat{\psi}(\boldsymbol{x}) + U_0\hat{\psi}^\dagger(\boldsymbol{x})\hat{\psi}(\boldsymbol{x})\hat{\psi}(\boldsymbol{x}) \right\rangle. \end{aligned} \tag{3.7}$$

Applying Equation 3.3, we obtain the desired equation of motion for $\phi(\boldsymbol{x})$:

$$i\hbar\frac{d\phi(\boldsymbol{x})}{dt} = -\frac{\hbar^2}{2m}\boldsymbol{\nabla}_{\boldsymbol{x}}^2\phi(\boldsymbol{x}) + V(\boldsymbol{x},t)\phi(\boldsymbol{x}) + U_0\left|\phi(\boldsymbol{x})\right|^2\phi(\boldsymbol{x}), \tag{3.8}$$

which is exactly the GPE (Equation 3.1). The astute reader will note that it resembles the Schrödinger equation of a single-particle wavefunction, with the addition of a nonlinear term $U_0\left|\phi(\boldsymbol{x})\right|^2\phi(\boldsymbol{x})$ describing interatomic scattering interactions. We have successfully reduced the intractable quantum field theory to a problem barely any more complicated than the quantum mechanics of a single particle.

It is crucial to note the normalisation of the order parameter, and the free parameters of the GPE. Unlike the Schrödinger wavefunction of a single particle, which is typically normalised to unity, the order parameter is normalised to the average number of particles (see Appendix A.2 or Ref. [102]):

$$\int d\boldsymbol{x}|\phi(\boldsymbol{x})|^2 = \int d\boldsymbol{x}\left\langle\hat{\psi}^\dagger(\boldsymbol{x})\hat{\psi}(\boldsymbol{x})\right\rangle = N. \tag{3.9}$$

Unlike the Schrödinger equation of a single particle, changes in the norm will alter the dynamics of the system due to the nonlinearity. However, the norm N and interaction strength U_0 are not independent free parameters: the dynamics depend only on the value of NU_0,[2] so an increase in N is equivalent to a proportional increase in U_0. There is only one free parameter, and so we may fix the norm to unity and vary U_0 when considering the change in effective interaction strength.

The GPE neglects quantum correlations.[3] Regardless, it is a very accurate model in cases where these are negligible. It captures the wave-like nature of a BEC, and thus accurately models interference [103, 104], reflection [105] and tunnelling [106, 107] effects. The nonlinear term allows interactions to be included, and therefore the GPE correctly models solitons [108–110] and vortices [111–113]. Most importantly for this thesis, the GPE has previously been used to model feedback control of a BEC [2].

It is crucial to note that there is nothing special about the coherent-state approximation

[2]The only term for which changing the norm will change the dynamics is the nonlinear term $U_0|\phi(\boldsymbol{x})|^2\phi(\boldsymbol{x})$. Any multiplier on the norm of $\phi(\boldsymbol{x})$ (N) could be absorbed into U_0: for example, doubling N for fixed U_0 would be equivalent to doubling U_0 for fixed N.

[3]This is a trivial consequence of the separability in Equation 3.2.

(Equation 3.2) beyond the fact that it ignores correlations: a BEC is not necessarily a coherent state, and there are different state approximations that lead to the same dynamics. In fact, under a density-like measurement of the type used in Refs. [3, 4] (and that we will apply in Chapters 5 and 6), a coherent-state approximation is completely inappropriate. This is due to a fundamental mismatch between the approximation and the underlying physics; a coherent state has non-negligible uncertainty in particle number (it is a Poissonian distribution of number states [102]), whereas a density-like measurement projects the system into a state of low number uncertainty.

3.1.3 The Gross-Pitaevskii equation in the Hartree-Fock approximation

The GPE can also be derived from other mean-field theories that neglect correlations, including by the assumption of a number state (the Hartree-Fock approximation, which also neglects quantum correlations [29]). This approach was used by Szigeti *et al.* [4] to derive a mean-field theory of BECs that is numerically stable under measurement; a full derivation can be found therein. The derivation uses the same Hamiltonian, and assumes that the system is Bose-condensed and certain in number, such that the state vector may be written as a single-mode Fock state:

$$|\Psi\rangle = |N, 0, 0, \ldots\rangle\,. \tag{3.10}$$

The occupied mode has a spatial wavefunction $\chi(\boldsymbol{x})$, which is the order parameter of this mean-field theory. Unfortunately, there is no simple expression for $\langle\hat{\psi}(\boldsymbol{x})\rangle$, necessitating a more complicated order parameter. By computing an equation of motion for the two-point correlation function $\langle\hat{\psi}^\dagger(\boldsymbol{x}_1)\hat{\psi}(\boldsymbol{x}_2)\rangle = N\chi^*(\boldsymbol{x}_1)\chi(\boldsymbol{x}_2)$ in the Heisenberg picture and finding an ansatz for the evolution of $\chi(\boldsymbol{x})$ that satisfies it, this leads to an equation of motion for $\chi(\boldsymbol{x})$:[4]

$$i\hbar\frac{d\chi(\boldsymbol{x})}{dt} = \left(-\frac{\hbar^2}{2m}\boldsymbol{\nabla}^2_{\boldsymbol{x}} + V(\boldsymbol{x}) + (N-1)U_0|\chi(\boldsymbol{x})|^2\right)\chi(\boldsymbol{x}). \tag{3.11}$$

This is the GPE (3.1), normalised to $N-1$ rather than N. In the large-N limit these two different state approximations lead to the same dynamics, illustrating our claim that there is nothing special about the state approximation beyond ignoring quantum correlations.

3.2 Mean-field theory of fermions: the Hartree-Fock approximation

We now use this approach as inspiration to develop a similar mean-field theory for fermions, so that we can simulate feedback control of fermionic systems. For the system's Hamiltonian, we will use the cold-atom Hamiltonian (Equation 2.22) in the fermionic, two-spin-component case:

$$\hat{H} = \sum_\sigma \int d\boldsymbol{x}\hat{\psi}^\dagger_\sigma\left(-\frac{\hbar^2}{2m}\boldsymbol{\nabla}^2_{\boldsymbol{x}} + V(\boldsymbol{x},t)\right)\hat{\psi}_\sigma(\boldsymbol{x}) + \frac{U_0}{2}\sum_{\sigma\sigma'}\int d\boldsymbol{x}\hat{\psi}^\dagger_\sigma(\boldsymbol{x})\hat{\psi}^\dagger_{\sigma'}(\boldsymbol{x})\hat{\psi}_{\sigma'}(\boldsymbol{x})\hat{\psi}_\sigma(\boldsymbol{x}), \tag{3.12}$$

[4] We are considering only the unitary evolution; this corresponds to $\alpha = 0$ in Ref. [4].

where $\sigma, \sigma' \in \{\uparrow, \downarrow\}$ and the field operators have fermionic anticommutation relations. Constructing a mean-field theory is harder in the fermionic case. Fermions obey the Pauli exclusion principle and cannot multiply occupy the same mode. We thus cannot use a coherent-state approximation or a single-mode Fock state.

A density-like measurement of the sort we intend to apply will approximately project the system onto a state of definite number [4]. We therefore approximate our system's quantum state by a Fock state (number state):

$$|\Psi\rangle = \prod_{n \in S} \hat{c}^\dagger_{n,\uparrow} \hat{c}^\dagger_{n,\downarrow} |0\rangle \,, \tag{3.13}$$

where the $\{\hat{c}^\dagger_{n,\sigma}\}$ are the creation operators for some *arbitrary* single-particle basis with principal index n and spin index σ, and S is some set of distinct principal indices in this basis.[5]

3.2.1 An order parameter for fermions

Much like the approach in Section 3.1.3, we use as our order parameter the *two-point correlation function*:

$$m_{\sigma\sigma'}(\boldsymbol{x}_1, \boldsymbol{x}_2) = \langle \Psi | \, \hat{\psi}^\dagger_\sigma(\boldsymbol{x}_1) \hat{\psi}_{\sigma'}(\boldsymbol{x}_2) \, | \Psi \rangle \,. \tag{3.14}$$

Expanding $|\Psi\rangle$ in the form of Equation 3.13, expanding the field operators into the same basis, using linearity and noting that $\hat{c}_{n,\sigma} |\Psi\rangle = 0$ for $n \notin S$, we obtain:

$$m_{\sigma\sigma'}(\boldsymbol{x}_1, \boldsymbol{x}_2) = \sum_{n,m \in S} \left[\underbrace{\left(\langle 0 | \prod_{a \in S} \hat{c}_{a,\downarrow} \hat{c}_{a,\uparrow} \right) \left(\hat{c}^\dagger_{n,\sigma} \hat{c}_{m,\sigma'} \right) \left(\prod_{b \in S} \hat{c}^\dagger_{b,\uparrow} \hat{c}^\dagger_{b,\downarrow} |0\rangle \right)}_{\delta_{nm}\delta_{\sigma\sigma'}} \chi^*_{n,\sigma}(\boldsymbol{x}_1) \chi_{m,\sigma'}(\boldsymbol{x}_2) \right] , \tag{3.15}$$

where the $\chi_{n,\sigma}(\boldsymbol{x})$ are the spatial wavefunctions for the modes of the number state $|\Psi\rangle$. Identifying the remaining bra-ket expression as $\delta_{nm}\delta_{\sigma\sigma'}$[6] and summing over m yields:

$$m_{\sigma\sigma'}(\boldsymbol{x}_1, \boldsymbol{x}_2) = \delta_{\sigma\sigma'} \left(\sum_{n \in S} \chi^*_{n,\sigma}(\boldsymbol{x}_1) \chi_{n,\sigma'}(\boldsymbol{x}_2) \right) . \tag{3.16}$$

Since the spin off-diagonal is zero, we often write only the diagonal components as:

$$m_\sigma(\boldsymbol{x}_1, \boldsymbol{x}_2) = \sum_{n \in S} \chi^*_{n,\sigma}(\boldsymbol{x}_1) \chi_{n,\sigma}(\boldsymbol{x}_2). \tag{3.17}$$

Much like the bosonic case, all observables of interest may be written in the form:

$$\langle \hat{O} \rangle = \sum_{n \in S, \sigma} \int d\boldsymbol{x} \left\langle \left(\hat{\psi}^\dagger_{n,\sigma}(\boldsymbol{x}) \right)^a \tilde{O}(\boldsymbol{x}) \left(\hat{\psi}_{n,\sigma}(\boldsymbol{x}) \right)^b \right\rangle . \tag{3.18}$$

[5] It should be noted that we have assumed an equal number of spin-up and spin-down fermions. There is also a sign ambiguity in the ordering of creation operators under the product, but this cancels when computing expectation values and is thus irrelevant.

[6] To see this without tedious operator algebra, note that this expression is equivalent to removing a particle in state $|m, \sigma'\rangle$ from $|\Psi\rangle$, removing a particle in state $\langle n, \sigma|$ from state $\langle \Psi|$, and taking the inner product, which is zero if particles were removed from different states.

Expanding out $|\Psi\rangle$ and the field operators into the usual basis and simplifying the operator expressions (a similar procedure to that of Equation 3.15, except with an arbitrary number of field operators and an operator on $L^2(\mathbb{R}^n)$ between the wavefunctions), we find:

$$\langle \hat{O} \rangle = \sum_{n \in S, \sigma} \int d\boldsymbol{x} \left(\chi^*_{n,\sigma}(\boldsymbol{x}) \right)^a \tilde{O}(\boldsymbol{x}) \left(\chi_{n,\sigma}(\boldsymbol{x}) \right)^b . \tag{3.19}$$

Instead of a single wavefunction-like order parameter, we now have N wavefunction-like order parameters. In fact, since our state approximation has no quantum correlations, we may treat the particles as independent, and these are actually the single-particle wavefunctions of each fermion.[7] This is a much more complicated state representation than we had in the bosonic case; nonetheless this grows linearly in complexity with respect to N, rather than exponentially as the full quantum state would.

3.2.2 Dynamics of the fermionic mean field

We now derive an equation of motion for the two-point correlation function. Once again, the Heisenberg equation of motion (2.24) gives:

$$\frac{d\hat{\psi}_{\sigma_1}(\boldsymbol{s})}{dt} = -\frac{i}{\hbar} \left[\hat{\psi}_{\sigma_1}(\boldsymbol{s}), \hat{H} \right]. \tag{3.20}$$

Defining:

$$\tilde{H}_a(\boldsymbol{x}) = -\frac{\hbar^2}{2m} \boldsymbol{\nabla}^2_{\boldsymbol{x}} + V(\boldsymbol{x}, t), \tag{3.21}$$

and expanding out Equation 3.20 by linearity, we obtain:

$$\begin{aligned} \frac{d\hat{\psi}_{\sigma_1}(\boldsymbol{s})}{dt} = &-\frac{i}{\hbar} \sum_{\sigma_2} \int d\boldsymbol{z} \Big[\underbrace{\hat{\psi}_{\sigma_1}(\boldsymbol{s})}_{\hat{A}_1}, \overbrace{\hat{\psi}^\dagger_{\sigma_2}(\boldsymbol{z})}^{\hat{B}_1} \underbrace{\tilde{H}_a(\boldsymbol{z}) \hat{\psi}_{\sigma_2}(\boldsymbol{z})}_{\hat{C}_1} \Big] \\ &- \frac{iU_0}{2\hbar} \sum_{\sigma_2 \sigma_3} \int d\boldsymbol{z} \Big[\underbrace{\hat{\psi}_{\sigma_1}(\boldsymbol{s})}_{\hat{A}_2}, \overbrace{\hat{\psi}^\dagger_{\sigma_2}(\boldsymbol{z}) \hat{\psi}^\dagger_{\sigma_3}(\boldsymbol{z})}^{\hat{B}_2} \underbrace{\hat{\psi}_{\sigma_3}(\boldsymbol{z}) \hat{\psi}_{\sigma_2}(\boldsymbol{z})}_{\hat{C}_2} \Big]. \end{aligned} \tag{3.22}$$

Applying the commutator-anticommutator identity $\left[\hat{A}, \hat{B}\hat{C}\right] = \left\{\hat{B}, \hat{A}\right\} \hat{C} - \hat{B} \left\{\hat{C}, \hat{A}\right\}$ to both commutators as labelled, and using anticommutation relations, we obtain:

$$\begin{aligned} \frac{d\hat{\psi}_{\sigma_1}(\boldsymbol{s})}{dt} = &-\frac{i}{\hbar} \sum_{\sigma_2} \int d\boldsymbol{z} \delta_{\sigma_1 \sigma_2} \delta(\boldsymbol{s} - \boldsymbol{z}) \tilde{H}_a(\boldsymbol{z}) \hat{\psi}_{\sigma_2}(\boldsymbol{z}) \\ &- \frac{iU_0}{2\hbar} \sum_{\sigma_2 \sigma_3} \int d\boldsymbol{z} \left\{ \hat{\psi}^\dagger_{\sigma_2}(\boldsymbol{z}) \hat{\psi}^\dagger_{\sigma_3}(\boldsymbol{z}), \hat{\psi}_{\sigma_1}(\boldsymbol{s}) \right\} \hat{\psi}_{\sigma_3}(\boldsymbol{z}) \hat{\psi}_{\sigma_2}(\boldsymbol{z}). \end{aligned} \tag{3.23}$$

[7] We can construct the full many-body wavefunction from these single-particle wavefunctions using a Slater determinant (see Chapter 2 of Ref. [114]).

Expanding the anticommutator, normal ordering with fermion anticommutation relations and simplifying yields:

$$\left\{\hat{\psi}^\dagger_{\sigma_2}(\boldsymbol{z})\hat{\psi}^\dagger_{\sigma_3}(\boldsymbol{z}), \hat{\psi}_{\sigma_1}(\boldsymbol{s})\right\} = 2\hat{\psi}^\dagger_{\sigma_2}(\boldsymbol{z})\hat{\psi}^\dagger_{\sigma_3}(\boldsymbol{z})\hat{\psi}_{\sigma_1}(\boldsymbol{s}) - \delta_{\sigma_1\sigma_3}\delta(\boldsymbol{s}-\boldsymbol{z})\hat{\psi}^\dagger_{\sigma_2}(\boldsymbol{z}) + \delta_{\sigma_1\sigma_2}\delta(\boldsymbol{s}-\boldsymbol{z})\hat{\psi}^\dagger_{\sigma_3}(\boldsymbol{z}). \tag{3.24}$$

Substituting Equation 3.24 into Equation 3.23, integrating and summing over all delta functions, relabelling sums, and applying an anticommutation relation to combine the last two terms yields:

$$\frac{d\hat{\psi}_{\sigma_1}(\boldsymbol{s})}{dt} = -\frac{i}{\hbar}\tilde{H}_a(\boldsymbol{s})\hat{\psi}_{\sigma_1}(\boldsymbol{s}) - \frac{iU_0}{\hbar}\sum_{\sigma_2\sigma_3}\int d\boldsymbol{z}\hat{\psi}^\dagger_{\sigma_2}(\boldsymbol{z})\hat{\psi}^\dagger_{\sigma_3}(\boldsymbol{z})\hat{\psi}_{\sigma_1}(\boldsymbol{s})\hat{\psi}_{\sigma_3}(\boldsymbol{z})\hat{\psi}_{\sigma_2}(\boldsymbol{z}) + \frac{iU_0}{\hbar}\sum_{\sigma_2}\hat{\psi}^\dagger_{\sigma_2}(\boldsymbol{s})\hat{\psi}_{\sigma_1}(\boldsymbol{s})\hat{\psi}_{\sigma_2}(\boldsymbol{s}). \tag{3.25}$$

We now use this to construct an equation of motion for the two-point correlation function. By the product rule and linearity, we find:

$$\frac{dm_{\sigma_1\sigma_2}(\boldsymbol{x}_1,\boldsymbol{x}_2)}{dt} = \left\langle\left(\frac{d\hat{\psi}^\dagger_{\sigma_1}(\boldsymbol{x}_1)}{dt}\right)\hat{\psi}_{\sigma_2}(\boldsymbol{x}_2)\right\rangle + \left\langle\hat{\psi}^\dagger_{\sigma_1}(\boldsymbol{x}_1)\left(\frac{d\hat{\psi}_{\sigma_2}(\boldsymbol{x}_2)}{dt}\right)\right\rangle. \tag{3.26}$$

Substituting Equation 3.25 into Equation 3.26 and applying anticommutation relations, we obtain:

$$\begin{aligned}\frac{dm_{\sigma_1\sigma_2}(\boldsymbol{x}_1,\boldsymbol{x}_2)}{dt} &= -\frac{i}{\hbar}\left(\tilde{H}_a(\boldsymbol{x}_2) - \tilde{H}_a(\boldsymbol{x}_1)\right)\left\langle\hat{\psi}^\dagger_{\sigma_1}(\boldsymbol{x}_1)\hat{\psi}_{\sigma_2}(\boldsymbol{x}_2)\right\rangle \\ &- \frac{iU_0}{\hbar}\sum_{\sigma_3}\left(\left\langle\hat{\psi}^\dagger_{\sigma_3}(\boldsymbol{x}_1)\hat{\psi}^\dagger_{\sigma_1}(\boldsymbol{x}_1)\hat{\psi}_{\sigma_3}(\boldsymbol{x}_1)\hat{\psi}_{\sigma_2}(\boldsymbol{x}_2)\right\rangle - \left\langle\hat{\psi}^\dagger_{\sigma_1}(\boldsymbol{x}_1)\hat{\psi}^\dagger_{\sigma_3}(\boldsymbol{x}_2)\hat{\psi}_{\sigma_2}(\boldsymbol{x}_2)\hat{\psi}_{\sigma_3}(\boldsymbol{x}_2)\right\rangle\right).\end{aligned} \tag{3.27}$$

So far, this equation of motion is still exact for any state, and we have not made use of our state approximation (3.13). By a corollary of Wick's Theorem (see Appendix B for a proof and detailed discussion), our Fock state approximation allows the factorisation of quartic terms:

$$\left\langle\hat{c}^\dagger_\alpha\hat{c}^\dagger_\beta\hat{c}_\gamma\hat{c}_\delta\right\rangle = \left\langle\hat{c}^\dagger_\alpha\hat{c}_\delta\right\rangle\left\langle\hat{c}^\dagger_\beta\hat{c}_\gamma\right\rangle - \left\langle\hat{c}^\dagger_\alpha\hat{c}_\gamma\right\rangle\left\langle\hat{c}^\dagger_\beta\hat{c}_\delta\right\rangle, \tag{3.28}$$

where these may be fermionic creation and annihilation operators in any basis.[8] Applying this factorisation to the quartic terms in Equation 3.27 yields:

$$\begin{aligned}\frac{dm_{\sigma_1\sigma_2}(\boldsymbol{x}_1,\boldsymbol{x}_2)}{dt} &= -\frac{i}{\hbar}\left(\tilde{H}_a(\boldsymbol{x}_2) - \tilde{H}_a(\boldsymbol{x}_1)\right)\left\langle\hat{\psi}^\dagger_{\sigma_1}(\boldsymbol{x}_1)\hat{\psi}_{\sigma_2}(\boldsymbol{x}_2)\right\rangle \\ &- \frac{iU_0}{\hbar}\sum_{\sigma_3}\Bigg(\left\langle\hat{\psi}^\dagger_{\sigma_1}(\boldsymbol{x}_1)\hat{\psi}_{\sigma_3}(\boldsymbol{x}_2)\right\rangle\left\langle\hat{\psi}^\dagger_{\sigma_3}(\boldsymbol{x}_2)\hat{\psi}_{\sigma_2}(\boldsymbol{x}_2)\right\rangle + \left\langle\hat{\psi}^\dagger_{\sigma_1}(\boldsymbol{x}_1)\hat{\psi}_{\sigma_2}(\boldsymbol{x}_2)\right\rangle\left\langle\hat{\psi}^\dagger_{\sigma_3}(\boldsymbol{x}_2)\hat{\psi}_{\sigma_3}(\boldsymbol{x}_2)\right\rangle \\ &\quad - \left\langle\hat{\psi}^\dagger_{\sigma_3}(\boldsymbol{x}_1)\hat{\psi}_{\sigma_2}(\boldsymbol{x}_2)\right\rangle\left\langle\hat{\psi}^\dagger_{\sigma_1}(\boldsymbol{x}_1)\hat{\psi}_{\sigma_3}(\boldsymbol{x}_1)\right\rangle - \left\langle\hat{\psi}^\dagger_{\sigma_3}(\boldsymbol{x}_1)\hat{\psi}_{\sigma_3}(\boldsymbol{x}_1)\right\rangle\left\langle\hat{\psi}^\dagger_{\sigma_1}(\boldsymbol{x}_1)\hat{\psi}_{\sigma_2}(\boldsymbol{x}_2)\right\rangle\Bigg).\end{aligned} \tag{3.29}$$

[8] Including a continuous basis, so these may be fermionic field operators.

All expecation values in Equation 3.29 are now two-point correlation functions and may be identified with $m_{\sigma_1\sigma_2}(\boldsymbol{x}_1, \boldsymbol{x}_2)$:

$$\frac{dm_{\sigma_1\sigma_2}(\boldsymbol{x}_1,\boldsymbol{x}_2)}{dt} = -\frac{i}{\hbar}\left(\tilde{H}_a(\boldsymbol{x}_2) - \tilde{H}_a(\boldsymbol{x}_1)\right) m_{\sigma_1\sigma_2}(\boldsymbol{x}_1,\boldsymbol{x}_2) - \frac{iU_0}{\hbar}\sum_{\sigma_3}\Big(m_{\sigma_1\sigma_3}(\boldsymbol{x}_1,\boldsymbol{x}_2)m_{\sigma_3\sigma_2}(\boldsymbol{x}_2,\boldsymbol{x}_2) + m_{\sigma_1\sigma_2}(\boldsymbol{x}_1,\boldsymbol{x}_2)m_{\sigma_3\sigma_3}(\boldsymbol{x}_2,\boldsymbol{x}_2) - m_{\sigma_3\sigma_2}(\boldsymbol{x}_1,\boldsymbol{x}_2)m_{\sigma_1\sigma_3}(\boldsymbol{x}_1,\boldsymbol{x}_1) - m_{\sigma_3\sigma_3}(\boldsymbol{x}_1,\boldsymbol{x}_1)m_{\sigma_1\sigma_2}(\boldsymbol{x}_1,\boldsymbol{x}_2)\Big). \quad (3.30)$$

It can be trivially seen from Equation 3.30 that since $m_{\sigma_1\sigma_2}(\mathbf{x}_1, \mathbf{x}_2) = 0$ for $\sigma_1 \neq \sigma_2$, the spin off-diagonal does not evolve and remains zero: we will therefore write only the spin diagonal component from here onwards in the form of Equation 3.17. Expanding the sum in Equation 3.30 gives the time evolution for the two non-zero spin components:

$$\frac{dm_{\sigma}(\boldsymbol{x}_1,\boldsymbol{x}_2)}{dt} = -\frac{i}{\hbar}\left(\tilde{H}_a(\boldsymbol{x}_2) - \tilde{H}_a(\boldsymbol{x}_1)\right) m_{\sigma}(\boldsymbol{x}_1,\boldsymbol{x}_2) - \frac{iU_0}{\hbar} m_{\sigma}(\boldsymbol{x}_1,\boldsymbol{x}_2)\left(m_{!\sigma}(\boldsymbol{x}_2,\boldsymbol{x}_2) - m_{!\sigma}(\boldsymbol{x}_1,\boldsymbol{x}_1)\right), \quad (3.31)$$

where:

$$!\,\sigma = \begin{cases} \downarrow, & \text{if } \sigma = \uparrow, \\ \uparrow, & \text{if } \sigma = \downarrow. \end{cases} \quad (3.32)$$

For simulation purposes, it is computationally favourable to evolve the basis functions $\chi_{n,s}(\boldsymbol{x}, t)$ rather than the two-point correlation function, since it is significantly easier to solve N 1D PDEs over a 2D PDE for small to moderate N.

Now that we have the dynamics of the two-point correlation function $m_s(\boldsymbol{x}_1, \boldsymbol{x}_2)$, we may find the corresponding dynamics of the $\chi_{n,\sigma}(\boldsymbol{x})$. Taking inspiration from the GPE (3.1) but accounting for the unique physics of fermions,[9] we construct the following ansatz for the evolution of the $\chi_{n,\sigma}(\boldsymbol{x})$:

$$\boxed{\frac{d\chi_{n,\sigma}(\boldsymbol{x},t)}{dt} = -\frac{i}{\hbar}\left(-\frac{\hbar^2}{2m}\boldsymbol{\nabla}^2_{\boldsymbol{x}} + V(\boldsymbol{x},t)\right)\chi_{n,\sigma}(\boldsymbol{x},t) - \frac{iU_0}{\hbar}\sum_{m\in S}\left|\chi_{m,!\sigma}(\boldsymbol{x},t)\right|^2\chi_{n,\sigma}(\boldsymbol{x},t).} \quad (3.33)$$

One can easily verify that this ansatz is correct by Equation 3.17 with the product rule, substituting in Equation 3.33 and simplifying. This yields Equation 3.31, verifying the ansatz.

We have successfully derived a GPE-like mean field theory for uncorrelated fermions, generalizing the unitary component of the approximation in Ref. [4] to fermions. Throughout the remainder of this thesis, we will refer to Equation 3.33 as the *fermion GPE* (FGPE).

[9] We expect an interaction field summed over the other particles, since we have multiple modes. Fermions with the same internal spin component do not interact by s-wave scattering at all [115], and so we expect the interaction field to be constructed from atoms of the opposite spin component only.

3.2.3 Notable properties of the FGPE

The $\chi_{n,\sigma}(\boldsymbol{x})$ are the single-particle wavefunctions of each fermionic atom. They each experience a potential proportional to the total density of atoms in the opposite spin component - the 'mean field' of our mean-field theory.

The Pauli exlcusion principle manifests itself as orthogonality of single-particle wavefunctions of the same spin component. We must construct creation and annihilation operators from an orthogonal single-particle basis to obtain the correct commutation relations, so the modes included in our Fock state are orthogonal:

$$\int d\boldsymbol{x}\chi^*_{n,\sigma}(\boldsymbol{x})\chi_{m,\sigma}(\boldsymbol{x}) = \delta_{nm}. \tag{3.34}$$

The evolution of $\chi_{n,\sigma}(\boldsymbol{x})$ is inner-product preserving for particles in the same spin component:

$$\begin{aligned}\frac{d}{dt}\int d\boldsymbol{x}\left(\chi^*_{n,\sigma}(\boldsymbol{x},t)\chi_{m,\sigma}(\boldsymbol{x},t)\right) &= \int d\boldsymbol{x}\left(\frac{d\chi^*_{n,\sigma}(\boldsymbol{x},t)}{dt}\chi_{m,\sigma}(\boldsymbol{x},t) + \chi^*_{n,\sigma}(\boldsymbol{x},t)\frac{\chi_{m,\sigma}(\boldsymbol{x},t)}{dt}\right)\\ &= \frac{i\hbar}{2m}\int d\boldsymbol{x}\left(\chi^*_{n,\sigma}(\boldsymbol{x},t)\boldsymbol{\nabla}^2_{\boldsymbol{x}}\chi_{m,\sigma}(\boldsymbol{x},t) - \chi_{m,\sigma}(\boldsymbol{x},t)\boldsymbol{\nabla}^2_{\boldsymbol{x}}\chi^*_{n,\sigma}(\boldsymbol{x},t)\right)\\ &= 0.\end{aligned} \tag{3.35}$$

Hence, Pauli exclusion is maintained; the wavefunctions in a given spin component may never evolve in such a way that they become non-orthogonal.[10]

Unlike the GPE, the FGPE has two free parameters: the particle number N and interaction strength U_0 are independent free parameters. Increasing N for a fixed U_0 will still increase the strength of the mean field experienced by the particles, but not necessarily in an equivalent manner to a proportional increase in U_0 for fixed N. The model also encapsulates the poor scattering properties of fermions; for a given N and U_0, the total effect of scattering is much less for an atomic gas governed by the FGPE than for the GPE. In the case of the GPE, a given atom scatters with every other atom: for the FGPE, a given atom only scatters with *half*[11] the atoms. Furthermore, since the GPE order parameter $\phi(\boldsymbol{x})$ interacts with its own density field, the scattering is greatest where the particle density is highest, maximising the effect. In the case of the FGPE, a given particle's wavefunction interacts with a density field formed by all particles in the opposite spin component. In principle, these could be localised anywhere, and thus the effect is weaker than the bosonic case.

As described in Section 2.2.2, we will frequently consider an effective 1D system of harmonically-trapped atoms with an arbitrary control potential, and so $V(x,t) = \frac{1}{2}m\omega^2x^2 + V_C(x,t)$. Using the dimensionless units for the harmonic oscillator described in Section 2.3.1, and defining a dimensionless interaction strength:

$$\boxed{\Upsilon_0 = \frac{U_0x_0}{\hbar\omega},} \tag{3.36}$$

[10] This constraint does not apply to atoms in different spin components: the interaction term in Equation 3.35 only cancels because particles of the same spin component experience the same mean field.

[11] Assuming an equal number of particles in each spin component, which is an assumption we will use consistently throughout this thesis.

we may rewrite the FGPE in dimensionless form:

$$\frac{d\chi_{n,\sigma}(x,t)}{dt} = -i\left(-\frac{1}{2}\frac{\partial^2}{\partial x^2} + \frac{1}{2}x^2 + V_C(\boldsymbol{x},t)\right)\chi_{n,\sigma}(x,t) - i\Upsilon_0\sum_m |\chi_{m,!\sigma}(x,t)|^2\,\chi_{n,\sigma}(x,t), \tag{3.37}$$

where x is in units of x_0 and t is in units of $t_0 = \omega^{-1}$. We will use this form for our numerical simulations. The exact same nondimensionalisation applies to the GPE (3.1).

3.3 Ground states

In previous studies of feedback cooling, the systems under simulation often failed to reach the ground state, being cooled to *dark states*: states which are not stationary, but the feedback schemes could not cool any further [2]. In Chapter 4, we will show how a different choice of feedback scheme can overcome this limitation. However, to demonstrate that we can always cool to the ground state, and not just some dark state, we must know the ground state energy. This is trivial for both bosons and fermions in the non-interacting case,[12] but the addition of a repulsive pair interaction changes the structure and raises the energy of the ground state in a non-trivial way. In this section, we describe methods to calculate ground states and their energies for the bosonic and fermionic mean-field theories described in Chapter 3.

Our Hamiltonians of interest may be written in the form $\hat{H} = \hat{H}_0 + \hat{U} + \hat{V}_C(t)$, where $\hat{H}_0$ is a single-particle term containing kinetic energy and a (typically harmonic) static trapping potential, $\hat{U}$ is a quartic scattering pair interaction, and $\hat{V}_C(t)$ is a time-dependent control potential. We seek the ground states of the trap itself, and so we always seek to find the state that minimises $E_0 = \left\langle \hat{H}_0 + \hat{U} \right\rangle$.

3.3.1 Mean-field ground states of a BEC: imaginary-time evolution

It is relatively straightforward to compute the ground state of a BEC in the mean-field approximation presented in Section 3.1. This is done by evolution in *imaginary time*.

For intuition, we first consider the linear full quantum field theory. For a system described by Hamiltonian $\hat{H}$ with eigenstates $|\psi_n\rangle$, corresponding eigenenergies E_n and initial state $|\Psi(0)\rangle = \sum_n c_n |\psi_n\rangle$, we could compute the time evolution in the spectral basis as:

$$|\Psi(t)\rangle = \sum_n c_n \exp\left(-\frac{iE_n t}{\hbar}\right)|\psi_n\rangle\,. \tag{3.38}$$

If we instead evolve in imaginary time $\tau = it$, we obtain:

$$|\Psi(\tau)\rangle = \sum_n c_n \exp\left(-\frac{E_n t}{\hbar}\right)|\psi_n\rangle\,. \tag{3.39}$$

Each component decays exponentially, with the higher-energy components decaying faster. This is, of course, not norm-preserving. We thus start with an inital guess of the ground-

[12] In the bosonic case, the ground state consists of all particles in the single-particle ground state: that is, a state of the form $|N, 0, \ldots\rangle$ in the energy eigenbasis. In the fermionic case, it is the 'Fermi sea' described in Section 2.1 - in occupation number notation, a state of the form $|1, 1, \ldots, 1, 0, \ldots\rangle$. For a harmonic trap, the energy can be calculated analytically - see Appendix A.4.

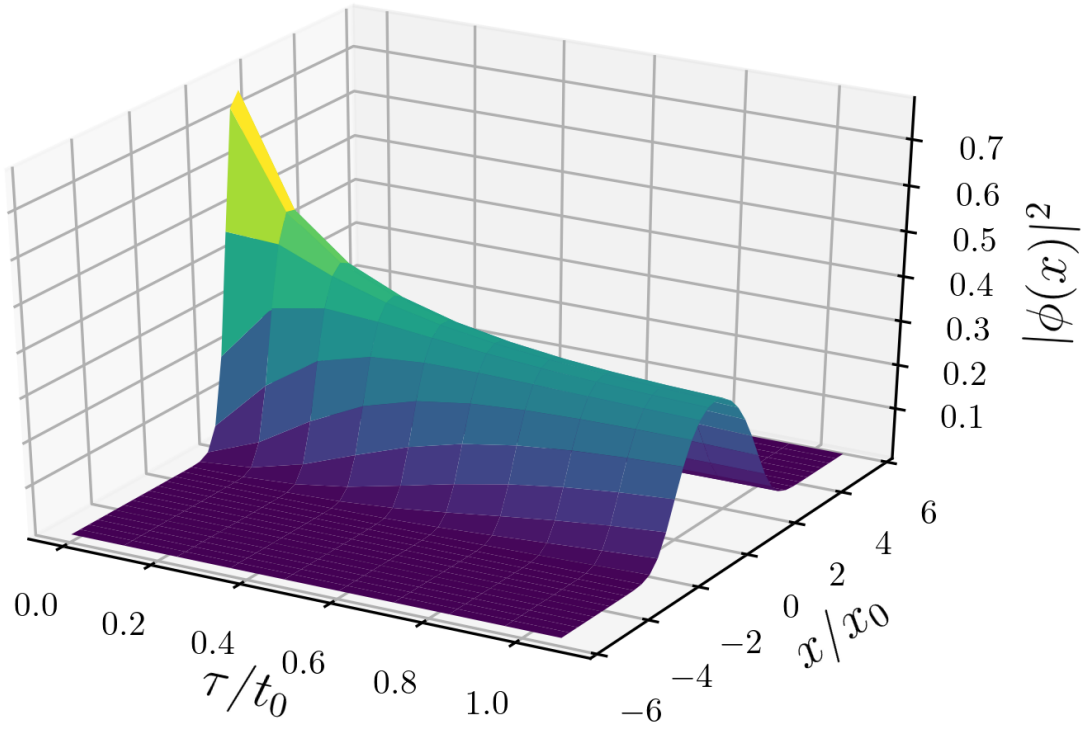

Figure 3.1: Computing the ground state of a harmonically-trapped one-dimensional BEC with $\Upsilon_0 = 10.0$ using the imaginary-time Gross-Pitaevskii equation with continuous renormalisation. All quantities are relative to the natural scales described in Section 2.3.1. The initial guess ($\tau = 0$) is the non-interacting ground state (a Gaussian). The evolution quickly produces the interacting ground state (convergence occurs by $\tau/t_0 \approxeq 1$). The addition of repulsive pair interactions widens the density profile.

state, evolve in imaginary time, and then renormalise the state. For sufficiently long evolution, what remains is approximately the ground state, since the higher-energy components decay away exponentially faster. In practice, the convergence is extremely fast.

Imaginary time evolution also works in the nonlinear problem, though the situation is more complicated. The method is not foolproof, and may converge to a false minimum for sufficiently poor initial guesses. Nonetheless, for a good initial guess it succeeds in finding the ground state. The method can be rigorously derived as a gradient-descent minimisation of energy [116].

Throughout this thesis, whenever a BEC ground state is required, we will start with the non-interacting ground state as an initial guess, and propagate it using the GPE in imaginary time:

$$\frac{d\phi(\boldsymbol{x})}{d\tau} = -\frac{1}{\hbar}\left(-\frac{\hbar^2}{2m}\boldsymbol{\nabla}_{\boldsymbol{x}}^2 + V(\boldsymbol{x}) + U_0|\phi(\boldsymbol{x})|^2\right)\phi(\boldsymbol{x}), \tag{3.40}$$

renormalising the order parameter at each integration time step, and testing the energy for convergence. This propagation will always be done with the XMDS2 package [98]. An example of our renormalised imaginary-time evolution is given in Figure 3.1.

3.3.2 Fermionic ground states: the Hartree-Fock self-consistent field method

It is much harder to find the ground state of an interacting fermionic system. The orthogonality preservation property of the FGPE (3.35) does not hold in imaginary time, and so the GPE ground state algorithm described in Section 3.3.1 evolves the system towards an unphysical state that violates Pauli exclusion. We therefore require another method to compute ground states. In this section, we present a full treatment of the Hartree-Fock *self-consistent field* (SCF) method, which is often used to this end in nuclear physics [117] and quantum chemistry [114] and is used to calculate all interacting fermionic ground states in this thesis. We then follow up with a brief justification of our choice of method.

Optimised variational estimates

Substituting the non-control terms of the Hamiltonian into Equation 3.19, the energy can be calculated from the single-particle wavefunctions:

$$E_0 = \left\langle \hat{H}_0 + \hat{U} \right\rangle = \sum_{n\in S,\sigma} \int d\boldsymbol{x} \Bigg(\chi^*_{n,\sigma}(\boldsymbol{x}) \left(-\frac{\hbar^2}{2m}\boldsymbol{\nabla}^2_{\boldsymbol{x}} + V_0(\boldsymbol{x}) \right) \chi_{n,\sigma}(\boldsymbol{x}) + \frac{U_0}{2} \left|\chi_{n,\sigma}(\boldsymbol{x})\right|^2 \sum_{m\in S} \left|\chi_{m,!\sigma}(\boldsymbol{x})\right|^2 \Bigg). \quad (3.41)$$

To compute ground states, recall the variational theorem: the expectation value of the Hamiltonian of *any* quantum state is bounded below by the ground state energy [28]. We may construct a variational estimate of the ground-state energy in the Hartree-Fock mean field by choosing a set of orthogonal single-particle wavefunctions $\{\chi_{n,s}(\boldsymbol{x})\}$ and substituting these into Equation 3.41. We wish to find the 'best' set of wavefunctions $\{\chi_{n,s}(\boldsymbol{x})\}$ that minimise E_0; these are the basis wavefunctions of our ground state, and substituting them into Equation 3.41 yields our ground state energy. We perform a constrained[13] optimisation of Equation 3.41 using the method of Lagrange multipliers to find states which locally minimise energy. The full calculation for a general system is presented in Ref. [114]. This yields the *Hartree-Fock equations in canonical form*:

$$\tilde{F}_s(\boldsymbol{x})\chi_{n,s}(\boldsymbol{x}) = \epsilon_{n,s}\chi_{n,s}(\boldsymbol{x}), \quad (3.42)$$

where for our system,

$$\tilde{F}_s(\boldsymbol{x}) = \left(-\frac{\hbar^2}{2m}\boldsymbol{\nabla}^2_{\boldsymbol{x}} + V_0(\boldsymbol{x}) + U_0 \sum_{m\in S} \left|\chi_{m,!s}\right|^2 \right). \quad (3.43)$$

The operator $\tilde{F}_s(\boldsymbol{x})\colon L^2(\mathbb{R}^n) \to L^2(\mathbb{R}^n)$ (3.43) is known as the Fock operator. It may be thought of as the Hamiltonian for the single-particle wavefunctions, and thus the Hartree-Fock equations for our system are essentially time-independent Schrödinger equations for the single-particle wavefunctions with a GPE-like nonlinear coupling.[14] This is a major caveat, however: $\tilde{F}_s(\boldsymbol{x})$ is dependent on all wavefunctions of the opposite spin state, which

[13] Subject to the normalisation constraint $\int d\boldsymbol{x} \left|\chi_{n,s}(\boldsymbol{x})\right|^2 = 1$.

[14] The GPE-like form is particular to s-wave scattering as a pair interaction: more general interactions will involve an extra spatial integral to construct the mean field. See Ref. [114] for a full treatment.

form the density-like interaction field. We cannot simply numerically solve Equation 3.42 as we would with a linear uncoupled eigenvalue problem.

The Roothan equations

One may easily verify if a set of wavefunctions $\{\chi_{n,s}(\boldsymbol{x})\}$ corresponds to a stationary state[15] by substituting into the left-hand side of Equation 3.42 and comparing to the right-hand side. If we can construct an iterative method that produces successively better guesses of the $\{\chi_{n,s}(\boldsymbol{x})\}$, we can apply this test to within some tolerance to determine whether it has converged. This is the essence of the Hartree-Fock self-consistent field method; we seek to find a set of wavefunctions that are eigenstates of their own mean field in a self-consistent fashion.

We choose some basis $\{\phi_d(\boldsymbol{x})\}$ of $L^2(\mathbb{R}^n)$. Truncating the basis at some finite dimension D, we rewrite Equation 3.42 in matrix form as [114]:

$$\boldsymbol{F}(\boldsymbol{C})\boldsymbol{C} = \boldsymbol{S}\boldsymbol{C}\boldsymbol{\epsilon}. \tag{3.44}$$

This form is typically known as the *Roothan equations*. Here, $\boldsymbol{C}$ is a $D \times N$ matrix whose columns are the coefficients of each single-particle state in the chosen basis, $\boldsymbol{\epsilon}$ is an $N \times N$ diagonal matrix whose diagonal components are the eigenenergies of these single-particle states, and $\boldsymbol{F}(\boldsymbol{C})$ is a $D \times D$ matrix representation of the Fock operator (written in this form to emphasise that it depends on the state $\boldsymbol{C}$). $\boldsymbol{S}$ is a $D \times D$ matrix of overlaps between the basis functions including an internal spin index, with components:

$$S_{\mu\sigma_1,\nu\sigma_2} = \delta_{\sigma_1\sigma_2} \int d\boldsymbol{x} \phi^*_\mu(\boldsymbol{x})\phi_\nu(\boldsymbol{x}). \tag{3.45}$$

For our purposes this will always be the identity matrix, since we will exclusively use orthonormal bases.[16] The Fock matrix has components of the form:[17]

$$F_{\mu\sigma_1,\nu\sigma_2} = \delta_{\sigma_1\sigma_2} \int d\boldsymbol{x} \phi^*_\mu(\boldsymbol{x})\tilde{F}_{\sigma_1}(\boldsymbol{x})\phi_\nu(\boldsymbol{x}). \tag{3.46}$$

Iterative solution for the self-consistent field

There are iterative procedures that may be used to find a self-consistent field for the ground state. The simplest[18] is the original algorithm proposed by Roothan [119]:

1. Construct a reasonable estimate of the ground state, and thus an initial guess for $\boldsymbol{C}$.
2. Construct $\boldsymbol{F}(\boldsymbol{C})$ for the current guess of $\boldsymbol{C}$.
3. Discard the current guess of $\boldsymbol{C}$, and numerically solve for the eigenvalue decomposition of $\boldsymbol{F}(\boldsymbol{C})$. Take the eigenvectors corresponding to the lowest N eigenvalues;

[15] Typically, this will be the ground state. Due to the way we numerically solve the eigenproblem, it is extremely unlikely that the algorithm would ever converge to an excited eigenstate of the Hamiltonian, especially for a good initial guess.

[16] Basis sets are almost never orthogonal in quantum chemistry, where this formalism originates. We are interested in the behaviour of a harmonically-trapped Fermi gas, so we will use the the Hermite-Gauss basis, which is orthonormal.

[17] We assume spin symmetry, since the algorithm does not converge if the ground state is phase-separated.

[18] Modern applications in quantum chemistry typically use convergence-acceleration algorithms (see [118] for examples), but the Roothan algorithm is more than adequate for our simple system.

these are the columns of the new guess of $\boldsymbol{C}$.

4. Repeat steps 2-3 until the field is self-consistent to within some desired tolerance: that is, some iteration produces approximately the same guess of $\boldsymbol{C}$ as the previous iteration.

Let us denote the iterative step as $I: L^2(\mathbb{R}^n) \times N \to L^2(\mathbb{R}^n) \times N$. We seek to find a fixed point of I. On a sufficiently restricted domain (if the initial guess is good enough), I may define a contractive mapping with respect to some metric, and therefore repeated applications may converge to the fixed point by the Banach fixed-point theorem[19] [120, 121]. The method is not guaranteed to converge, however, and care must be taken to supply the algorithm with a good initial guess.

There are several important details for successful implementation of the Roothan algorithm. In practice, when comparing the state at the nth iteration with that at the $(n-1)$th iteration, we chose to use a relative measure of the energy difference

$$\Delta_{n-1,n} = \frac{|E_{n-1} - E_n|}{E_n} \tag{3.47}$$

as a proxy for state similarity. This may seem risky, as one can easily construct non-identical states with the same energy. It would therefore be tempting to instead use the fidelity:

$$|\langle \Psi_{n-1} | \Psi_n \rangle|^2 , \tag{3.48}$$

since it is an exact measurement of similarity between states that cannot be 'fooled' in such a way. However, computing the overlap of two Slater determinant states is a computationally demanding task [122] that would be impractical to use as part of an iteration loop. We can justify energy as a safe proxy for state similarity by considering the limiting behaviour of the Roothan algorithm. There are only two possible behaviours of the iteration: either it converges, or it oscillates between two states, possibly accompanied by slow drifts of these two states [123]. Therefore, in the case where the algorithm does not converge, the relative energy difference (3.47) will never be vanishingly small, and our approach is safe.

Initial guesses and convergence

As discussed in Section 3.3.2, the Roothan algorithm only converges for a sufficiently good initial guess. Fortunately, for the purposes of this thesis, it is easy to construct a good initial guess. We will always consider a harmonically-trapped one-dimensional Fermi gas, corresponding to the choice $V_0(x) = \frac{1}{2} m\omega^2 x^2$. In the non-interacting case ($U_0 = 0$), Equation 3.42 is just the time-independent Schrödinger equation for a one-dimensional harmonic oscillator, the solution to which is well known. The ground state in this case for N fermions per spin component is just a Fermi sea, with one fermion in each of the first N eigenstates of the harmonic oscillator. For low interaction strengths, we expect the many-body ground state to be a small perturbation to the non-interacting ground state, so the Fermi sea is a sufficiently close initial guess. When we require ground states for higher interaction strengths where the Roothan algorithm does not converge with the Fermi sea as an initial guess, we may 'bootstrap' our way to an acceptable initial guess: use the

[19] This is sometimes known as the Contraction Mapping Theorem. The theorem was originally proven by Banach [120], and a more modern treatment can be found in Ref. [121].

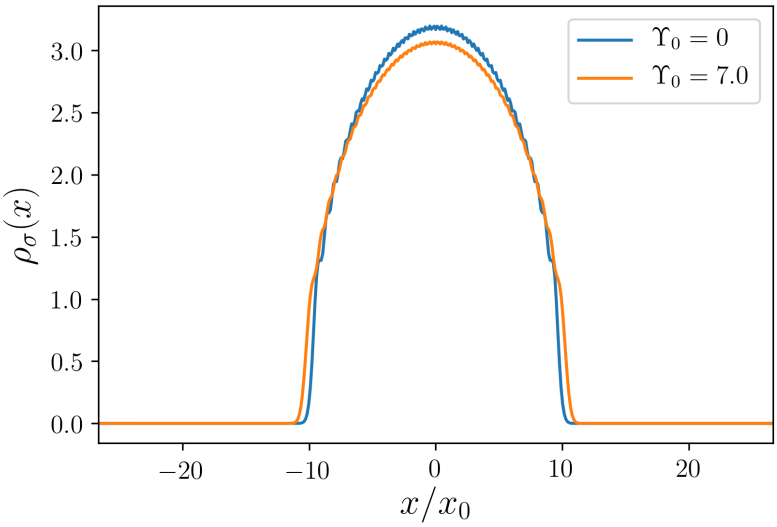

Figure 3.2: The total density per spin component $\rho_\sigma(x) = \sum_{n\in S}|\chi_{n,\sigma}(x)|^2$ for a one-dimensional, harmonically-trapped, spin-symmetric, two-component Fermi gas of 100 particles, in the non-interacting limit ($\Upsilon_0 = 0$) and with moderate interactions ($\Upsilon_0 = 7.0$). Position is given relative to the natural length scale described in Section 2.3.1. The addition of repulsive interactions widens the total density profile slightly, and increases the ground state energy: for $\Upsilon_0 = 0$, the ground state energy is $2500\hbar\omega$, but for $\Upsilon_0 = 7.0$, it is $\sim 3413\hbar\omega$.

Fermi sea as an initial guess for a lower interaction strength, use the resulting weakly interacting ground state as the initial guess for a slightly higher interaction strength, and repeat until one has the ground state at the desired value of Υ_0.

Ground states of the interacting Fermi gas

We now have all the tools to calculate the ground state of an interacting Fermi gas within the Hartree-Fock approximation. Throughout this thesis, whenever a ground state of an interacting Fermi gas is required, we apply the tools described thus far. Qualitatively, at low interaction strengths where the dominant effects are due to kinetic and potential energy, the ground states obtained are extremely similar to the non-interacting case, and are spin-symmetric. The crucial difference is a widening of the state: adding repulsive pair interactions introduces an additional energy cost to localisation, leading to an overall widening of the density profile (Figure 3.2). The widening effect is more extreme for atoms in higher-energy modes, since they have broader density profiles in the non-interacting limit and thus see the lower-energy atoms as a localised perturbing potential at the centre of the trap (Figure 3.3). This results in a modest increase in the total energy of the ground state (for example, the non-interacting ground state of 100 atoms depicted in Figure 3.2 has an energy of $2500\hbar\omega$, while the interacting ground state at $\Upsilon_0 = 7.0$ has an energy of $\sim 3413\hbar\omega$).

The situation is more complicated for large interaction strengths, in the regime where repulsive effects dominate. Two-component atomic gases can be *miscible* (it is relatively favourable for the components to mix spatially) or *immiscible* (it is unfavourable for the components to mix spatially); this is true for Fermi-Fermi mixtures of the type we are

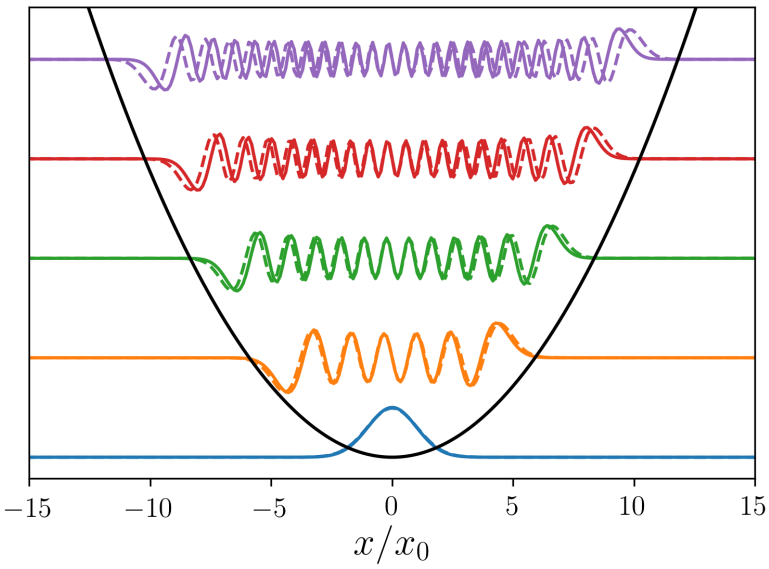

Figure 3.3: Ground-state wavefunctions for $n = 0$, $n = 11$, $n = 23$, $n = 35$, $n = 47$ in the non-interacting limit ($\Upsilon_0 = 0$, solid lines) and with moderate interactions ($\Upsilon_0 = 7.0$, dashed lines) for a one-dimensional, harmonically-trapped, spin-symmetric, two-component Fermi gas of 100 particles in the Hartree-Fock approximation. Position is given relative to the natural length scale described in Section 2.3.1. The harmonic potential is superimposed in black. The addition of repulsive interactions widens the wavefunctions slightly, with this effect being more extreme for higher-order modes.

considering [124] as well as Bose-Fermi mixtures [125, 126]. For sufficiently high interaction strengths, it becomes favourable for the spin components to separate, since there is no s-wave scattering within the same spin component, but there is an enormous energy cost to particles in opposite components occupying the same space. Consequently, the strongly-interacting ground states are no longer spin-symmetric (and may even be highly degenerate). As we increase interaction strength from zero, the ground state will initially be a widened spin-symmetric state (as seen in Figures 3.2 and 3.3); this is the miscible regime. At some threshold interaction strength, spin symmetry becomes energetically unfavourable due to strong inter-component repulsion - beyond this threshold, the spin-symmetry is spontaneously broken, and the ground states are degenerate and have strong spatial separation between spin components. We found that the Roothan algorithm fails to converge beyond this threshold, and so we will be mostly limited to weakly repulsive interactions and the miscible regime in this thesis.

Alternative methods

It is important to justify our choice of method. Finding ground states of interacting fermions is a common problem in condensed matter physics, nuclear physics and quantum chemistry, and several approaches exist. We also considered using the perturbative Green's function method [82], and adiabatic real-time evolution [93].

The Green's function method for calculating expectation values involves a perturbative expansion of the system's full interacting equilibrium Green's function, which can be evaluated to a given order by constructing a set of Feynman diagrams and evaluating

their amplitudes. We will not detail the method here, but an excellent treatment of the zero-temperature version can be found in Chapter 5 of Ref. [82]. This approach includes the full effect of quantum correlations and provides a single expression that can be re-evaluated for various parameters. However, it does not produce the state vector for the ground state, but only the ground state energy. Furthermore, the first-order correction for our system is zero (see Appendix A.3 for the calculation), and so a much more involved calculation is required to successfully apply the method.

In contrast to the Green's function method, the Hartree-Fock SCF method we have elected to use is advantageous for a number of reasons. It is completely self-consistent with the approximation used to derive the FGPE, and so we can be confident that the ground state energy produced by a successful application of the method will be exactly the same as that of the ground state in our simulation. We do not actually want to model the full quantum correlations, since we want a reference value with which to compare an uncorrelated dynamical approximation. Furthermore, it produces the single-particle-like wavefunctions $\chi_{n,s}(\boldsymbol{x}, t)$ for the ground state, a tool we will use often. It is computationally cheap and based on a simple iteration that can easily be implemented on a computer.

Adiabatic real-time evolution also produces ground states that are self-consistent with our mean-field theory. It involves initializing the system in a known ground state of the non-interacting system (in our case, the Fermi sea of a harmonic oscillator), and slowly turning on interactions. By the adiabatic theorem [93], if the evolution is slow with respect to the natural timescales of the system, the evolved state will approximately remain in the ground state of the evolved Hamiltonian. In principle, this would produce the same ground states as the Hartree-Fock SCF method, but we found it to be too computationally expensive in practice - the Roothan algorithm produces the same output with far less computational resources. However, this can produce ground states that are self-consistent with *any* dynamical approximation, and should be considered for future works that model higher-order quantum field effects.

3.4 Summary of mean-field theory

This chapter has reviewed existing techniques for mean-field dynamics of BECs, and generalised them to derive a mean-field description of multimode atomic Fermi gases. Using state approximations that neglect quantum correlations (coherent state and Fock state), we derived the GPE (3.1) for BECs, by which we can simulate the unitary dynamics of a BEC under feedback control. Using a Fock state approximation, we derived an equivalent mean-field equation of motion for Fermi gases (Equation 3.33, which we dubbed the FGPE), which describes uncorrelated fermions with single-particle-like wavefunctions interacting with a density field formed by atoms of the opposite spin. This enables us to simulate the unitary dynamics of a Fermi gas under feedback control, which is the focus of Chapter 4. We then described algorithms which could be used to find the ground states of these mean-field theories - imaginary-time evolution for bosons, and the Roothan algorithm (Hartree-Fock SCF) for fermions. This provides us with the tools to simulate feedback control of interacting quantum gases in the no-measurement and mean-field limits, and benchmark successful cooling by comparing to the ground state.

Feedback cooling without measurement effects

We have now developed the tools for a simple description of feedback cooling. Recall from Section 2.2.2 that our cold-atom Hamiltonian for bosons or fermions (2.22) could be written as:

$$\hat{H} = \sum_{\sigma} \int d\boldsymbol{x} \hat{\psi}_{\sigma}^{\dagger}(\boldsymbol{x}) \left(-\frac{\hbar^2}{2m} \boldsymbol{\nabla}_{\boldsymbol{x}}^2 + V(\boldsymbol{x}, t) \right) \hat{\psi}_{\sigma}(\boldsymbol{x}) + \frac{U_0}{2} \sum_{\sigma\sigma'} \int d\boldsymbol{x} \hat{\psi}_{\sigma}^{\dagger}(\boldsymbol{x}) \hat{\psi}_{\sigma'}^{\dagger}(\boldsymbol{x}) \hat{\psi}_{\sigma'}(\boldsymbol{x}) \hat{\psi}_{\sigma}(\boldsymbol{x}), \tag{4.1}$$

where $V(\boldsymbol{x}, t)$ is an arbitrary time-dependent potential. We will now separate this out as $V(\boldsymbol{x}, t) = V_0(\boldsymbol{x}) + V_C(\boldsymbol{x}, t)$, where $V_0(\boldsymbol{x})$ is a time-independent trapping potential, and $V_C(\boldsymbol{x}, t)$ is the *control potential* - a time-dependent perturbation that we may use to influence the system's dynamics. In an experimental setting, it is possible to create arbitrary optical potentials at high resolution and bandwidth using digital-micromirror devices [47], and so we will assume throughout this thesis that $V_C(\boldsymbol{x}, t)$ can be arbitrarily be varied by the experimenter in real time. We will thus often write our Hamiltonian in the form:

$$\hat{H} = \hat{H}_0 + \hat{U} + \hat{V}_C(t), \tag{4.2}$$

where:

$$\begin{aligned} \hat{H}_0 &= \sum_{\sigma} \int d\boldsymbol{x} \hat{\psi}_{\sigma}^{\dagger}(\boldsymbol{x}) \left(-\frac{\hbar^2}{2m} \boldsymbol{\nabla}_{\boldsymbol{x}}^2 + V_0(\boldsymbol{x}) \right) \hat{\psi}_{\sigma}(\boldsymbol{x}), \\ \hat{U} &= \frac{U_0}{2} \sum_{\sigma\sigma'} \int d\boldsymbol{x} \hat{\psi}_{\sigma}^{\dagger}(\boldsymbol{x}) \hat{\psi}_{\sigma'}^{\dagger}(\boldsymbol{x}) \hat{\psi}_{\sigma'}(\boldsymbol{x}) \hat{\psi}_{\sigma}(\boldsymbol{x}), \\ \hat{V}_C(t) &= \sum_{\sigma} \int d\boldsymbol{x} \hat{\psi}_{\sigma}^{\dagger}(\boldsymbol{x}) V_C(\boldsymbol{x}, t) \hat{\psi}_{\sigma}(\boldsymbol{x}). \end{aligned} \tag{4.3}$$

Therefore, $\hat{H}_0$ is a time-independent, single-particle Hamiltonian describing kinetic energy and trapping (for our numerical simulations, it will always be the harmonic oscillator Hamiltonian and thus analytically solvable), $\hat{U}$ describes two-body atom-atom interactions, and $\hat{V}_C(t)$ describes a time-dependent control potential applied to the system.

In this chapter, we assume that we have perfect knowledge of the system observables, and investigate how a judicious choice of the form and dynamics of the control poten-

tial $V_C(\boldsymbol{x}, t)$ can be used to remove energy and therefore cool the system. This treatment neglects the effect of measurement backaction, which as we will show in Chapters 5 and 6, does have a significant effect. Nonetheless, investigating the no-measurement limit illustrates the best-case behaviour of feedback cooling. This will be done using the mean-field and numerical simulation techniques presented in Chapter 3. The absence of measurement effects and many-particle quantum correlations allow for rapid prototyping of measurement-independent properties, such as the best choice of control potential.

This chapter is structured as follows. In Section 4.1, we will briefly discuss the approach and results of a similar study for BECs by Haine *et al.* [2], and compare two choices of $V_C(\boldsymbol{x}, t)$. In Section 4.2, we will prove that both choices of control remove energy from appropriate states, and discuss the implications of this. We motivate our simulations of the GPE (3.1) and FGPE (3.33) under feedback control in Section 4.3. In Section 4.4, we simulate an atomic Fermi gas under the 'moment control' used in previous studies [2–4]. We then compare this to the new 'energy-damping control' in Section 4.5. We find that the key physics of feedback-controlled fermions is captured by a two-fermion model, which we simulate and discuss in Section 4.6. We briefly discuss single-component Fermi gases in Section 4.7. Finally, in Section 4.8, we summarise the chapter's results in the context of the key questions posed in Section 4.3.

4.1 Previous work and control choice

Feedback cooling of atomic gases was first studied in a mean-field, no-measurement limit by Haine *et al.* [2], who simulated the dynamics of a feedback-controlled BEC using the Gross-Pitaevskii equation (3.1). They considered a control potential of the form:

$$V_C(\boldsymbol{x}, t) = \sum_n a_n(t) f_n(\boldsymbol{x}), \tag{4.4}$$

where the $f_n(\boldsymbol{x})$ may be any set of spatial functions. We will refer to this as the *moment control*. They considered an effective 1D condensate for which the trap position and strength could be changed, and thus had spatial functions $f_1(x) = x$, $f_2(x) = x^2$, and $f_n(x) = 0$ for $n > 2$. This study was conducted in 2004, when optical trap technology was significantly less advanced - the control was chosen for its ease of experimental implementation, since it only requires one to change the position and strength of the trap. In the intervening years, there have been major developments in trap technology, and it is now possible to create high-bandwidth, high-resolution optical potentials of arbitrary shape using digital-micromirror devices [47]. This control scheme was used in subsequent studies including measurement effects [3, 4]. When applied to a BEC, it damps oscillations in $\langle \hat{x} \rangle$ and $\langle \hat{x}^2 \rangle$ very efficiently, hence the name 'moment control'. However, it does not directly remove oscillations in the higher-order moments of atomic density, and relies upon the condensate's nonlinear interactions to slowly couple oscillations into the controllable moments. Haine *et al.* found that this limited the effectiveness of the control scheme, and the system often entered *dark states*: states which are not eigenstates of the Hamiltonian, but nonetheless cannot be further cooled. This limitation is in principle even more significant for fermions due to their poor scattering properties, and a different control scheme is required.

We will compare this to a different choice of control potential, which we will refer to as

the *energy-damping control*. The potential is given as:

$$V_C(\boldsymbol{x},t) = -k_{\mathrm{ED}}\boldsymbol{\nabla}_{\boldsymbol{x}}\cdot\left\langle\hat{\boldsymbol{j}}(\boldsymbol{x})\right\rangle, \tag{4.5}$$

where $k_{\mathrm{ED}} > 0$ is a constant that may alter the effectiveness of the feedback, and $\hat{j}(x)$ is the particle current:

$$\hat{\boldsymbol{j}}(\boldsymbol{x}) = \frac{\hbar}{2mi}\sum_{\sigma}\left[\hat{\psi}^{\dagger}_{\sigma}(\boldsymbol{x})\Big(\boldsymbol{\nabla}_{\boldsymbol{x}}\psi_{\sigma}(\boldsymbol{x})\Big) - \Big(\boldsymbol{\nabla}_{\boldsymbol{x}}\hat{\psi}^{\dagger}_{\sigma}(\boldsymbol{x})\Big)\hat{\psi}_{\sigma}(\boldsymbol{x})\right]. \tag{4.6}$$

This control potential is inspired by the energy-damping term of the simple-growth projective Gross-Pitaevskii equation (SPGPE) (see Ref. [127]). The details of the SPGPE are irrelevant to this thesis, and it is merely sufficient to note that the functional form is known to efficiently remove energy from a single-spatial-mode BEC.

4.2 Why feedback works

We are interesting in minimising the system's energy in the absence of feedback, and so we will define its energy as:[1]

$$E_0 = \left\langle\hat{H}_0 + \hat{U}\right\rangle. \tag{4.7}$$

Combining this definition with the Heisenberg equation of motion (2.24), we obtain:

$$\begin{aligned}\frac{dE_0}{dt} &= -\frac{i}{\hbar}\left\langle\left[\hat{H}_0+\hat{U},\hat{H}\right]\right\rangle\\ &= \frac{i}{\hbar}\left\langle\left[\hat{H}_0+\hat{U}+\hat{V}_C(t),\hat{H}_0+\hat{U}\right]\right\rangle\\ &= \frac{i}{\hbar}\left\langle\left[\hat{V}_C(t),\hat{H}\right]\right\rangle\\ &= \frac{i}{\hbar}\left\langle\left[\sum_j\int d\boldsymbol{x}\hat{\psi}^{\dagger}_j(\boldsymbol{x})V_C(\boldsymbol{x},t)\hat{\psi}_j(\boldsymbol{x}),\hat{H}\right]\right\rangle.\end{aligned} \tag{4.8}$$

Substituting the moment control (4.4) and using linearity, we obtain:

$$\begin{aligned}\frac{dE_0}{dt} &= \frac{i}{\hbar}\sum_n a_n(t)\left\langle\left[\sum_j\int d\boldsymbol{x}\hat{\psi}^{\dagger}_j(\boldsymbol{x})f_n(\boldsymbol{x})\hat{\psi}_j(\boldsymbol{x}),\hat{H}\right]\right\rangle\\ &= -\sum_n a_n(t)\frac{d\left\langle f_n(\boldsymbol{x})\right\rangle}{dt}.\end{aligned} \tag{4.9}$$

It is immediately clear from Equation 4.9 that choosing $a_n(t) = c_n\left(d\left\langle f_n(\boldsymbol{x})/dt\right\rangle\right)$ gives $\frac{dE_0}{dt}\leq 0$, meaning that energy is non-increasing for this feedback scheme, and furthermore that energy is strictly decreasing when there are oscillations in a controlled moment of the system. Hence, this choice of control removes energy from the system, unless it is in a 'dark state' with no fluctuations in the $\langle f_n(\boldsymbol{x})\rangle$. The fluctuations $d\left\langle f_n(\boldsymbol{x})\right\rangle/dt$ are the

[1] The quantity $\left\langle\hat{H}_0+\hat{U}+\hat{V}_C(t)\right\rangle$ is not important, since we will switch off the feedback once we have cooled the system, and minimising it does not minimise E_0 in general. One could make this quantity instantaneously very small by simply making $\hat{V}_C(t)$ very negative, but this would achieve nothing.

error signals of this control: they are a measurable quantity that, when nonzero, provide information that can be used to cool the system.

A similar result can be shown for the energy-damping control. First, we note the continuity equation [128]:

$$-\boldsymbol{\nabla}_{\boldsymbol{x}} \cdot \left\langle \hat{\boldsymbol{j}}(\boldsymbol{x}) \right\rangle = \frac{d \langle \hat{\rho}(\boldsymbol{x}) \rangle}{dt} = \frac{d \left\langle \sum_j \hat{\psi}_j^\dagger(\boldsymbol{x}) \hat{\psi}_j(\boldsymbol{x}) \right\rangle}{dt}. \tag{4.10}$$

If we substitute the energy-damping control (4.5) into Equation 4.8, and apply linearity and the continuity equation, we obtain:

$$\begin{aligned} \frac{dE_0}{dt} &= \frac{i}{\hbar} \left\langle \left[\sum_j \int d\boldsymbol{x} \hat{\psi}_j^\dagger(\boldsymbol{x}) \left(-k_{\mathrm{ED}} \boldsymbol{\nabla}_{\boldsymbol{x}} \cdot \left\langle \hat{\boldsymbol{j}}(\boldsymbol{x}) \right\rangle \right) \hat{\psi}_j(\boldsymbol{x}), \hat{H} \right] \right\rangle \\ &= k_{\mathrm{ED}} \frac{i}{\hbar} \int d\boldsymbol{x} \left(\frac{d \langle \hat{\rho}(\boldsymbol{x}) \rangle}{dt} \right) \left[\sum_j \hat{\psi}_j^\dagger(\boldsymbol{x}) \hat{\psi}(\boldsymbol{x}), \hat{H} \right] \\ &= -k_{\mathrm{ED}} \int d\boldsymbol{x} \left(\frac{d \langle \hat{\rho}(\boldsymbol{x}) \rangle}{dt} \right)^2 \leq 0. \end{aligned} \tag{4.11}$$

Clearly, the energy is also non-increasing for this control, and is strictly decreasing as long as there are fluctuations in the atomic density. The density fluctuations at each position $d \langle \hat{\rho}(x) \rangle / dt$ are the error signals of this control. Hence, the energy-damping control can cool from the dark states of the moment control seen in Ref. [2], since it can in principle cool any state with density fluctuations. In fact, for a single spatial mode with linear evolution (such as a BEC or single atom) in a 1D harmonic trap, it can cool from any state that is not an eigenstate of the Hamiltonian, since all superpositions have density fluctuations (see Appendix A.5 for a proof), and thus it provably has no dark states in this case. It appears that the energy-damping control resolves the limitations of the moment control, which we will investigate in our simulations.

These two proofs do not rely upon (anti)commutation relations, and thus both controls work for both Bose and Fermi gases. Furthermore, they do not rely upon any particular state approximation or mean-field theory. We will use the mean-field techniques of Chapter 3 to numerically simulate these controls. However, since these proofs apply to any atomic gas,[2] these controls may be effective for more complex systems beyond the scope of this thesis, including strongly correlated atomic gases, 'hot' Bose gases above the critical temperature T_c, and atomic gases with attractive interactions.

4.3 Aims of numerical simulation

The remainder of this chapter is dedicated to numerically simulating the mean-field atomic dynamics under the influence of these two controls. We will conduct extensive simulations of Fermi gases using the FGPE (3.33), and a small number of BEC simulations using the GPE (3.1) for comparison. We will use the XMDS2 open-source software package [98] to numerically solve all PDEs in this chapter. All simulations will be conducted in an

[2] Assuming energy scales well below the first ionisation energy, such that we may safely consider each atom to be a self-contained particle. It is not necessary to approximate scattering solely as s-wave, since all orders of scattering are diagonal in the position basis, and thus commute with $\hat{V}_C(t)$.

effective 1D harmonically-trapped system (see Section 2.2.2), with trapping potential:

$$V_0(x) = \frac{1}{2}m\omega^2 x^2. \tag{4.12}$$

Thus, all quantities in this chapter are given in the natural units of the harmonic oscillator described in Section 2.3.1. Unless stated otherwise, all times are given in units of the trapping period $t_0 = \omega^{-1}$, all positions are given in units of $x_0 = \sqrt{\hbar/m\omega}$, all energies are in units of $\hbar\omega$ (the energy quantum of the harmonic oscillator), and all interaction strengths are given in the dimensionless form Υ_0 (3.36).

By numerically simulating feedback control in the absence of measurement backaction, we seek to answer the following questions:

- Can the new 'energy-damping control' overcome the limitations of the 'moment control' used in Refs. [2–4]?
- Do the results for BECs obtained in Haine *et al.* [2] generalise to Fermi gases?
- Are there any fundamental differences between cooling Bose gases and Fermi gases?
- Can we directly cool a large number of fermions effectively?

The higher-order Hermite-Gauss modes (2.27) are extremely oscillatory, and thus representing many Pauli-excluded fermions in x-space requires a prohibitively large number of grid points. Consequently, most simulations in this chapter are conducted in the Hermite-Gauss basis (using the exact quadrature methods of Section 2.3.3), to enable scaling up to large particle number. The BEC simulations (Section 4.5.1) and the two-fermion model (Section 4.6) are conducted in the position basis using Fourier methods (as discussed in Section 2.3.2).

We will frequently compare the *excitation energy per particle*:

$$\frac{\Delta E}{N} = \frac{E_0(t) - E_g}{N}, \tag{4.13}$$

where E_g is the ground state energy. The ground state energy of many non-interacting atoms in a harmonic trap can be calculated analytically (Appendix A.4), and for interacting systems, we calculate the ground state energy numerically using the methods of Section 3.3. This quantity approaches zero as the system approaches its ground state, and allows a fair comparison of systems with different N.

4.4 Simulation of the moment control

We are now equipped to numerically simulate feedback control of an atomic Fermi gas up to a relatively large number of particles (∼400 atoms). We will initially consider application of the moment control to a one-dimensional Fermi gas of 100 atoms (50 per spin state). For our initial state, we use the ground-state for $\Upsilon_0 = 1.0$ (slightly widened compared to the non-interacting case), displaced[3] by $10x_0$. This is similar to the initial states used in

[3]This is slightly challenging to construct in the Hermite-Gauss basis: the quadrature points are not evenly spaced, and the integral $c'_n = \sum_m c_m \int dx \phi^*_n(x)\phi_m(x+L)$ cannot accurately be computed for large D with equally spaced grid points nor with Hermite-Gaussian quadrature. Instead, we use the Roothan algorithm and add a term to the Fock operator such that the trap centre is shifted, causing the ground

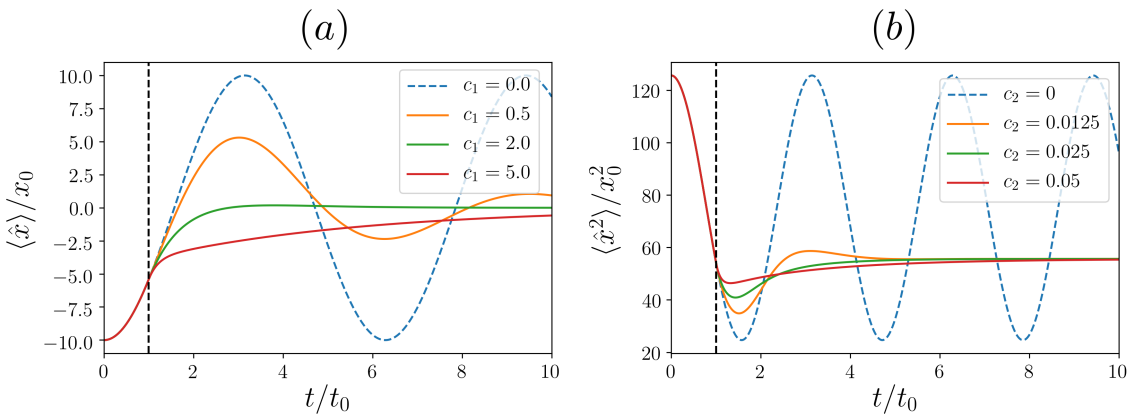

Figure 4.1: Oscillations in the first two moments of atomic density (a) $\langle\hat{x}\rangle$ and (b) $\langle\hat{x}^2\rangle$ for a non-interacting, two-component, 100-atom Fermi gas, across a range of control parameters. Feedback is switched on at $t/t_0 = 1.0$, denoted by the vertical black dashed line. Optimal control occurs in the case of critical damping, and the scheme is slower for an underdamped or overdamped control.

studies of BEC feedback control [2–4].

We will follow the example of Haine *et al.* [2] and consider linear and quadratic feedback of the form:

$$V_C(x,t) = \left(c_1 \frac{d\langle\hat{x}\rangle}{dt}\right) x + \left(c_2 \frac{d\langle\hat{x}^2\rangle}{dt}\right) x^2, \tag{4.14}$$

corresponding to the choice $f_1(x) = x$, $f_2(x) = x^2$, and $f_n(x) = 0$ for $n > 2$ in Equation 4.4, and the appropriate time-dependent coefficients to decrease energy. We now consider how to select values of feedback strength c_1 and c_2 that optimise this control. By Ehrenfest's theorem [28] we find that:[4]

$$\frac{d^2\langle\hat{x}\rangle}{dt^2} = -\left\langle\frac{\partial V(x,t)}{\partial x}\right\rangle = -\left(1 + 2c_2\frac{d\langle\hat{x}^2\rangle}{dt}\right)\langle x\rangle - c_1\frac{d\langle\hat{x}\rangle}{dt}. \tag{4.15}$$

This is the equation of motion for a damped, coupled classical harmonic oscillator (uncoupled when $c_2 = 0$). In the uncoupled limit, setting $c_1 = 2.0$ leads to critical damping, causing the fastest removal of energy. One must choose parameters carefully: overdamped and underdamped controls are slower at removing energy from the system.

A simple expression for the motion of $\langle\hat{x}^2\rangle$ does not exist [2], so we independently optimised for c_2 numerically, finding that $c_2 = 0.025$ was close to critical damping. A comparison of feedback strengths on each moment is presented in Figure 4.1.

Due to the coupling between the first and second moment (apparent in Equation 4.15), the exact optimal combination of parameters may depend on the initial state. However, the choice $c_1 = 2.0$, $c_2 = 0.025$ is in practice always close to optimal. It is highly effective and rapidly removes all oscillations in the first and second moments of atomic density within a few oscillator cycles. For this particular initial state (a displaced, slightly widened ground

state finder to converge to the desired initial state.

[4] See Sakurai [28] for a version of the proof that holds for a general many-body system.

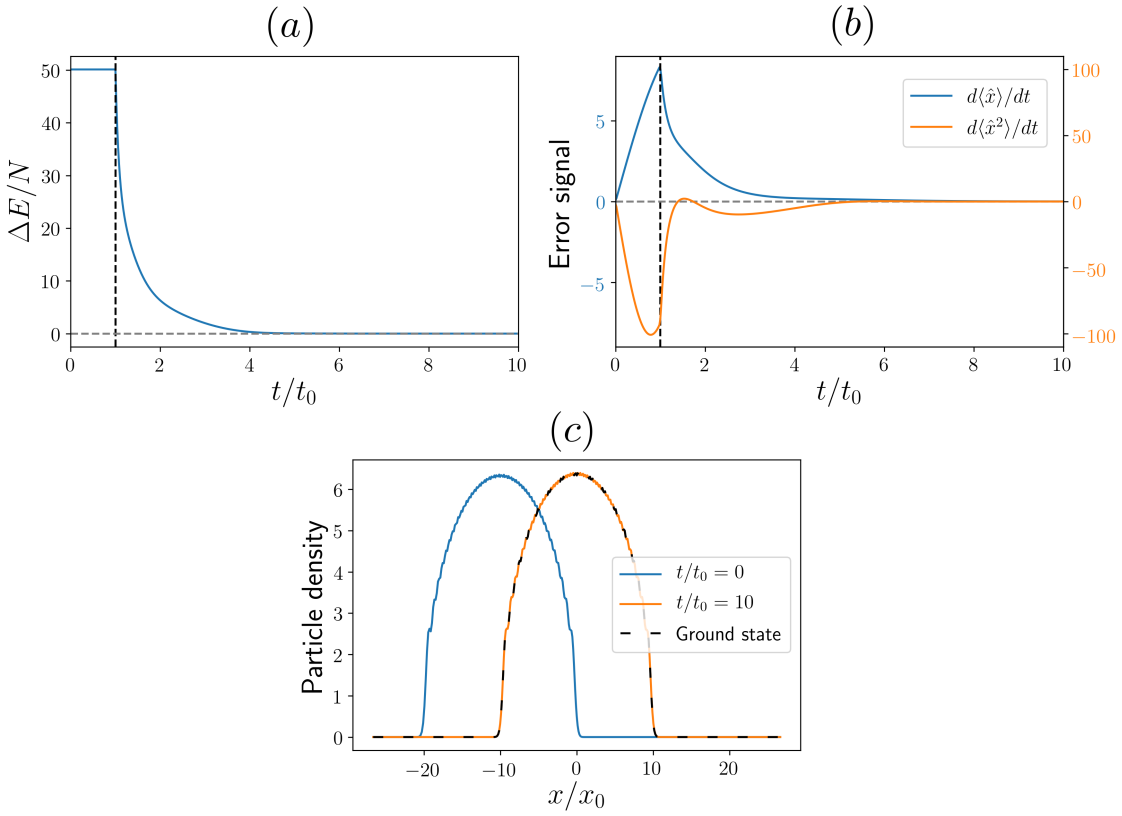

Figure 4.2: Successfully cooling a non-interacting, two-component, 100-atom Fermi gas from a displaced, widened ground state using the moment control for $c_1 = 2.0$, $c_2 = 0.025$. We have plotted (a) the excitation energy per particle, (b) the error signals in the first two moments of atomic density and (c) the initial, final and ground state density profiles. Feedback is switched on at $t/t_0 = 1.0$, corresponding to the vertical black dotted line. The system approaches the ground state (horizontal grey dotted line), and the error signals vanish. All quantities are in the harmonic oscillator units of Section 2.3.1.

state), the moment control is successful in cooling close to the ground state (Figure 4.2).

However, this initial state is biased towards being easily cooled by the moment control, since almost all of its energy corresponds to oscillations in $\langle\hat{x}\rangle$ and $\langle\hat{x}^2\rangle$. The moment control fails to be effective for more general initial states. We constructed a 'random' initial state for a 100-atom Fermi gas by randomly populating Hermite-Gauss modes, subject to an exponential windowing and orthogonality constraints to ensure Pauli exclusion (Figure 4.3c). This initial state is spin-asymmetric. The moment control is only able to remove a tiny fraction of the system's energy: it hits a dark state with no oscillations in $\langle\hat{x}\rangle$ or $\langle\hat{x}^2\rangle$, but significant oscillations in other moments of atomic density. Although we can use the nonlinear interatomic scattering interactions to couple oscillations into the controllable moments as Haine *et al.* did for BECs [2], this is still ineffective for fermions. We have provided plots of the energy, error signals, initial state, and density profiles for an example of the moment control failing to cool such an initial state in both the interacting ($\Upsilon_0 = 1.0$) and non-interacting cases (Figure 4.3). To cool complicated initial states, we will need to look beyond the moment control.

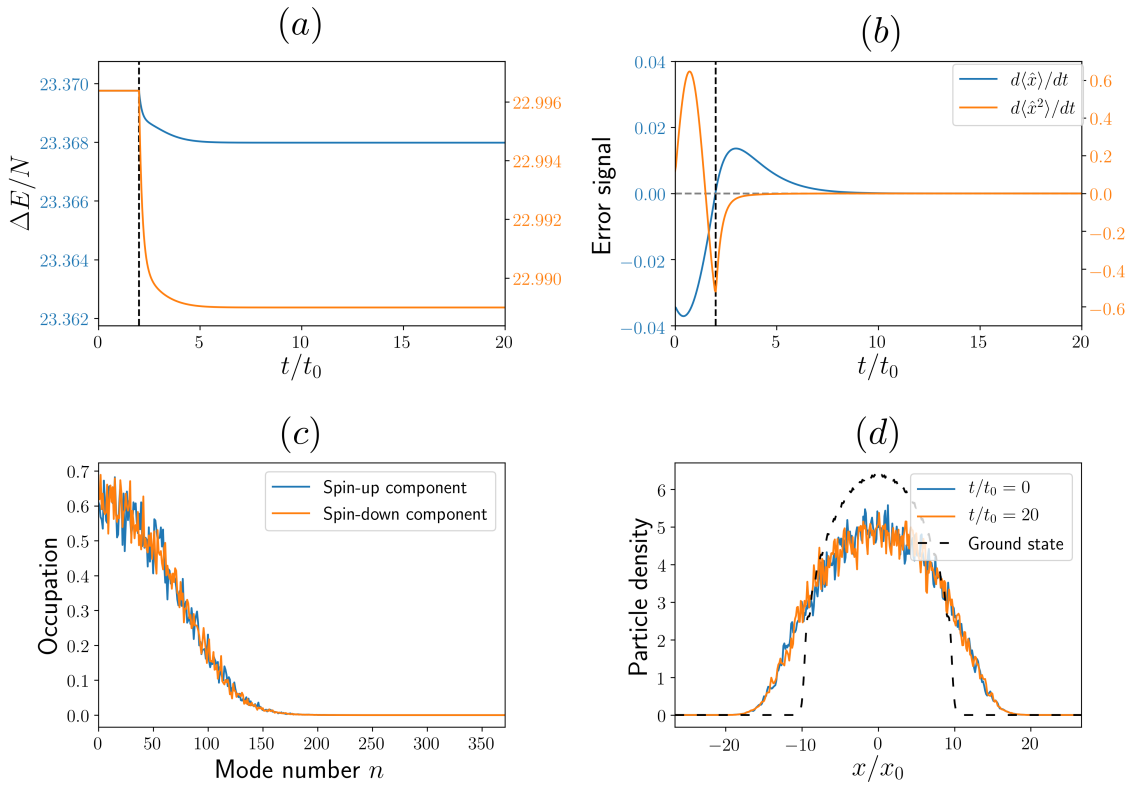

Figure 4.3: Unsuccessful attempt at cooling a two-component, 100-atom Fermi gas from a complicated initial state using the moment control for $c_1 = 2.0$, $c_2 = 0.025$ in both the interacting ($\Upsilon_0 = 1.0$) and non-interacting cases. Feedback is switched on at $t/t_0 = 2.0$. We have plotted (a) the excitation energy per particle, with both y-axes on the same scale, (b) the error signals in the first two moments of atomic density, (c) the initial mode occupation in the energy eigenbasis and (d) the initial, final and ground state density profiles. The control is only able to remove a miniscule fraction of the excitation energy, and the error signals vanish even though the system is far from the ground state. With interactions on, the cooling is better but still extremely ineffective. All quantities are in the harmonic oscillator units of Section 2.3.1.

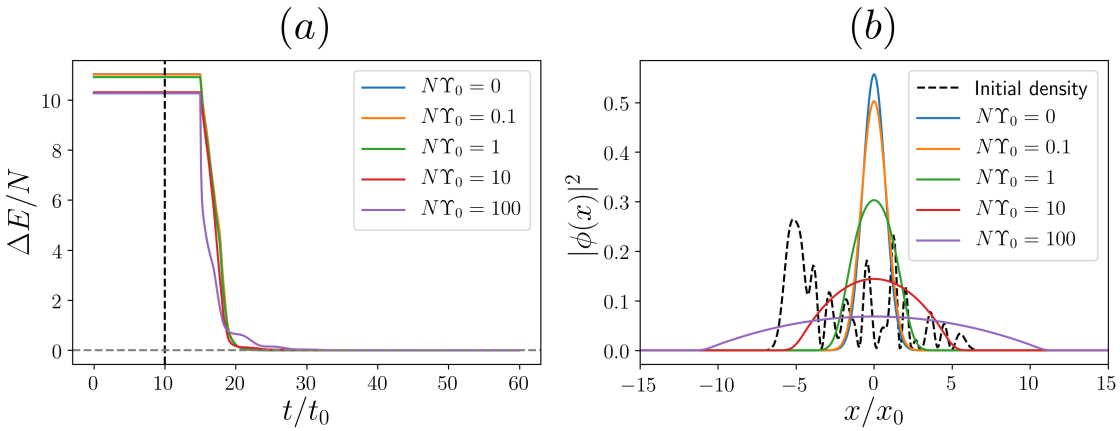

Figure 4.4: Successfully cooling a BEC from a complicated initial state with the energy-damping control across a range of interaction strengths. Feedback is switched on at $t/t_0 = 10.0$. We have plotted (a) the excitation energy per particle and (b) the density profile of the initial state and ground states at each simulated interaction strength. The cooling is extremely efficient, rapidly bringing the system to its ground state within tens of oscillator cycles. All quantities are in the harmonic oscillator units of Section 2.3.1.

4.5 Simulation of the energy-damping control

4.5.1 Energy-damping control of a BEC

As noted in Section 4.1, the energy-damping control is inspired by the energy-damping term of the SPGPE [127], which is known to efficiently remove energy from a single-mode BEC. Since it has not been presented in any published works, we simulated feedback cooling with the energy-damping control for a BEC. We constructed a complicated initial state by randomly populating the first 20 Hermite-Gauss modes, and found that it is extremely efficient in cooling to the ground state for a wide range of interaction strengths (Figure 4.4).

For a given initial state and parameter choice, there is an optimal value of feedback strength k_{ED} which removes energy the fastest. This depends on the initial state, but the control is not particularly sensitive to small variations in k_{ED}, and any value of k_{ED} around the right order of magnitude works extremely well. As discussed in Section 3.1.2, the dynamics depend only on the value of NU_0. However, we can show analytically that the optimal value of k_{ED} depends solely on N. Expanding our choice of potential in the GPE (3.1) yields:

$$\underbrace{i\hbar\frac{d\phi(x)}{dt}}_{\sim\sqrt{N}} = \underbrace{-\frac{\hbar^2}{2m}\frac{\partial^2\phi(x)}{\partial x^2}}_{\sim\sqrt{N}} + \underbrace{\frac{1}{2}m\omega^2x^2\phi(x)}_{\sim\sqrt{N}} + \underbrace{k_{\mathrm{ED}}\frac{d\left(|\phi(x)|^2\right)}{dt}\phi(x)}_{\sim N\sqrt{N}} + \underbrace{U_0\left|\phi(x)\right|^2\phi(x)}_{\sim NU_0\sqrt{N}}. \quad (4.16)$$

To preserve identical dynamics as we change the expected number of particles N, we would require all terms of Equation 4.16 to scale by the exact same factor when N is changed. The time-derivative, kinetic and potential terms scale proportionally to $\sqrt{N}$, and as discussed in Section 3.1.2, so does the interaction term as long as we also scale U_0 proportionally to $1/N$ (thus making NU_0 the only free parameter). The control term, however, is proportional to

$N\sqrt{N}$. Therefore, when changing particle number, we must also scale k_{ED} proportionally to $1/N$ to obtain identical dynamics and thus preserve optimal control.

4.5.2 Energy-damping control of a Fermi gas

We now turn our attention to the Fermi gas, and investigate whether the energy-damping control is actually successful in cooling it. Although the energy-damping control is extremely efficient in cooling a single spatial mode such as a BEC, there is no guarantee it will be as effective for multiple spatial modes sharing the same control potential (such as the many orthogonal wavefunctions $\chi_{n,s}(x)$ for a Fermi gas). Unlike the single-mode case, the total particle density is now a sum over the densities of many individual particles, and so fluctuations in density may cancel out.

Despite this, the energy-damping control is successful in cooling the initial state that the moment control failed to cool (Figure 4.3c). As depicted in Figure 4.5, with no scattering interactions it succeeds in removing a majority of the energy, but cools to a dark state, with a non-negligible excitation energy above the ground state ($\sim$5.47$\hbar\omega$ per particle). Although dark states do not exist in the case of a single spatial mode with linear evolution, we have shown the existence of dark states in the many-fermion case. Much like the moment control of a BEC in Ref. [2], the addition of scattering interactions ($\Upsilon_0 = 1.0$) provides a coupling which perturbs the system from the dark state, allowing cooling arbitrarily close to the ground state. However, this cooling is much slower. While the energy-damping control was able to cool a BEC extremely close to its ground state within 30 harmonic oscillator periods (Figure 4.4), an optimised energy-damping control for a Fermi gas takes hundreds of harmonic oscillator cycles to achieve the same result. Regardless, this suggests that interactions play an important role in cooling a Fermi gas with the energy-damping control.

We are particularly interested in how the method's effectiveness scales with particle number, so it is important to consider how the optimal value of k_{ED} should scale with N. As discussed in Section 4.5.1, to maintain optimal control of a BEC, we require $k_{\mathrm{ED}} \propto 1/N$. For a Fermi gas, however, U_0 and N are separate parameters, and no such result can be proven analytically. We must numerically investigate whether this scaling is appropriate.

We constructed a set of random orthogonal initial wavefunctions $\chi_{n,\sigma}(x)$ with similar energies, and found that the energy-damping control had similar optimal values of k_{ED} for each of these states ($k_{\mathrm{ED}} \sim 15$). We constructed simulations across a range of feedback strengths k_{ED} and atom numbers N, sampling the initial single-particle wavefunctions from this set (in a spin-asymmetric manner). Although the behaviour is more complicated, we found that the scaling $k_{\mathrm{ED}} \propto 1/N$ produced close to optimal feedback as we varied N, and so this scaling rule is a sensible choice for both fermionic and bosonic species. Figure 4.6 demonstrates this scaling for a Fermi gas.

Now that we are able to appropriately scale our feedback strength, we are equipped to consider how the effectiveness of cooling depends on atom number N. We constructed two sets of 200 orthogonal wavefunctions with similar energies and optimal values of k_{ED} by randomly populating Hermite-Gauss modes. We simulated the energy-damping control with near-optimal k_{ED} (scaled by $k_{\mathrm{ED}} \propto 1/N$), varying N and sampling our initial states from these wavefunctions. For the multi-particle configurations, we did this for both no interactions ($\Upsilon_0 = 0$) and moderate repulsive interactions ($\Upsilon_0 = 1.0$). The results are

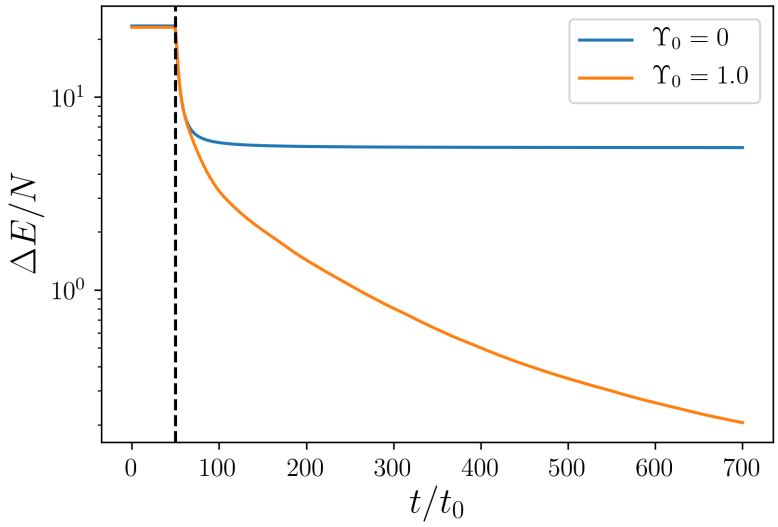

Figure 4.5: Successfully cooling a two-component, 100-atom Fermi gas from the complicated initial state in Figure 4.3c using the energy-damping control for $k_{\mathrm{ED}} = 0.6$. Feedback is switched on at $t/t_0 = 50.0$. With interactions turned off, the cooling removes significant amounts of energy, and asymptotes to a dark state. With interactions on, the system continues to cool towards the ground state, suggesting that interactions play an important role in energy-damping control of a Fermi gas. All quantities are in the harmonic oscillator units of Section 2.3.1.

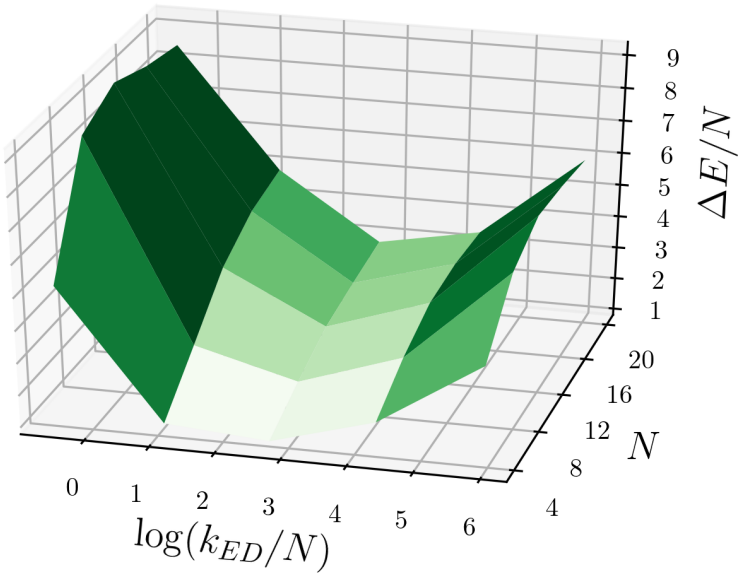

Figure 4.6: The excitation energy per particle after 10 trapping periods of a two-component Fermi gas cooled by the energy-damping control, across a range of values of k_{ED} and N. For each N, the 'valley' in the centre corresponds to near-optimal control, which has the expected scaling $k_{\mathrm{ED}} \propto 1/N$. All quantities are in the harmonic oscillator units of Section 2.3.1.

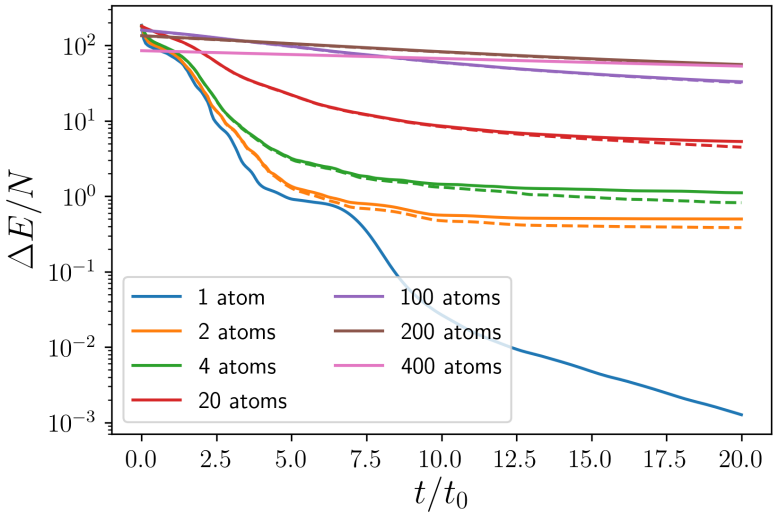

Figure 4.7: Cooling a two-component Fermi gas with the energy-damping control, for a range of values of N and near-optimal k_{ED} ($k_{\mathrm{ED}} = 5/N$). Feedback is active for the entire simulation. Solid lines correspond to $\Upsilon_0 = 0$, and dashed lines correspond to $\Upsilon_0 = 1.0$. The interacting case for $N = 400$ is not included due to difficulties in computing its ground state energy.[5] Cooling becomes significantly worse for just two atoms, and the cooling rate continues to decrease with increasing N. All quantities are in the harmonic oscillator units of Section 2.3.1.

depicted in Figure 4.7.

For one fermion, we have a single spatial mode, and the cooling works extremely well. This is to be expected as it is mathematically identical to a non-interacting BEC, which we previously noted was efficiently cooled by the energy-damping control (Section 4.5.1). For this initial state, the energy settles into a steady exponential decay after about 10 harmonic oscillator cycles.

For just two particles, however, the cooling becomes significantly worse. In the non-interacting case, it initially removes some energy, but cools to a dark state with a non-negligible excitation energy above the ground state ($\sim 2\hbar\omega$ per atom) - much like the 100-particle example in Figure 4.5. Crucially, as the number of particles increases, the cooling becomes much slower, and at least in the case of 4 and 20 atoms, asymptotes at a higher excitation energy per particle. Not only is it harder to cool multiple fermions, but it becomes harder with increasing N. With interactions on, the cooling is slightly better, but still extremely slow beyond a certain threshold.

4.6 The two-fermion model: why are fermions hard to cool?

We now attempt to understand why multi-component Fermi gases are hard to cool. The dark states of the energy-damping control are those for which there are no fluctuations in the total atomic density. Thus, it seems likely that in these dark states, the probability density of each atom oscillates in a non-trivial way, but the oscillations cancel out when

[5] Hermite-Gaussian quadrature converges with double-precision floating point arithmetic up to $D = 371$. This ground state cannot be accurately represented without a larger basis set, and higher-precision arithmetic is non-trivial to implement.

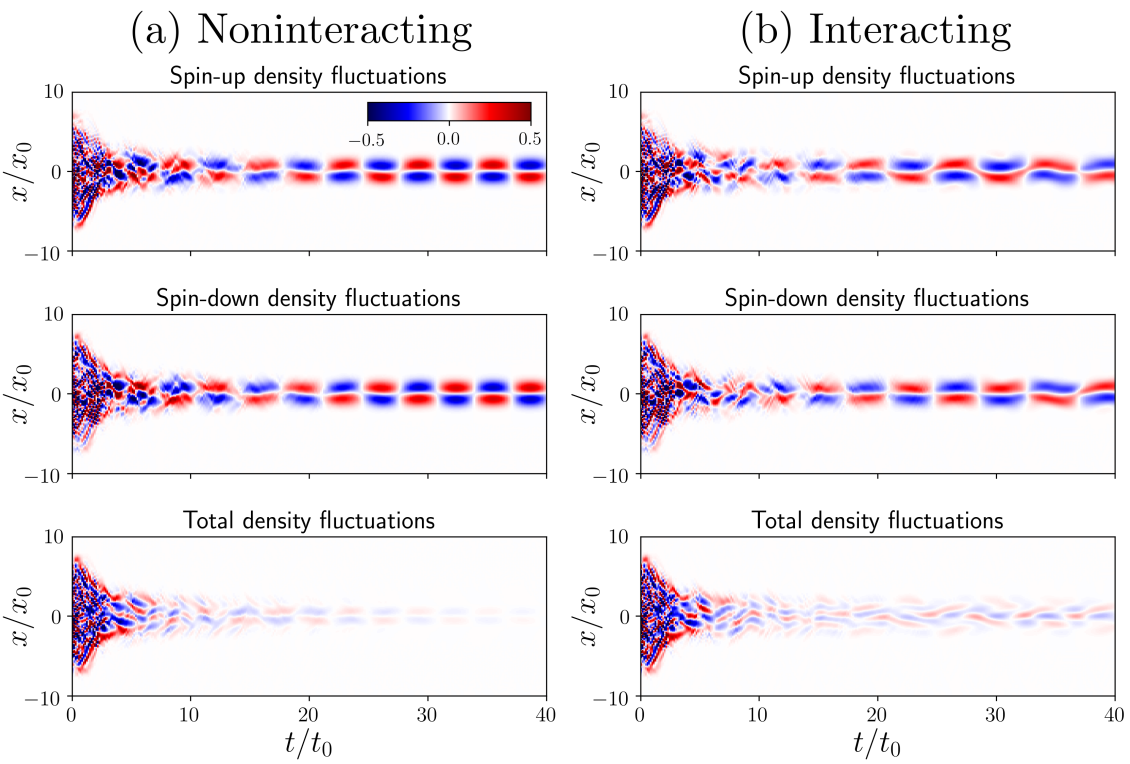

Figure 4.8: Feedback cooling in the two-fermion model with the energy-damping control for near-optimal control ($k_{\mathrm{ED}} = 5.0$). The individual density fluctuations $d|\chi_\sigma(x,t)|^2/dt$ and total density fluctuations $\sum_\sigma d|\chi_\sigma(x,t)|^2/dt$ are depicted for both (a) the non-interacting case and (b) the interacting case ($\Upsilon_0 = 2.0$). In the non-interacting case, the atoms settle into a total counter-oscillation, in which they have identical periodic density fluctuations with a phase difference of π, causing the total fluctuations to cancel out despite the significant individual motion. In the interacting case, the system is weakly perturbed from counter-oscillation by the scattering-induced asymmetry, and so there are always small density fluctuations through which the system may be cooled.

summed over all atoms. We say that the atoms are counter-oscillating. The essential physics of this phenomenon should be captured in a two-atom model, with one atom in each spin component. The FGPE (3.33) reduces to two coupled equations (corresponding to $\sigma =\uparrow$ and $\sigma =\downarrow$):

$$i\hbar\frac{d\chi_\sigma(x,t)}{dt} = \left(-\frac{\hbar^2}{2m}\frac{\partial^2}{\partial x^2} + \frac{1}{2}m\omega^2x^2 + k_{\mathrm{ED}}V_C(x,t) + U_0\left|\chi_{!\sigma}(x,t)\right|^2\right)\chi_\sigma(x,t). \quad (4.17)$$

The atoms are coupled both symetrically (both atoms experience the same control potential $V_C(x,t)$) and asymetrically (each atom interacts with the density field of its counterpart, and these density fields are necessarily non-identical due to Pauli exclusion).

We simulated the two-fermion model for both the non-interacting ($\Upsilon_0 = 0$) and moderately interacting ($\Upsilon_0 = 1.0$) case, using initial wavefunctions from the ensemble in Section 4.5.2. We plotted the density fluctuations for both cases, depicted in Figure 4.8.

The mechanism behind dark states is extremely clear. In the non-interacting case (Figure 4.8a), the individual densities $|\chi_\uparrow(x,t)|^2$ and $|\chi_\downarrow(x,t)|^2$ quickly settle from their compli-

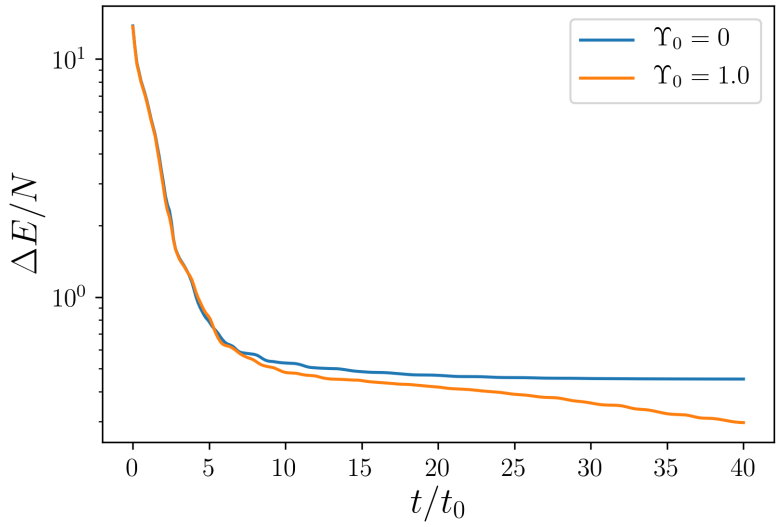

Figure 4.9: Feedback cooling in the two-fermion model with the energy-damping control for near-optimal control ($k_{\mathrm{ED}} = 5.0$). In the non-interacting case, the system asymptotes to a dark state due to the total counter-oscillation of the atoms. In the interacting case, the system is weakly perturbed from counter-oscillation by the scattering-induced asymmetry, allowing the system to slowly further cool. All quantities are in the harmonic oscillator units of Section 2.3.1.

cated initial states to a well-defined periodic oscillation that is antisymmetric about the centre of the trap. However, the two atoms have a phase difference of π in their oscillations, and when summed together, cancel out. As the atoms are coupled in a symmetric manner - they both see the same control and trapping potentials - there is no asymmetry that can perturb them from this counter-oscillation, leading to a dark state that cannot be cooled. In the interacting case (Figure 4.8b), there is a weak asymmetry due to the difference in density fields. This continuously perturbs the system from the counter-oscillating state, ensuring that there are always total density fluctuations. The energy of the counter-oscillation is therefore gradually coupled out - albeit very slowly. Figure 4.9 compares the energy removal for the non-interacting and interacting cases: they have a nearly identical initial behaviour as most of the energy is rapidly removed, but the non-interacting system asymptotes to a dark state, while the interacting system slowly couples out energy via this asymmetry.

4.7 Single-spin-component Fermi gases

It should be noted that the total counter-oscillation is unique to multi-component Fermi gases. In the absence of feedback or interactions (e.g. for a dark state of the energy-damping control), we may write the evolution of the single-particle wavefunctions $\chi_{n,\sigma}(x,t)$ in the energy eigenbasis:

$$\chi_{n,\sigma}(x,t) = \sum_m c_m \phi_m(x) e^{-i\omega_m t}, \tag{4.18}$$

where the $\phi_m(x)$ are the harmonic oscillator energy eigenfunctions, and the $\omega_m = E_m/\hbar$ are the characteristic rotation frequencies of each component. For the 1D trap we are

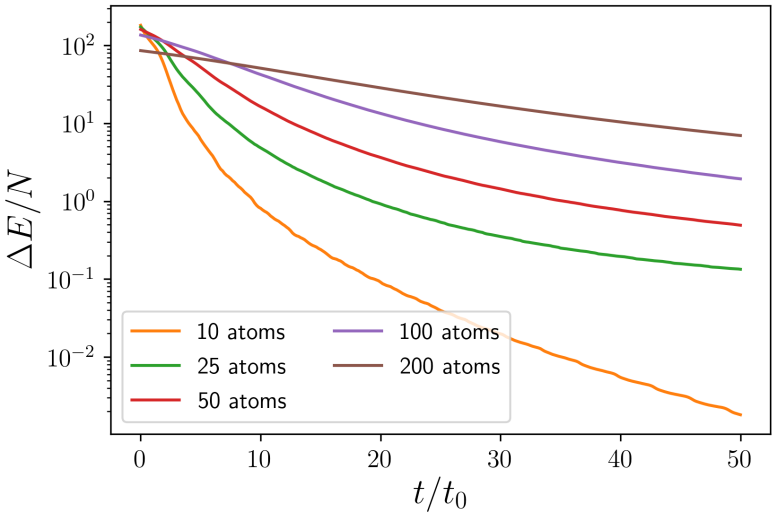

Figure 4.10: Cooling a single-component Fermi gas with the energy-damping control, for a range of values of N and near-optimal k_{ED} ($k_{\mathrm{ED}} = 5/N$). Feedback is active for the entire simulation. The cooling rate decreases with increasing N. All quantities are in the harmonic oscillator units of Section 2.3.1.

considering, the ω_m are nondegenerate. The oscillations can only cancel out totally if multiple atoms oscillate at the same frequency with the same spatial structure, which is only possible if we have more than one internal component. Thus, dark states of the energy-damping control should not exist for a Fermi gas with a single spin component as there will always be some total density fluctuations, and so energy must be strictly decreasing according to Equation 4.11.

Discarding one spin component from the FGPE (3.33), we obtain a set of single-particle Schrödinger equations, coupled by a shared control potential $V_C(x,t)$ (as there are no s-wave interactions for fermions in the same spin component):

$$i\hbar\frac{d\chi_n(x,t)}{dt} = \left(-\frac{\hbar^2}{2m}\frac{\partial^2}{\partial x^2} + \frac{1}{2}m\omega^2x^2 + V_C(x,t)\right)\chi_n(x,t). \tag{4.19}$$

We simulated Equation 4.19 for near-optimal k_{ED} across a range of atom numbers N. The results are depicted in Figure 4.10. Although the system does not asymptote to a dark state, the cooling rate still decreases as we increase N, since density fluctuations may still partially cancel out, and are more likely to for larger N.

However, spin-polarised ultracold Fermi gases have negligible interactions,[6] and so are of little use to directly produce analogue quantum simulators. We thus choose to focus on two-component Fermi gases for the remainder of this thesis.

4.8 Conclusions from no-measurement simulations

Although we have not included measurement effects in the simulations presented in this chapter, we have still produced significant insights into the challenges of cooling Fermi

[6] As discussed in Section 2.2.2, ultracold atoms are dominated by s-wave scattering, and fermions of the same internal component experience no s-wave scattering.

gases. Before we progress to a measurement-feedback model, we summarise and discuss the results obtained in the no-measurement limit. We will review the four questions posed in Section 4.3 in the context of our results.

4.8.1 Can the new 'energy-damping control' overcome the limitations of the 'moment control'?

Yes. The energy-damping control is unequivocally better than the moment control applied to the first two moments of atomic density. Our simulations showed that the moment control was ineffective in cooling complicated initial states, reaching 'dark states' with high excitation energies above the ground state. The energy-damping control resolved this limitation. It may, however, be more difficult to impliment experimentally: this is a prospect we will discuss in Chapter 7.

4.8.2 Do the results for BECs obtained in Haine *et al.* generalise to Fermi gases?

Mostly. We have succesfully implemented a fermionic version of the model in Haine *et al.* [2]. We have demonstrated that many of their key results apply to Fermi gases: we demonstrated that the moment control can be used to successfully cool simple initial states, that feedback is optimised for certain parameters, that 'dark states' exist from which the system cannot be cooled, and that interactions can be used to slowly perturb the system from a dark state (for both controls). There are some differences, however, which we will shortly address.

4.8.3 Are there any fundamental differences between cooling Bose gases and Fermi gases?

Yes. Although near-optimal control seems to be preserved for both BECs and Fermi gases by the scaling $k_{\mathrm{ED}} \propto 1/N$, fermions are harder to cool directly. A BEC has only one spatial mode to control, but a Fermi gas of N atoms has N spatial modes, all competing for the same control potential. Their individual density fluctuations may partially or totally cancel out when looking at the total atom density. In the non-interacting case, we even saw dark states of the energy-damping control, where atoms exactly counter-oscillated, cancelling out the total density fluctuations. Although we showed that interactions could slowly perturb the system from a counter-oscillating state, this coupling is slow.

4.8.4 Can we directly cool a large number of fermions effectively?

Possibly not for the energy-damping control. However, until we introduce measurement effects, this question will remain open. It seems that in the no-measurement limit, with interactions on, we can continue to remove energy indefinitely, as there will always be some total density fluctuations. However, we saw that the cooling rate decreased as we increased N. Once again, this is caused by density fluctuations cancelling out: at each position, each atom contributes either a positive or negative value to the total density fluctuation, and the more atoms in the trap, the more likely that these will cancel out on average. When we introduce measurement, our cooling rate will compete with a measurement-induced heating rate: it seems likely that the slower cooling for many atoms will be problematic. Nonetheless, it is impossible to ascertain how these rates actually compete without simulating measurement effects, which we do in Chapter 6.

Chapter 5

Theory of quantum gases under continuous measurement

In Chapter 4, we assumed perfect knowledge of the system's state vector and ignored the effects of measurement backaction, implementing a fermionic version of the model of Haine *et al.* [2]. Although this provides useful insights into the control-specific aspects and best-case performance of feedback cooling, it is unrealistic. In practice, we only have imperfect knowledge of the system's quantum state, and must continuously measure it to obtain this knowledge. As our control schemes are based on density fluctuations, we will attempt to continuously measure the system's spatial density. This will cause measurement-induced heating, as it will narrow the position-space wavefunction, leading to increased kinetic energy. A realistic model of feedback control must account for the competition between the rates of feedback cooling and measurement-induced heating.

This chapter contains both background theory and original work. In Section 5.1, we introduce system-reservoir techniques from quantum optics to describe open quantum systems. In Section 5.2, we will discuss a generalisation of these techniques suitable for modelling active feedback control of a continuously-monitored system. In Section 5.3, we summarise the model and results of Szigeti *et al.* [3, 4], who applied these techniques to model a BEC under measurement. We will then develop a new fermionic version of this model in Section 5.4, and show that the single-fermion limit agrees with the single-boson limit of Ref. [3].

5.1 Open quantum systems

The quantum-mechanical methods used thus far describe closed systems that do not interact with their environment (beyond the removal of energy due to a time-dependent external potential). Almost all realistic quantum systems have non-negligible interactions with their surrounding environment, but a full quantum model of the environment would be computationally intractable. We refer to such systems that have non-negligible interactions with their environment as *open quantum systems*. In this section, we present a brief introduction to system-reservoir methods from quantum optics used to describe open quantum systems. For a more comprehensive introduction, we refer the interested reader to the treatment of Gardiner and Zoller [102].

5.1.1 The density matrix

A classical ensemble of quantum states may be represented by a *density matrix*, given by

$$\hat{\rho} = \sum_j P_j \left|\psi_j\right\rangle \left\langle\psi_j\right| , \tag{5.1}$$

where the $|\psi_j\rangle$ can be any quantum states (not necessarily orthonormal or spanning), and the $P_j \in [0,1]$ are their associated probabilities in the ensemble, and thus $\sum_j P_j = 1$. When there is exactly one state (denoted $|\Psi\rangle$) in the ensemble, the associated probability is 1, and the density matrix (5.1) reduces to:

$$\hat{\rho} = \left|\Psi\right\rangle \left\langle\Psi\right| . \tag{5.2}$$

We call this a *pure state*, as opposed to a *mixed state*, which is an ensemble of multiple states. Expectation values in a mixed state take the form of an *ensemble average*, defined as[1]

$$\langle\hat{O}\rangle = \mathrm{Tr}\left\{\hat{O}\hat{\rho}\right\} = \sum_j P_j \left\langle\psi_j\right| \hat{O} \left|\psi_j\right\rangle , \tag{5.3}$$

which clearly reduces to the usual definition for a pure state. In a closed quantum system, density matrices have a Heisenberg-like unitary evolution:

$$\frac{d\hat{\rho}}{dt} = -\frac{i}{\hbar}\left[\hat{H}, \hat{\rho}\right] , \tag{5.4}$$

where $\hat{H}$ is the system's Hamiltonian. This can in principle be integrated to find $\hat{\rho}(t)$, and thus the full dynamics of the state.

5.1.2 System-reservoir methods: Lindbladian master equations

Consider an open quantum system with Hilbert space $\mathcal{H}_S$, coupled to a reservoir with Hilbert space $\mathcal{H}_R$. Suppose that the system and reservoir are initially separable, such that $\hat{\rho}_{SR}(0) = \hat{\rho}_S(0) \otimes \hat{\rho}_R(0)$, where the subscript S denotes the system, R the reservoir, and SR the full space formed by both. In principle, we could compute the full dynamics of the system by finding the full Hamiltonian evolution:

$$\frac{d\hat{\rho}_{SR}}{dt} = -\frac{i}{\hbar}\left[\hat{H}_{SR}, \hat{\rho}_{SR}\right] , \tag{5.5}$$

then finding the reduced density matrix for the system as $\hat{\rho}_S(t) = \mathrm{Tr}_R\left\{\hat{\rho}_{SR}(t)\right\}$ [28]. However, this method is generally computationally intractable when $\mathcal{H}_R$ hosts a system large enough to act as a reservoir.

Fortunately, there are tractable methods to simplify this. Suppose the following approximations hold:

1. The system and reservoir are always separable, and the reservoir can be treated as unchanging, such that $\hat{\rho}_{SR}(t) = \hat{\rho}_S(t) \otimes \hat{\rho}_R(0)$. This is the *Born approximation*.

2. The system is *Markovian*: the dynamics are unaffected by the past history of the

[1] To verify the second equality, expand out the trace in a complete basis $\{|\phi_n\rangle\}$, rearrange, and use the completeness relation $\sum_n |\phi_n\rangle \langle\phi_n| = \hat{1}$.

system and depend only on the current system state.[2]

3. Terms of the form $\mathrm{Tr}_R\left\{\left[\hat{H}_{SR}(t), \hat{\rho}_{SR}(0)\right]\right\}$ are zero.[3]

Under these approximations, we can derive a *master equation in Lindblad form* describing the evolution of the system's density matrix:

$$\frac{d\hat{\rho_S}}{dt} = \underbrace{-\frac{i}{\hbar}\left[\hat{H}_S, \hat{\rho}_S\right]}_{\text{Hamiltonian evolution}} + \underbrace{\sum_j \mathcal{D}\left[\hat{L}_j\right]\hat{\rho}_S}_{\text{Decoherence}}, \tag{5.6}$$

where $\mathcal{D}$ denotes the *decoherence superoperator* defined by:

$$\mathcal{D}\left[\hat{L}\right]\hat{\rho} \equiv \hat{L}\hat{\rho}\hat{L}^\dagger - \frac{1}{2}\hat{L}^\dagger\hat{L}\hat{\rho} - \frac{1}{2}\hat{\rho}\hat{L}^\dagger\hat{L}. \tag{5.7}$$

This formalism describes the system's behaviour without also needing to account for the state of the reservoir, since $\hat{\rho}_S \in \mathcal{H}_S$. The intractable system-reservoir problem can therefore be reduced to a problem barely any more complex than the dynamics of the system in isolation. Inspecting Equation 5.6, we see that Lindbladian evolution is composed of the usual unitary evolution according to the system's Hamiltonian (the first term), and an additional term describing *decoherence*. Loosely speaking, decoherence is the introduction of classical uncertainty to a quantum system due to interactions with the environment. As a quantum system decoheres, information contained in phase relations of the state is lost, and a pure state will typically become mixed.

5.1.3 Decoherence demystified

We will now consider a simple example in order to gain an intuitive understanding of decoherence. Consider an observable $\hat{O}$ with eigenbasis $\{|n\rangle\}$, such that $\hat{O}|O_n\rangle = O_n|O_n\rangle$. We assume a nondegenerate spectrum, such that $O_n \neq O_m$ for $n \neq m$. Suppose our system (described by density matrix $\hat{\rho}$) is dominated by decoherence in this observable, such that the master equation may be written:

$$\frac{d\hat{\rho}}{dt} = \mathcal{D}[\hat{O}]\hat{\rho}. \tag{5.8}$$

Suppose that the system begins in a pure state $\hat{\rho} = |\Psi\rangle\langle\Psi|$ of some superposition in the eigenbasis of $\hat{O}$:

$$|\Psi\rangle = \sum_n c_n |O_n\rangle. \tag{5.9}$$

It can be shown (see Appendix A.6 for the derivation) that in the long-term limit, we have

$$\hat{\rho}(t \to \infty) = \sum_n |c_n|^2 |O_n\rangle\langle O_n|. \tag{5.10}$$

[2]Naively, this may seem equivalent to the Born approximation. However, they must be stated separately: the Born approximation does not by itself exclude the possibility of the *system* being non-Markovian, but it is a much stronger approximation on the reservoir.

[3]For many systems, these terms include exectation values of single field operators in the vacuum due to bilinear couplings, and so this is often the case.

Thus, over time, this decoherence process projects the pure state onto the eigenbasis of $\hat{O}$ according to the Born rule (i.e. the classical probability for a state $|O_n\rangle$ is given by $|c_n|^2$). The state becomes mixed, and the information contained in the phase relationships between the c_n is lost. This is why decoherence is often understood as a loss of information from the system, making it the most significant barrier to reliably storing quantum information for quantum computing [43].

5.2 Conditional quantum measurement theory

We require a dynamical theory of quantum measurement to describe experiments conditioned on measurement outcomes, such as feedback control. Although the methods described in Section 5.1 can describe decoherence, they are insufficient to describe quantum measurement. It was a necessary assumption that the reservoir be completely passive and time-invariant, and thus it cannot 'react' to the system. Furthermore, there is no mechanism in the theory for wavefunction collapse. Further generalisations are required in order to describe behaviour conditioned on measurement results. Broadly, these techniques are known as *conditional quantum measurement theory*. We will only review the essentials: for further details, the interested reader is directed to the leading texts on the topic [129, 130].

We will model nondestructive continuous measurement processes. These are *not* fully projective measurements that collapse a system into an eigenstate, but rather a weaker way of gathering information about the system state. The system is coupled to a reservoir (such as the optical field of an incident laser), which then undergoes projective measurement. Due to this coupling, information from projective measurement of the reservoir can be used to gain information about the system state, without fully collapsing it into an eigenstate. The system can thus be continuously weakly measured without completely arresting its dynamics (e.g. the quantum Zeno effect [131]).

5.2.1 Stochastic master equations

Quantum measurement is inherently probabilistic, and so to describe a system undergoing measurement we follow the evolution of a *conditional density matrix* $\hat{\rho}_c$, representing the system state conditioned on a particular measurement result. The average behaviour of the system is recovered by taking a stochastic average over all possible *trajectories* (different dynamical outcomes of the system, dependent on the history of random noise processes):

$$\hat{\rho} = \mathbb{E}\left\{\hat{\rho}_c\right\}. \tag{5.11}$$

The evolution of $\hat{\rho}_c$ is described by a *stochastic master equation* in Itô form,[4] given by (c.f. Equation 5.6):

$$d\hat{\rho}_c = \underbrace{-\frac{i}{\hbar}\left[\hat{H},\hat{\rho}_c\right]dt}_{\text{Hamiltonian evolution}} + \underbrace{\sum_j \mathcal{D}\left[\hat{L}_j\right]\hat{\rho}_c dt}_{\text{Decoherence}} + \underbrace{\sum_j \mathcal{H}\left[\hat{L}_j\right]\hat{\rho}_c dW_j(t)}_{\text{Innovations}}, \tag{5.12}$$

[4]The use of the Itô integral is a natural consequence of the formalism used for quantum stochastic calculus: see Ref. [102] for details. We will later cast our mean-field equations to Stratonovich form.

where $\hat{H}$ is the system's Hamiltonian, the $\hat{L}_j$ are Lindblad operators describing the measurement process, and the $dW_j(t)$ are Wiener increments (see Section 2.4), which are totally uncorrelated such that $\mathbb{E}\{dW_j dW_k\} = \delta_{jk}dt$. $\mathcal{D}$ is the usual Lindbladian decoherence superoperator (Equation 5.7), and the *innovations superoperator* $\mathcal{H}$ is defined:

$$\mathcal{H}\left[\hat{L}\right]\hat{\rho} \equiv \hat{L}\hat{\rho} + \hat{\rho}\hat{L}^\dagger - \mathrm{Tr}\left\{\left(\hat{L}+\hat{L}^\dagger\right)\hat{\rho}\right\}\hat{\rho}. \tag{5.13}$$

The first term of Equation 5.12 describes the usual unitary evolution according to the system's evolution. The second term describes decoherence due to the measurement process, in exactly the same manner as the Lindbladian evolution described in Section 5.1. The third term is known as the *innovations term*, and represents new information gathered about the state via the measurement process. Quantum measurement is inherently probabilistic, and so it may depend on a number[5] of Wiener processes[6] $dW_j(t)$.

This is not *a priori* different to the theory of open quantum systems discussed in Section 5.1, and the difference is quite subtle. Suppose that $\hat{H}$ does not depend on the system state. If we compute the average behaviour of the system by taking $d\hat{\rho} = \mathbb{E}\{d\hat{\rho}_c\}$ in Equation 5.12, then we obtain:

$$d\hat{\rho} = \mathbb{E}\{d\hat{\rho}_c\} = -\frac{i}{\hbar}\left[\hat{H}, \mathbb{E}\{\hat{\rho}_c\}\right]dt + \sum_j \mathcal{D}\left[\hat{L}_j\right]\mathbb{E}\{\hat{\rho}_c\}\,dt + \sum_j \mathcal{H}\left[\hat{L}_j\right]\mathbb{E}\{\hat{\rho}_c dW_j(t)\}, \tag{5.14}$$

where we have used the fact that $\hat{H}$ and the $\hat{L}_j$ do not vary between trajectories. We note that $\hat{\rho}_c$ is a nonanticipating function of t (see Section 4.2.4 of Ref. [97] for elaboration on this property), and thus the noise and conditional state at time t are uncorrelated:

$$\mathbb{E}\{\hat{\rho}_c dW_j(t)\} = \mathbb{E}\{\hat{\rho}_c\}\,\mathbb{E}\{dW_j(t)\} = 0, \tag{5.15}$$

where we have used the fact that $\mathbb{E}\{dW_j(t)\} = 0$ in the last step. Therefore, the last term of Equation 5.14 is zero, and identifying $\mathbb{E}\{\hat{\rho}_c\} = \hat{\rho}$, this reduces to:

$$d\hat{\rho} = -\frac{i}{\hbar}\left[\hat{H}, \hat{\rho}\right]dt + \sum_j \mathcal{D}\left[\hat{L}_j\right]\hat{\rho}\,dt, \tag{5.16}$$

which is exactly the standard Lindbladian evolution of an open quantum system (c.f. Equation 5.6).

Thus, the stochastic master equation (5.12) represents an *unravelling* of the Lindbladian dynamics, conditioned on particular measurement outcomes, but the average dynamics are preserved. This may seem redundant: why would we compute many conditional trajectories and average over them, if we could just compute the average behaviour with standard Lindbladian evolution (5.6)? In most cases, this would be sufficient, but recall from Chapter 4 that the control terms of a Hamiltonian for a feedback-controlled system include expectation values in the system state. In Equation 5.14, we assumed that $\hat{H}$ did

[5] The index may be a continuous one, such as position, in which case the sum becomes an integral.

[6] It is also possible to describe a fully projective measurement onto a discrete basis with the same techniques, which leads to a Poissonian noise process dN rather than a Wiener process. This is irrelevant to this thesis, and thus not treated here: further details may be found in Chapter 3 of Ref. [130].

not depend on the system state, allowing the simplification:

$$\mathbb{E}\left\{\left[\hat{H},\hat{\rho}_c\right]\right\} = \mathbb{E}\left\{\hat{H}\hat{\rho}_c\right\} - \mathbb{E}\left\{\hat{\rho}_c\hat{H}\right\} = \hat{H}\mathbb{E}\left\{\hat{\rho}_c\right\} - \mathbb{E}\left\{\hat{\rho}_c\right\}\hat{H} = \left[\hat{H},\hat{\rho}\right]. \tag{5.17}$$

If $\hat{H}$ depends on the system state, then it varies between trajectories; $\hat{H}$ and $\hat{\rho}_c$ are highly correlated, and thus it is not true that $\mathbb{E}\{\hat{H}\hat{\rho}_c\} = \mathbb{E}\{\hat{H}\}\mathbb{E}\{\hat{\rho}_c\}$. Therefore, there is no way to describe the average behaviour without individually evolving each trajectory if our system is feedback-controlled.

The upshot is that we require a conditional treatment that follows each trajectory if we actively respond to the information gained from measurement, such as in feedback control. It is extremely important to realise that these trajectories have physical meaning. Each trajectory corresponds to a physical realisation of the experiment under continuous measurement, conditioned on the measurement outcomes. We want to perform feedback *in real time* based on measurement results, not 'on average'. Thus, we need a description that follows a single quantum state, not the ensemble average. The general strategy for simulating a quantum system undergoing measurement and feedback control is as follows:

1. Construct an initial state $\hat{\rho}(t=0)$. We wish to know the average state at some later time t.
2. Create many[7] copies of this initial state, and designate them $\hat{\rho}_c$.
3. Evolve each $\hat{\rho}_c$ separately according to the stochastic master equation (Equation 5.12), using a pseudorandom number generator to generate the Wiener noise $dW_j(t)$, with a different seed for each trajectory.
4. Each trajectory will evolve differently due to differing noise. After evolution, average the observables of interest over all trajectories: this is our estimate of their average value, with uncertainty calculated by taking the standard error in the mean over all trajectories.

This enables us to calculate the average behaviour of a continuously monitored quantum system, allowing us to model feedback control.

5.2.2 Filtering theory and system-filter separation

Ideally, solving the stochastic master equation (Equation 5.12) gives knowledge of the current condition system state $\hat{\rho}_c$, which can be used to decide upon an effective control potential at the next time step. However, we cannot simply use $\hat{\rho}_c$ to determine our feedback without justification. $\hat{\rho}_c$ describes the 'true' full quantum state of the system, yet it is impossible to measure *all* information about a quantum state, and thus an experimenter will never actually know the full state $\hat{\rho}_c$. Measurement can only give limited information about the composition of a quantum state, and so we must account for this in our model.

We can model the effect of an experimenter's imperfect knowledge of the underlying system by simulating two coupled stochastic master equations for the *system* $\hat{\rho}_c$ and the *filter* $\hat{\pi}_c$ [132, 133]. Both are density matrices; the system $\hat{\rho}_c$ describes the true state of the system (hidden from the experimenter), and evolves according to Equation 5.12. The filter $\hat{\pi}_c$

[7] For the purposes of this thesis, several hundred trajectories are sufficient for an excellent prediction of the average behaviour.

describes the *experimenter's best guess* of the system state, given the measurement record. The filter evolves by a similar stochastic master equation, of the form:

$$d\hat{\pi}_c = -\frac{i}{\hbar}\left[\hat{H}, \hat{\pi}_c\right] dt + \sum_j \mathcal{D}\left[\hat{L}_j\right]\hat{\pi}_c dt + \sum_j \mathcal{H}\left[\hat{L}_j\right]\hat{\pi}_c \left(d\tilde{Y}_j(t) - \left\langle \hat{L}_j + \hat{L}_j^\dagger \right\rangle_{\hat{\pi}_c}\right). \quad (5.18)$$

We define the *measurement signal* as:

$$dY_j(t) = \left\langle \hat{L}_j + \hat{L}_j^\dagger \right\rangle_{\hat{\rho}_c} + dW_j(t). \quad (5.19)$$

The subscripts $\hat{\pi}_c$ and $\hat{\rho}_c$ indicate that the expectation values are calculated with respect to the filter and the true system state, respectively. The filter is updated by measurements on the system, whereas the filter is used to choose the control that influences both the system and filter. All expectation values used in the control Hamiltonian are calculated with respect to the filter, since this is the only information the experimenter has access to. The same Hamiltonian is used in both Equations 5.12 and 5.18. In a realistic experiment, the measurement signal $dY_j(t)$ will be corrupted by some classical noise channel[8] $d\eta_j(t)$ (also a Wiener process, assuming the noise is Gaussian), leading to the *corrupted measurement signal*:

$$d\tilde{Y}_j(t) = dY_j(t) + \sqrt{\nu} d\eta_j(t), \quad (5.20)$$

which appears in the filter equation (5.18). Here, ν is the strength of the measurement noise process. This process forms a continuous measurement-feedback loop, depicted in Figure 5.1.

In the limit of no corrupting noise ($\nu = 0$), if $\hat{\pi}_c = \hat{\rho}_c$, then the filter equation (5.18) reduces exactly to the stochastic master equation of the system itself (5.12). We say that the system and filter have *converged* if they are approximately the same, and unless severely perturbed by interfering classical noise, they will stay converged due to this property. Except in pathological cases, it is typically safe to assume that the system and filter will eventually converge, and that the convergence thereafter will be fairly robust to realistic experimental imperfections (see Ref. [132] for an in-depth example and discussion of the robustness of system-filter separation). The convergence rate is determined by system parameters: stronger measurement[9] will result in faster convergence.

Most previous works [3, 4, 77] assumed best-case performance of measurement and neglected the classical noise channel $d\eta_j(t)$. Due to the eventual convergence and robustness to experimental imperfections, they assumed that the system and filter are initially converged (and thus converged for all time). This leads to a single, uncoupled stochastic master equation of the form in Equation 5.12, and it is common to refer to the filter and quantum state interchangeably in this limit. This is likely a good assumption provided that the measurement strength is not too weak. We will mostly follow this convention, but will discuss the prospect of separately simulating the coupled equations of the system (5.12) and filter (5.18) in Section 7.1.3, an approach known as a *system-filter separation.*

[8] This is equivalent to just having imperfect detection efficiency.

[9] We will give a concrete example of measurement 'strength' in Section 5.3.

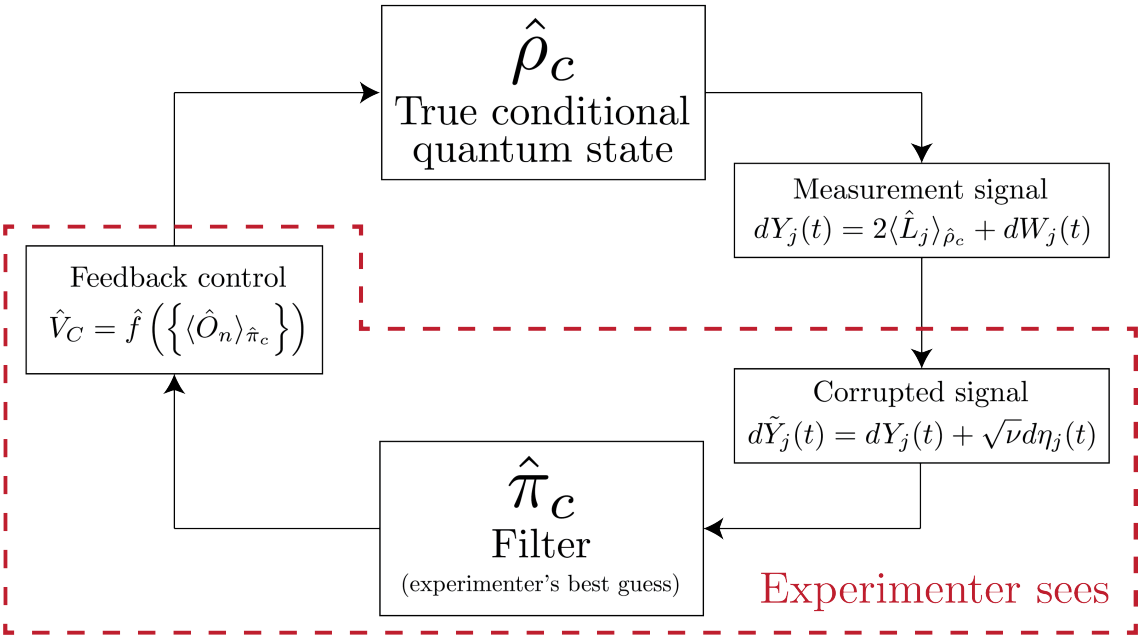

Figure 5.1: A diagrammatic representation of the measurement-feedback process. Measurement signals $dY_j(t)$ are obtained, corresponding to (Hermitian) measurement of system expectation values $\langle \hat{L}_j \rangle_{\hat{\rho}_c}$ corrupted by unavoidable white noise associated with random wavefunction collapse. These signals may be further corrupted by classical noise channels $d\eta_j(t)$ (e.g. due to technical noise sources), before being used by the experimenter to update the filter $\hat{\pi}_c$. The filter is then used to calculate the control potential, which is applied to the system $\hat{\rho}_c$. This forms a measurement-feedback loop.

5.3 Previous work: BECs under continuous measurement

We will now summarise the measurement model introduced by Szigeti *et al.* [3] and used in subsequent works [4, 77]. Consider a harmonically-trapped atomic gas, with $\omega_x \ll \omega_y = \omega_z$, leading to tight confinement in the y and z directions,[10] and thus a 'cigar' shape that is comparatively thin in the transverse directions. As discussed in Section 2.2.2, this leads to an effective 1D system. In the limit of no measurement (and assuming perfect knowledge of the state), this reduces to the one-dimensional model used for the simulations of Chapter 4.

Szigeti *et al.* considered the case of a Bose gas undergoing continuous density measurements via phase-contrast imaging [52, 53]. This is a technique which non-destructively images a quantum gas by shining coherent light highly detuned from resonance onto the system, and using the scattered phase profile to reconstruct the density profile of the condensate. Although this is minimally destructive, it still heats the system, causing decoherence. Since information about the atomic density is encoded in the phase of the light, this information can be extracted via homodyne detection. This signal is then used to update the filter. Knowledge of the observables from the filter is used to configure the control potential $V_C(x,t)$ in a way that removes energy, as discussed extensively in Chapter 4. A diagram of the system is provided in Figure 5.2

As discussed in Section 5.2.2, filter convergence is a reasonable assumption, and so they derived a single filter equation. We will not follow the full filter derivation - it is an extremely involved process that is well beyond the scope of this thesis. The full derivation can be found in the Appendix of Ref. [3], and leads to the stochastic master equation:

$$d\hat{\rho}_c = \underbrace{-\frac{i}{\hbar}\left[\hat{H},\hat{\rho}_c\right]dt}_{\text{Unitary evolution}} + \underbrace{\alpha\int dx\mathcal{D}\left[\hat{M}(x)\right]\hat{\rho}_c dt}_{\text{Decoherence}} + \underbrace{\sqrt{\alpha}\int dx\mathcal{H}\left[\hat{M}(x)\right]\hat{\rho}_c dW(x,t)}_{\text{Innovations}}. \quad (5.21)$$

This contains the full quantum field theory of the BEC: no approximations are made yet on $\hat{\rho}_c$. It is of the same form discussed in Section 5.2. It consists of unitary evolution according to the system's Hamiltonian $\hat{H}$, (the usual cold-atom Hamiltonian (2.22) in the bosonic, single-spin-component case, plus control terms), decoherence in the quantum field due to application of the laser, and updates to the filter due to new knowledge from measurement (innovations). The 'measurement strength' α is factored out of the Lindblad operator to emphasise its role as the driving strength of the measurement backaction. It is given by:[11]

$$\alpha = \frac{3}{4}\frac{\Gamma_{\text{sp}}}{\omega_x}\frac{\Omega^2}{\Delta^2}, \quad (5.22)$$

where Γ_{sp} is the rate at which a single atom spontaneously emits into the environment,[12] Ω is the Rabi frequency and Δ is the detuning of the laser. In principle, this could be controlled arbitrarily, as the Rabi frequency Ω increases with laser intensity. A larger α

[10] A more general model with tight- confinement only in the z direction, leading to a 'pancake' shape, is discussed in Ref. [3] but has never been simulated.

[11] Szigeti *et al.* made minor modifications to the parameter definitions between the initial derivation of the filter equation [3] and the subsequent Hartree-Fock mean-field study [4]. We present the conventions of the latter in this section, but have slightly altered some notation for consistency with more modern work.

[12] Our model does not explicitly include the effect of spontaneous emission. Spontaneous emission cannot be entirely avoided, but the effect has been shown to be negigible in carefully contructed experiments based on dispersive imaging [54].

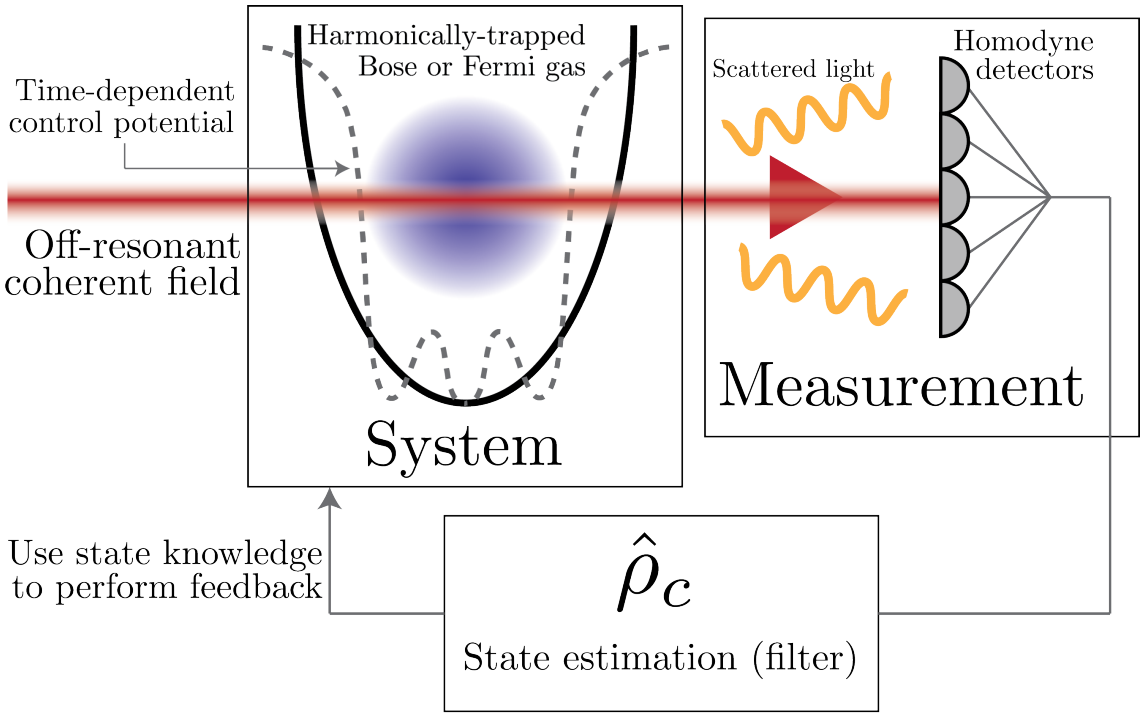

Figure 5.2: A diagram of the measurement-feedback scheme studied for BECs in Refs. [3, 4, 77] and for Fermi gases in this thesis. A harmonically-trapped atomic gas is illuminated with laser light highly detuned from resonance, which is scattered and subjected to a homodyne measurement. This measurement signal is used to update the filter $\hat{\rho}_c$. Feedback control is then applied via an additional control potential, the form of which is calculated based on expectation values in the filter. This forms a continuous measurement-feedback loop (see Figure 5.1).

gathers more information about the state through the innovations term, but also results in greater heating through the decoherence term. Both terms are a direct result of the measurement, with 'measurement operator':

$$\hat{M}(x) = \int dx' \hat{\psi}^\dagger(x') K(x - x') \hat{\psi}(x'), \tag{5.23}$$

where the *measurement kernel* $K(x)$ is defined (in the harmonic oscillator units of Section 2.3.1) as:

$$K(x) = \sqrt{\frac{\eta}{2\pi\eta_\perp}} \int dk \exp\left(-\frac{1}{16}\left(\frac{\eta_\perp}{\eta^2}\right)k^4\right) e^{ikx}. \tag{5.24}$$

We write the wavenumber of the incoming laser light as $k_0 = 2\pi/\lambda$, where λ is the wavelength of the laser. The Lamb-Dicke parameter is defined in the x direction as $\eta = k_0 x_0$ and in the transverse directions as $\eta_\perp = k_0 R_\perp$, for condensate width $R_\perp$ in the transverse directions. The measurement $\hat{M}(x)$ consists of a density operator convolved with the kernel $K(x)$: therefore, the kernel is a point-spread function which 'blurs' the density measurement, making it imperfect (as perfect measurement of density is physically impossible). The width of the kernel thus gives the measurement resolution, and so a larger η leads to more precise measurement.

The stochastic master equation (5.21) is an equation of motion for a full-field quantum model. For the reasons outlined in Section 1.1, it is computationally intractable to integrate directly. The techniques of mean-field theory are therefore required to numerically simulate it for multiple particles.[13] Szigeti *et al.* proposed the use of mean-field theory in their original paper [3], but found that the use of a coherent-state approximation (see Section 3.1.1) led to numerically unstable equations, since a coherent state is a Poissonian distribution of particle numbers, and a density-like measurement projects the system towards a state of well-defined number. They thus conducted all their simulations in the single-particle limit (which we will discuss in Section 5.5).

In a subsequent paper [4], Szigeti *et al.* used the Fock state approximation discussed in Section 3.1.3 to derive mean-field dynamics for a strongly interacting BEC. Although the coherent state and number state approximations give the same unitary dynamics (up to the approximation $N \approxeq N - 1$), the form of the measurement terms differs greatly between the two. This resulted in a tractable and numerically stable mean-field theory with measurement. In the following section, we pursue a fermionic generalisation of this approach.

5.4 Fermions under measurement

5.4.1 Full-field quantum model

We now generalise the results of Szigeti *et al.* [3, 4] to fermions, using the mean-field approach used to derive the unitary dynamics of an atomic Fermi gas in Section 3.2 and simulated in Chapter 4. We now consider fermionic atoms subjected to the measurement process discussed in Section 5.3 and depicted in Figure 5.2. Intuitively, we expect a density-like measurement of fermionic atoms to be similar to that of bosonic atoms. This is indeed

[13] In the bosonic case, it is actually possible to include higher-order quantum field effects with the number-phase Wigner (NPW) method [78, 79], an approach used by Hush *et al.* [77]. This, however, is beyond the scope of this thesis, particularly as a fermionic generalisation of the method does not yet exist.

the case, which can be shown by a straightforward (but lengthy) minor modification[14] to the full quantum filter derivation of Szigeti *et al.* [3]. This leads to the full-field Itô stochastic master equation:

$$d\hat{\rho}_c = \underbrace{-\frac{i}{\hbar}\left[\hat{H},\hat{\rho}_c\right]dt}_{\text{Unitary evolution}} + \underbrace{\alpha\int dx\mathcal{D}\left[\hat{M}(x)\right]\hat{\rho}_c dt}_{\text{Decoherence}} + \underbrace{\sqrt{\alpha}\int dx\mathcal{H}\left[\hat{M}(x)\right]\hat{\rho}_c dW(x,t)}_{\text{Innovations}}, \quad (5.25)$$

where the filter $\hat{\rho}_c$ now describes a fermionic field, and the measurement operator $\hat{M}(x)$ now accounts for measurement of multiple spin components:

$$\hat{M}(x) = \sum_\sigma \int dx' \hat{\psi}^\dagger_\sigma(x') K_r(x-x') \hat{\psi}_\sigma(x'). \quad (5.26)$$

As before, $K_r(x)$ is the *measurement kernel*, a function which is convolved with the spatial density operator in order to 'blur' it, representing imperfect measurement. We will once again use the harmonic oscillator units of Section 2.3.1, but use a different kernel normalisation to Szigeti *et al.* (c.f. Equation 5.24):

$$K_r(x) = \frac{1}{\sqrt{2\pi}}\int dk \left(\sqrt{\frac{r}{2\Gamma(5/4)}}e^{(-rk)^4/2}\right)e^{ikx}, \quad (5.27)$$

where $\Gamma(s)$ is the gamma function, and we now parameterise measurement precision by the *measurement resolution* r:

$$r \equiv \frac{\sqrt{R_\perp \lambda/\pi}}{2x_0}, \quad (5.28)$$

where $R_\perp$ is the transverse width of the Fermi gas, λ is the wavelength of the measurement laser, and $x_0 = \sqrt{\frac{\hbar}{m\omega_x}}$ is the natural length scale in the x direction. Equation 5.28 is in fact the smallest possible measurement resolution - it is the diffraction limit, and r may be effectively varied to longer length scales by controlling imperfections in the measurement scheme. This normalisation convention ensures that $\int dx|K_r(x)|^2 = 1$, and thus we may vary the measurement resolution independently of the measurement strength. We will use this in Section 6.1 to re-investigate the parameter effects of Szigeti *et al.* [3] that were affected by this inability to vary measurement strength and resolution individually. As a consequence of this normalisation, there is a slight rescaling of the measurement strength α:

$$\alpha \equiv \frac{3\Gamma(5/4)}{16\sqrt{2}\pi^4}\left(\frac{\lambda}{R_\perp}\right)^{3/2}\frac{\Gamma_{sp}}{\omega_x}\frac{\Omega^2}{\Delta^2}, \quad (5.29)$$

where as before, Γ_{sp} is the rate at which a single atom spontaneously emits into the environment, Ω is the Rabi frequency and Δ is the detuning of the laser. This is purely a rescaling of parameters, and so the measurement strength α has the same interpretation as before: a larger α gathers more information about the system state, but also heats it more. It can essentially be arbitrarily controlled by varying the intensity of the measurement laser. The kernel in this form has some useful properties that we use in Section 5.4.2. It

[14] The modified derivation differs only in the (anti)commutation relations of the atomic field, which is of little consequence as most operator algebra in the derivation is for the optical field, which is bosonic in either case. It has been verified [134] to lead to a stochastic master equation of the same form as Equation 5.21.

is even and real, and thus $\hat{M}(x)$ is Hermitian. Furthermore, we have:

$$\int dy K_r(x-y)K_r(x'-y) = \sqrt{\frac{\pi r}{2^{1/4}\Gamma(5/4)}}K_{2^{1/4}r}(x-x'). \tag{5.30}$$

We will also have to evaluate the kernel at the origin:

$$K_r(0) = \frac{1}{\sqrt{2\pi}}\int dk \left(\sqrt{\frac{r}{2\Gamma(5/4)}}e^{(-rk)^4/2}\right) = 2^{1/4}\sqrt{\frac{\Gamma(5/4)}{\pi r}}. \tag{5.31}$$

5.4.2 Mean-field theory: the stochastic FGPE

The fermionic stochastic master equation (5.25) is a full-field quantum model. Once again, for the reasons outlined in Section 1.1, it is computationally intractable to directly integrate. We therefore use a mean-field approach in the vein of Section 3.2, and derive a stochastic version of the FGPE (3.33): that is, the usual mean-field Hamiltonian evolution captured in the FGPE, plus the appropriate stochastic and deterministic terms to account for the probabilistic quantum measurement. This is unfortunately a more involved process than the BEC mean-field theory of Szigeti *et al.* [4] due to the N occupied modes for N fermions, but is nonetheless tractable. The density-like measurement of this model will approximately project the system into a state of well-defined number [4]. Thus, we once again approximate our system's quantum state by a Fock state (number state):

$$|\Psi\rangle = \prod_{n\in S}\hat{c}^\dagger_{n,\uparrow}\hat{c}^\dagger_{n,\downarrow}|0\rangle\,, \tag{5.32}$$

where the $\{\hat{c}^\dagger_{n,\sigma}\}$ are the creation operators for some *arbitrary* single-particle basis with principal index n and spin index σ, and S is some set of distinct principal indices in this basis. We consider a pure state:

$$\hat{\rho}_c = |\Psi\rangle\langle\Psi|\,. \tag{5.33}$$

Once again, we seek an equation of motion for the two-point correlation function:

$$m_\sigma(x_1,x_2) = \left\langle\hat{\psi}^\dagger_\sigma(x_1)\hat{\psi}_\sigma(x_2)\right\rangle = \sum_{n\in S}\chi^*_{n,\sigma}(x_1)\chi_{n,\sigma}(x_2). \tag{5.34}$$

Noting that $dm_\sigma(x_1,x_2) = \mathrm{Tr}\left\{\hat{\psi}^\dagger_\sigma(x_1)\hat{\psi}_\sigma(x_2)d\hat{\rho}_c\right\}$ and substituting the dimensionless form of the stochastic master equation (5.25), we obtain:

$$\begin{aligned} dm_\sigma(x_1,x_2) = -i\,\mathrm{Tr}\left\{\hat{\psi}^\dagger_\sigma(x_1)\hat{\psi}_\sigma(x_2)\left[\hat{H},\hat{\rho}_c\right]\right\}dt + \alpha\int dx\,\mathrm{Tr}\left\{\hat{\psi}^\dagger_\sigma(x_1)\hat{\psi}_\sigma(x_2)\mathcal{D}\left[\hat{M}(x)\right]\hat{\rho}_c\right\}dt \\ + \sqrt{\alpha}\int dx\,\mathrm{Tr}\left\{\hat{\psi}^\dagger_\sigma(x_1)\hat{\psi}_\sigma(x_2)\mathcal{H}\left[\hat{M}(x)\right]\hat{\rho}_c\right\}dW(x,t). \end{aligned} \tag{5.35}$$

As we are considering a pure state, the unitary evolution term of Equation 5.35 is exactly what we derived in Section 3.2. For convenience, we write it as:

$$-i\,\mathrm{Tr}\left\{\hat{\psi}_\sigma^\dagger(x_1)\hat{\psi}_\sigma(x_2)\left[\hat{H},\hat{\rho}_c\right]\right\} = -i\Bigg[\sum_{n\in S}\Big(\chi^*_{n,\sigma}(x_1)\tilde{H}_a(x_2)\chi_{n,\sigma}(x_2) - \chi_{n,\sigma}(x_2)\tilde{H}_a(x_1)\chi^*_{n,\sigma}(x_1)\Big) + U_0\sum_{n,m\in S}\chi^*_{n,\sigma}(x_1)\chi_{n,\sigma}(x_2)\left(|\chi_{m,!\sigma}(x_2)|^2 - |\chi_{m,!\sigma}(x_1)|^2\right)\Bigg]dt, \tag{5.36}$$

where $\tilde{H}_a(x) = -\frac{\hbar^2}{2m}\frac{\partial^2}{\partial x^2} + V_0(x) + V_C(x,t)$ is the position-space representation of the single-particle terms in the Hamiltonian. We now consider the decoherence term of Equation 5.35. Expanding out the decoherence superoperator $\mathcal{D}$ (5.7), using linearity of trace and identifying expectation values, normally ordering the field operators using anticommutation relations, and simplifying, we obtain:

$$\alpha\int dx\,\mathrm{Tr}\left\{\hat{\psi}_\sigma^\dagger(x_1)\hat{\psi}_\sigma(x_2)\mathcal{D}\left[\hat{M}(x)\right]\hat{\rho}_c\right\}dt = \alpha\int dx\Big(K_r(x-x_1)K_r(x-x_2) - \frac{1}{2}K_r(x-x_1)K_r(x-x_1) - \frac{1}{2}K_r(x-x_2)K_r(x-x_2)K_r(x-x_2)\Big)\left\langle\hat{\psi}_s^\dagger(x_1)\hat{\psi}_s(x_2)\right\rangle dt. \tag{5.37}$$

Applying the kernel product property (5.30), evaluating the kernel at the origin (5.31) expanding the expectation value in the Hartree-Fock approximation, and simplifying, this becomes:

$$\alpha\int dx\,\mathrm{Tr}\left\{\hat{\psi}_\sigma^\dagger(x_1)\hat{\psi}_\sigma(x_2)\mathcal{D}\left[\hat{M}(x)\right]\hat{\rho}_c\right\}dt = \alpha\sqrt{\frac{\pi r}{2^{1/4}\Gamma(5/4)}}\left(K_{2^{1/4}r}(x_1-x_2) - 2^{3/8}\pi\right)\cdot\left(\sum_{n\in S}\chi^*_{n,\sigma}(x_1)\chi_{n,\sigma}(x_2)\right)dt. \tag{5.38}$$

We now compute the innovations term of Equation 5.35. Expanding the innovations superoperator (5.13) and noting that $\hat{M}(x)$ is Hermitian, we have:

$$\mathcal{H}\left[\hat{M}(x)\right]\hat{\rho}_c = \hat{M}(x)\hat{\rho}_c + \hat{\rho}_c\hat{M}(x) - 2\left\langle\hat{M}(x)\right\rangle\hat{\rho}_c. \tag{5.39}$$

Inserting Equation 5.39 into the innovations term, using linearity of trace, identifying expectation values, normally ordering with anticommutation relations and simplifying, we obtain:

$$\begin{aligned}\sqrt{\alpha}\int dx\,\mathrm{Tr}&\left\{\hat{\psi}_\sigma^\dagger(x_1)\hat{\psi}_\sigma(x_2)\mathcal{H}\left[\hat{M}(x)\right]\hat{\rho}_c\right\}dW(x,t)\\ &= \sqrt{\alpha}\sum_{\sigma'}\int dx\Big[\left(K_r(x-x_1)+K_r(x-x_2)\right)\left\langle\hat{\psi}_\sigma^\dagger(x_1)\hat{\psi}_\sigma(x_2)\right\rangle\\ &\quad - 2\int dy K_r(x-y)\Big(\left\langle\hat{\psi}_{\sigma'}^\dagger(y)\hat{\psi}_{\sigma'}(y)\right\rangle\left\langle\hat{\psi}_\sigma^\dagger(x_1)\hat{\psi}_\sigma(x_2)\right\rangle\\ &\qquad + \left\langle\hat{\psi}_{\sigma'}^\dagger(y)\hat{\psi}_\sigma^\dagger(x_1)\hat{\psi}_{\sigma'}(y)\hat{\psi}_\sigma(x_2)\right\rangle\Big)\Big]dW(x,t).\end{aligned} \tag{5.40}$$

Applying Wick's Theorem (see Appendix B) to the quartic term, expanding out quadratic expectation values in the Hartree-Fock approximation and simplifying:

$$\sqrt{\alpha}\int dx\,\mathrm{Tr}\left\{\hat{\psi}^\dagger_\sigma(x_1)\hat{\psi}_\sigma(x_2)\mathcal{H}\left[\hat{M}(x)\right]\hat{\rho}_c\right\}dW(x,t) = \sqrt{\alpha}\int dx\Big(\left(K_r(x-x_1)+K_r(x-x_2)\right)$$
$$\cdot\sum_n \chi^*_{n,\sigma}(x_1)\chi_{n,\sigma}(x_2) - 2\int dy K(x-y)\sum_{nm}\chi^*_{n,\sigma}(y)\chi^*_{m,\sigma}(x_1)\chi_{n,\sigma}(x_2)\chi_{m,\sigma}(y)\Big). \quad (5.41)$$

Substituting Equations 5.36, 5.38 and 5.41 into Equation 5.35, our equation of motion for the two-point correlation function is:

$$\begin{aligned} dm_\sigma(x_1,x_2) = -i\Bigg[&\sum_{n\in S}\left(\chi^*_{n,\sigma}(x_1)\tilde{H}_a(x_2)\chi_{n,\sigma}(x_2) - \chi_{n,\sigma}(x_2)\tilde{H}_a(x_1)\chi^*_{n,\sigma}(x_1)\right)\\ &+U_0\sum_{n,m\in S}\chi^*_{n,\sigma}(x_1)\chi_{n,\sigma}(x_2)\left(|\chi_{m,!\sigma}(x_2)|^2 - |\chi_{m,!\sigma}(x_1)|^2\right)\Bigg]dt\\ &+\alpha\sqrt{\frac{\pi r}{2^{1/4}\Gamma(5/4)}}\left(K_{2^{1/4}r}(x_1-x_2)-2^{3/8}\pi\right)\left(\sum_{n\in S}\chi^*_{n,\sigma}(x_1)\chi_{n,\sigma}(x_2)\right)dt\\ &+\sqrt{\alpha}\int dx\Big(\left(K_r(x-x_1)+K_r(x-x_2)\right)\sum_{n\in S}\chi^*_{n,\sigma}(x_1)\chi_{n,\sigma}(x_2)\\ &-2\int dy K(x-y)\sum_{n,m\in S}\chi^*_{n,\sigma}(y)\chi^*_{m,\sigma}(x_1)\chi_{n,\sigma}(x_2)\chi_{m,\sigma}(y)\Big). \quad (5.42)\end{aligned}$$

By the Itô product rule (2.44) and the Hartree-Fock approximation on $m_\sigma(x_1,x_2)$ (3.17), this must match the form:

$$dm_\sigma(x_1,x_2) = \sum_{n\in S}\left(\chi^*_{n,\sigma}(x_1)d\chi_{n,\sigma}(x_2) + d\chi^*_{n,\sigma}(x_1)\chi_{n,\sigma}(x_2) + d\chi^*_{n,\sigma}(x_1)d\chi_{n,\sigma}(x_2)\right), \quad (5.43)$$

We will attempt to find an ansatz for $d\chi_{n,\sigma}(x)$ such that Equations 5.42 and 5.43 are consistent. Finding such an ansatz is difficult without a systematic approach: we will first constrain its form to aid in this process. It must have deterministic terms (that may depend on particle index and spin) and purely local stochastic terms. Thus, the ansatz must be of the form:

$$d\chi_{n,\sigma}(x) = A_{n,\sigma}(x)dt + \int dy B_{n,\sigma}(x,y)dW(y,t), \quad (5.44)$$

where the $A_{n,\sigma}(x)$ and $B_{n,\sigma}(x,y)$ are functions of the $\chi_{n,\sigma}(x,t)$ and are yet to be determined. Substituting Equation 5.44 into Equation 5.43, applying the properties of the Wiener increment $dt^2 = 0$, $dW(y,t)dt = 0$, and $dW(y_1,t)dW(y_2,t) = \delta(y_1-y_2)dt$, and simplifying, we find:

$$\begin{aligned} dm_\sigma(x_1,x_2) = \sum_{n\in S}\Big[&\chi^*_{n,s}(x_1)A_{n,\sigma}(x_2)dt + \int dy B^*_{n,\sigma}(x_1,y)B_{n,\sigma}(x_2,y)dt\\ &+\int dy\left(\chi^*_{n,\sigma}(x_1)B_{n,\sigma}(x_2,y) + B^*_{n,\sigma}(x_1,y)\chi_{n,\sigma}(x_2)\right)dW(y,t)\Big]. \quad (5.45)\end{aligned}$$

Comparing Equation 5.45 to Equation 5.42 allows us to determine[15] the necessary form of $A_{n,\sigma}(x)$ and $B_{n,\sigma}(x,y)$. The correct expressions are:

$$\begin{aligned} A_{n,\sigma}(x) = &-i\tilde{H}(x)\chi_{n,\sigma}(x) - 2^{-5/8}\pi\alpha\chi_{n,\sigma}(x) \\ &+ \alpha\sqrt{\frac{\pi r}{2^{1/4}\Gamma(5/4)}}\left(\sum_{a\in S}\int dz K_{2^{1/4}r}(x-z)\chi^*_{a,\sigma}(z)\chi_{a,\sigma}(x)\chi_{n,\sigma}(z)\right. \\ &\left. - \frac{1}{2}\sum_{a,b\in S}\int dz_1\int dz_2 K_{2^{1/4}r}(z_1-z_2)\chi^*_{a,\sigma}(z_1)\chi^*_{b,\sigma}(z_2)\chi_{n,\sigma}(z_1)\chi_{b,\sigma}(x)\chi_{a,\sigma}(z_2)\right) \end{aligned} \tag{5.46}$$

$$B_{n,\sigma}(x,y) = \sqrt{\alpha}\left(K_r(y-x)\chi_{n,\sigma}(x) - \sum_{a\in S}\int dz K(y-z)\chi^*_{a,\sigma}(z)\chi_{a,\sigma}(x)\chi_{n,\sigma}(z)\right). \tag{5.47}$$

One can easily verify that this choice is correct by substituting Equations 5.46 and 5.47 into Equation 5.45, and observing that this yields Equation 5.42. Thus, we have successfully found the Itô SDE describing the mean-field evolution.

For simulation purposes, it is convenient to cast our SDE to Stratonovich form (as the XMDS2 package [98] is significantly more efficient when performing the Stratonovich integral). The Stratonovich SDE for $d\chi_{n,\sigma}(x)$ can be written:

$$d\chi_{n,s}(x) = \left(A_{n,\sigma}(x) + c_{n,\sigma}(x)\right)dt + \int dy B_{n,\sigma}(x,y)\circ dW(y,t), \tag{5.48}$$

where the $\circ dW(y,t)$ now indicates that the SDE should be integrated using the Stratonovich integral, not the Itô integral, and $c_{n,\sigma}(x)$ is the *Stratonovich correction*, given by (c.f. Equation 2.47):

$$\begin{aligned} c_{n,\sigma}(x) = &-\frac{1}{2}\sum_{m\in S,\sigma'}\int dy\int dx' B_{m,\sigma'}(x',y)\partial_{\chi_{m,\sigma'}(x',t)}B_{n,\sigma}(x,y) \\ &- \frac{1}{2}\sum_{m\in S,\sigma'}\int dy\int dx' B^*_{m,\sigma'}(x',y)\partial_{\chi^*_{m,\sigma'}(x',t)}B_{n,\sigma}(x,y). \end{aligned} \tag{5.49}$$

This can be computed by substituting Equations 5.46 and 5.47 into Equation 5.49, summing and integrating over all delta functions, combining identical terms, using the kernel product property (5.30), and applying the identity:

$$\sum_{m\in S}\int dz\chi^*_{m,\sigma}(z)\chi_{m,\sigma}(x)\chi_{n,\sigma}(z) = \sum_{m\in S}\delta_{mn}\chi_{n,\sigma}(x) = \chi_{n,\sigma}(x). \tag{5.50}$$

[15] We are able to match the necessary form of $B_{n,\sigma}(x,y)$ by comparing the stochastic terms. Then, the deterministic term in Equation 5.45 can be expanded out, and the necessary form of the $A_{n,\sigma}(x)$ can be determined to offset this and yield the correct expression.

Thus, the Stratonovich correction is:

$$c_{n,\sigma}(x) = -2^{-5/8}\pi\alpha\chi_{n,\sigma}(x)+\alpha\sqrt{\frac{\pi r}{2^{1/4}\Gamma(5/4)}}\Bigg(\sum_{m\in S}\int dz K_{2^{1/4}r}(x-z)\chi^*_{m,\sigma}(z)\chi_{m,\sigma}(x)\chi_{n,\sigma}(z)$$
$$-\frac{3}{2}\sum_{a,b\in S}\int dz_1\int dz_2 K_{2^{1/4}r}(z_1-z_2)\chi^*_{b,\sigma}(z_2)\chi^*_{a,\sigma}(z_1)\chi_{b,\sigma}(x)\chi_{a,\sigma}(z_2)\chi_{n,\sigma}(z_1)\Bigg). \quad (5.51)$$

Substituting Equations 5.46, 5.47 and 5.51 into Equation 5.48 and simplifying, the mean-field Stratonovich SDE for the wavefunctions $\chi_{n,\sigma}(x)$ is:

$$d\chi_{n,\sigma}(x) = \Bigg[-i\tilde{H}(x)\chi_{n,\sigma}(x)+2\alpha\sqrt{\frac{\pi r}{2^{1/4}\Gamma(5/4)}}\Big(\sum_{a\in S}\int dz K_{2^{1/4}r}(x-z)\chi^*_{a,\sigma}(z)\chi_{a,\sigma}(x)\chi_{n,\sigma}(z)$$
$$-\sum_{a,b\in S}\int dz_1\int dz_2 K_{2^{1/4}r}(z_1-z_2)\chi^*_{a,\sigma}(z_1)\chi^*_{b,\sigma}(z_2)\chi_{b,\sigma}(x)\chi_{a,\sigma}(z_2)\chi_{n,\sigma}(z_1)\Big)\Bigg]dt$$
$$+\sqrt{\alpha}\int dy\left(K_r(y-x)\chi_{n,\sigma}(x)-\sum_{a\in S}\int dz K_r(y-z)\chi^*_{a,\sigma}(z)\chi_{a,\sigma}(x)\chi_{n,\sigma}(z)\right)\circ dW(y,t). \quad (5.52)$$

We will henceforth refer to Equation 5.52 as the *stochastic fermion GPE* (SFGPE). We have successfully reduced the full-field quantum model of fermions under measurement (5.25) to a much simpler problem with the dimensionality of the FGPE (3.33), since we need only follow the evolution of N single-particle wavefunctions. This is still more complicated than the FGPE: each trajectory is an FGPE driven by white noise and decoherence, but we must average over hundreds of these trajectories for a good estimate of the system's average behaviour. Nonetheless, we may still tractably study the system for a moderate number of particles by following the procedure described in Section 5.2.1. It is once again important to realise that each of these individual trajectories has real physical meaning, and is the actual outcome of the system for particular measurement results.

5.5 The single-particle limit

Much of the essential physics of feedback control - in particular, parameter dependence of measurement backaction effects - can be seen in the single-particle limit. This also provides an important comparison to previous works in feedback cooling of bosonic species. Exchange symmetry has no effect for a single particle, and so we should expect the single-particle limit of the fermionic model to agree with the single-particle limit of the bosonic model, which was derived and studied in Ref. [3]. In the limit of a single particle, our system is described by a single wavefunction $\chi(x)$. Thus, the SFGPE (5.52) reduces to the *stochastic Schrödinger equation*:

$$d\chi(x) = \Big[-i\tilde{H}_a(x)\chi(x) + 2\alpha\Big(m(x)-\bar{m}\Big)\chi(x)\Big]\,dt + \sqrt{\alpha}\left[\vartheta(x)-\bar{\vartheta}\right]\chi(x), \quad (5.53)$$

where:

$$\begin{aligned} m(x) &= \sqrt{\frac{\pi r}{2^{1/4}\Gamma(5/4)}} \int dz K_{2^{1/4}r}(x-z)|\chi(z)|^2, \\ \bar{m} &= \int dz m(z)|\chi(z)|^2, \\ \vartheta(x) &= \int dy K_r(y-x) \circ dW(y,t), \\ \bar{\vartheta} &= \int dz \vartheta(z)|\chi(z)|^2. \end{aligned} \tag{5.54}$$

As we would expect, this is the same as the single-particle limit of the bosonic model (see Ref. [3], or set $N = 1$ in the mean-field theory of Ref. [4]). There is a minor difference in some constants due to the different normalisation of the measurement kernel, but this is exactly what we would obtain by using our kernel normalisation (5.27) in the model of Ref. [3].

We now have the tools to simulate a single particle under measurement. Although we used mean-field theory to derive the SFGPE (5.52), the assumption of well-defined number is exactly true for a single particle. Thus, the stochastic Schrödinger equation (5.53) is exact: there is no approximation made to simplify the quantum field.[16]

5.6 Summary of measurement theory

In this chapter, we have introduced the theory to include measurement effects in quantum dynamics, and used this to derive the tools to simulate continuously measured fermions. In Section 5.1, we reviewed the fundamentals of system-reservoir methods for open quantum systems, introducing Lindbladian evolution and decoherence processes. In Section 5.2, we discussed generalisations to these techniques that allowed us to model open quantum systems for which the Hamiltonian was correlated with the quantum state (such as a feedback-controlled system in which measurement results are used to make decisions about how to control the system). In Section 5.3, we summarised the model and results of Szigeti *et al.* [3, 4], introducing phase-contrast imaging to continuously monitor the density of a Bose or Fermi gas. In Section 5.4, we introduced a fermionic version of this model, and derived a multimode fermionic equivalent to the mean-field theory of BECs in Ref. [4], culminating in the SFGPE (5.52), which is of much higher dimension than the mean-field theory of Szigeti *et al.*, since it requires N wavefunctions for N fermions. Finally, in Section 5.5, we showed how a stochastic Schrödinger equation (5.53) emerges as the single-fermion limit of the SFGPE, and noted that this agrees with the single-boson limit studied in Ref. [3].

[16] We have assumed system-filter convergence, but this is unrelated to the dimensionality of the system.

Chapter 6

Feedback cooling with measurement effects

In Chapter 4, we considered a simple model of feedback control of fermions which neglected the effect of measurement backaction. Using this model, we showed that an atomic Fermi gas can be feedback cooled arbitrarily close to its ground state using the energy-damping control, given sufficient time. However, the cooling rates became extremely slow closer to the ground state, and furthermore, were slower for more particles. In a realistic model of feedback control, these cooling rates must compete with measurement-induced heating rates, casting doubt on the best-case results obtained in Chapter 4. In this chapter, we use the tools developed in Chapter 5 to simulate feedback control of an atomic Fermi gas undergoing a continuous density measurement, providing a more realistic assessment of the capabilities and limitations of our feedback control schemes.

In Section 6.1 we simulate the stochastic Schrödinger equation (5.53) to understand the dynamics (Section 6.1.3) and parameter dependence (Sections 6.1.4 and 6.1.5) of a single fermion undergoing measurement and feedback control. In Section 6.2 we extend these results to many fermions by simulating the SFGPE (5.52), showing that the energy-damping control scales poorly for a large number of atoms (Section 6.2.2) and discussing the effect of interatomic scattering interactions (Section 6.2.3).

All simulations in this chapter were implemented using the XMDS2 open-source software package [98] and executed on the Raijin supercomputer at the National Computational Infrastructure. All quantities in this chapter are given in the harmonic oscillator units of Section 2.3.1.

6.1 Feedback control of a single fermion with measurement effects

The limit of a single atom contains much of the essential physics of feedback control. Recall that in Section 5.5, we derived the (Stratonovich) stochastic Schrödinger equation for the conditional state of a single fermion undergoing density measurement via phase-contrast imaging:

$$d\chi(x) = \left[-i\tilde{H}_a(x)\chi(x) + 2\alpha\Big(m(x) - \bar{m}\Big)\chi(x)\right] dt + \sqrt{\alpha}\left[\vartheta(x) - \bar{\vartheta}\right]\chi(x), \tag{6.1}$$

where:

$$\begin{aligned} m(x) &= \sqrt{\frac{\pi r}{2^{1/4}\Gamma(5/4)}} \int dz K_{2^{1/4}r}(x-z)|\chi(z)|^2, \\ \bar{m} &= \int dz m(z)|\chi(z)|^2, \\ \vartheta(x) &= \int dy K_r(y-x) \circ dW(y,t), \\ \bar{\vartheta} &= \int dz \vartheta(z)|\chi(z)|^2. \end{aligned} \tag{6.2}$$

The system dynamics will depend on the measurement strength α, the measurement resolution r, and the feedback parameters (k_{ED} for the energy-damping control and c_j for the moment control). These all alter the effectiveness of feedback control. We are limited in the number of simulations we can conduct for many particles with the SFGPE (5.52), since it is $\mathcal{O}(N^3)$ for fixed dimension and must also be averaged over hundreds of trajectories. Thus, the single-atom limit is an opportunity to tractably study how measurement effects depend on system parameters. As noted in Section 5.5, the single-boson and single-fermion limit are identical, and so this limit is an important link between the present study of Fermi gases and previous studies of BECs under the same measurement scheme [3, 4, 77]. It is also exact and does not rely upon any state approximations or mean-field theories, and is thus an important test case when considering the validity of our approximations.

The single-atom limit was previously simulated by Szigeti *et al.* [3], but there are good reasons to investigate it further in this thesis. As noted in Section 5.4.1, the kernel normalisation used by Szigeti *et al.* meant that measurement resolution could not be varied independently of measurement strength, and so their conclusions regarding the effect of measurement resolution are not necessarily correct. Furthermore, they only simulated the moment control, and so it is useful to gain an understanding of the comparative performance of the energy-damping and moment controls when measurement effects are accounted for.

In this section, we simulate a single fermion undergoing measurement and feedback control. All simulations shown in this section[1] were conducted with the same initial wavefunction constructed from a random superposition of the first 30 Hermite-Gauss modes, with density profile depicted in Figure 6.1. This state has a significant energy ($E_0 = 8.394\hbar\omega$) relative to the ground state and is chosen by a random procedure. It thus lacks any symmetries or special structure that would hide important effects in the system.

6.1.1 Efficient simulation of the stochastic Schrödinger equation

When simulating the system using the stochastic Schrödinger equation (6.1), we must average over hundreds of trajectories per simulation to accurately estimate average behaviour, and furthermore run many simulations to understand the effects of different parameter combinations. It is thus extremely important that we compute our evolution in the most computationally efficient manner possible. A significant optimisation can be achieved by

[1] The long-term behaviour of the system is extremely robust to initial state, but we used the same initial state between simulations for consistency.

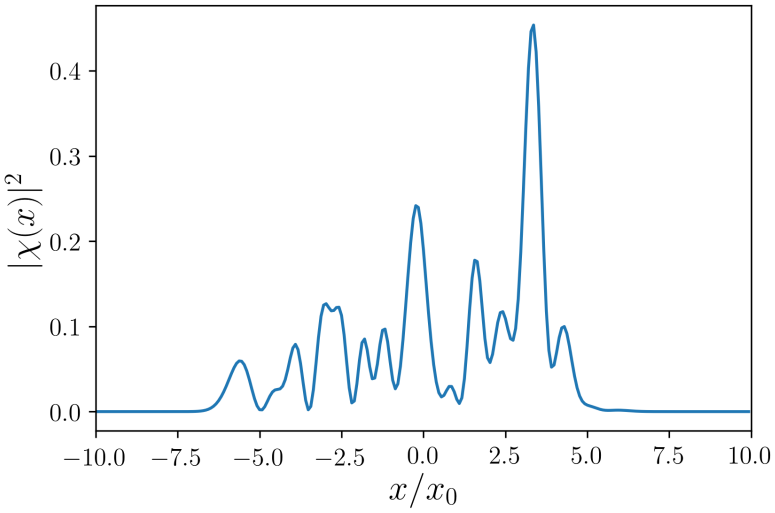

Figure 6.1: The probability density of the initial wavefunction used for all single-fermion measurement simulations in this thesis. The state has energy $E_0 = 8.394\hbar\omega$.

exploiting properties of *convolutions*.

A convolution $(f \star g)(x)$ of functions $f(x)$ and $g(x)$ is an integral of the form:

$$(f \star g)(x) = \int_{-\infty}^{\infty} dy f(y) g(x-y). \tag{6.3}$$

Direct numerical integration of Equation 6.3 on D grid points has complexity $\mathcal{O}(D^2)$, since we must compute an $\mathcal{O}(D)$ integral at each of the D grid points. Fortunately, the convolution theorem allows us to compute this as a product in Fourier space:

$$(f \star g)(x) = \sqrt{2\pi}\mathcal{F}^{-1}\left\{\mathcal{F}\left\{f(x)\right\}(k) \cdot \mathcal{F}\left\{g(x)\right\}(k)\right\}(x). \tag{6.4}$$

The most computationally expensive parts of this calculation are the Fourier transforms $\mathcal{F}[\cdot]$, which may be computed in $\mathcal{O}(D \log D)$ using the fast Fourier transform (FFT). This enables much faster computation of convolutions.

In the stochastic Schrödinger equation (6.1), the most computationally expensive terms are convolutions. We may compute $m(x)$ and $\vartheta(x)$ (Equation 6.2) in $\mathcal{O}(D \log D)$ using this approach:

$$\begin{aligned}
m(x) &= \sqrt{\frac{\pi r}{2^{1/4}\Gamma(5/4)}} \int dz K_{2^{1/4}r}(x-z)|\chi(z)|^2 \\
&= \sqrt{\frac{2^{7/4}\pi^2 r}{\Gamma(5/4)}}\mathcal{F}^{-1}\left\{\mathcal{F}\left\{K_{2^{1/4}r}(x)\right\}(k) \cdot \mathcal{F}\left\{|\chi(x)|^2\right\}(k)\right\}(x), \\
\vartheta(x) &= \int dy K_r(y-x) \circ dW(y,t) \\
&= \sqrt{2\pi}\mathcal{F}^{-1}\left\{\mathcal{F}\left\{K_r(x)\right\}(k) \cdot \mathcal{F}\left\{\circ\, dW(x,t)\right\}(k)\right\}(x).
\end{aligned} \tag{6.5}$$

Consequently, each time evolution step is $\mathcal{O}(D \log D)$, as there are no terms in the stochastic Schrödinger equation (6.1) that are more costly to compute. Further simplification is possible by reducing the number of FFTs required. The efficient computation of $\vartheta(x)$ (6.5) requires the Fourier transform of the Wiener process $dW(x,t)$. However, this can be constructed directly in k-space using a real Wiener process in k-space, denoted $\eta(k,t)$:

$$\mathcal{F}\Big\{ \circ\, dW(x,t) \Big\}(k) = \frac{1}{2}\,(i-1)\,(\circ\eta(k,t) + i \circ \eta(-k,t))\,, \tag{6.6}$$

thus saving us one FFT. The unitary terms are also computed using spectral methods (Section 2.3.2), and so are also $\mathcal{O}(D \log D)$.

6.1.2 Choice of control

In Chapter 4, we found that the energy-damping control vastly outperformed the moment control for $n \leq 2$, even in the absence of measurement backaction. Although both are experimentally feasible, a currently planned experimental implementation of the BEC feedback control modelled in Refs. [3, 4] will use the moment control [135], and so it is pertinent to determine whether it would be effective for Fermi gases. It is particularly important to choose an effective control before doing extensive simulations, since the stochastic simulations of this chapter are computationally demanding.

Recall from Chapter 4 that the moment control for $n \leq 2$ removes energy by damping oscillations in $\langle \hat{x} \rangle$ and $\langle \hat{x}^2 \rangle$, relying on nonlinearities to couple higher-order oscillations into the controlled moments. In the case of a single atom, there are no nonlinear scattering interactions, but the measurement process induces a slight nonlinearity [3]. As we saw in Chapter 4, the moment control is extremely efficient in damping oscillations in $\langle \hat{x} \rangle$ and $\langle \hat{x}^2 \rangle$, so oscillations coupled into these moments will be rapidly damped. However, the measurement will continuously create oscillations in all moments of atomic density. Thus, successful cooling depends almost entirely on the competition between this coupling rate and the measurement-induced heating rate.

We also saw in Chapter 4 that the energy-damping control is largely independent of scattering properties, since it directly removes energy from all moments. In the absence of measurement backaction, it appeared to be vastly superior. This effect is even more pronounced when accounting for measurement effects - we see in Figure 6.2 that for the same initial state and very weak measurement ($\alpha = 0.005$), the energy-damping control rapidly brings the atom close to its ground state, whereas the moment control rapidly removes a small amount of energy and is then overcome by measurement-induced heating.

As discussed extensively in Refs. [2, 4], for BECs the moment control is extremely reliant on a strong nonlinearity to provide inter-moment coupling, and had only modest performance. As we saw in Chapter 4, the scattering properties of fermions are poor, and this is not a useful approach for fermionic species (which should not come as a suprise, since the poor scattering properties of fermions are the key limitation in evaporative cooling of fermions, motivating this entire thesis). Furthermore, as discussed in Section 3.3.2, a two-component Fermi gas will phase-separate for strong repulsive interactions. It thus seems likely that the moment control would be even worse for many fermions, and so we will only apply the energy-damping control for the remainder of this chapter.

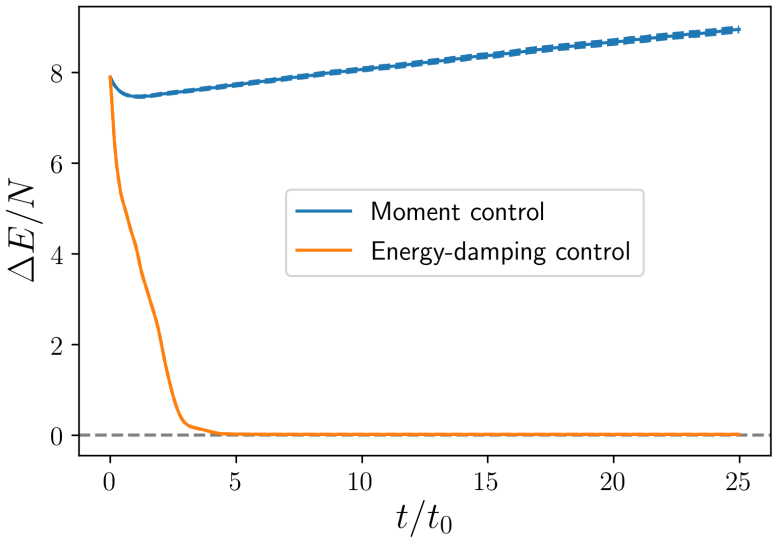

Figure 6.2: A comparison of near-optimal feedback cooling with the moment control ($c_1 = 2$, $c_2 = 0.025$) and the energy-damping control ($k_{\mathrm{ED}} = 4$) for very weak measurement ($\alpha = 0.005$) and $r = 0.1$. Solid lines depict the mean of 300 trajectories, and coloured dashed lines indicate twice the standard error in the mean (95% confidence interval). The energy-damping control succeeds in cooling the system close to the ground state, equilibrating at a small excitation energy. The moment control initially removes some energy, but is overcome by the heating rate.

6.1.3 Dynamics of feedback cooling under measurement

Now that we have selected a control, we aim to better understand the dynamics of our system under measurement and feedback control. The *average* behaviour is qualitatively the same across parameter combinations: the energy E_0 rapidly decreases until it reaches an equilibrium between average cooling rate and average heating rate. The system approaches an eqiulibrium energy above the ground state, which varies depending on system parameters. In Chapter 4, since we could always get a single spatial mode or multiple interacting spatial modes arbitrarily close to the ground state, we used the speed of the cooling as our metric for success. However, since the system quickly reaches an equilibrium when measurement is accounted for, we will now use this equilibrium energy as our measure of success, and our goal is to achieve the lowest possible equilibrium excitation energy per particle.

It is important to distinguish between the system's average and conditional (single-trajectory) behaviour. We compare the dynamics of a single trajectory to the mean of hundreds of trajectories in Figure 6.3. The average energy displays the aforementioned behaviour, rapidly decreasing to an equilibrium above the ground state. However, at 'equilibrium', the single trajectory continues to fluctuate about a well-defined mean, since the measurement process is probabilistic. Similarly, the average density of the system approaches a smooth Gaussian close to that of the ground state, and the density fluctuations mostly average out in the long-term limit, but significant density fluctuations continue forever for a single trajectory (which are the reason the system has nonzero excitation energy).

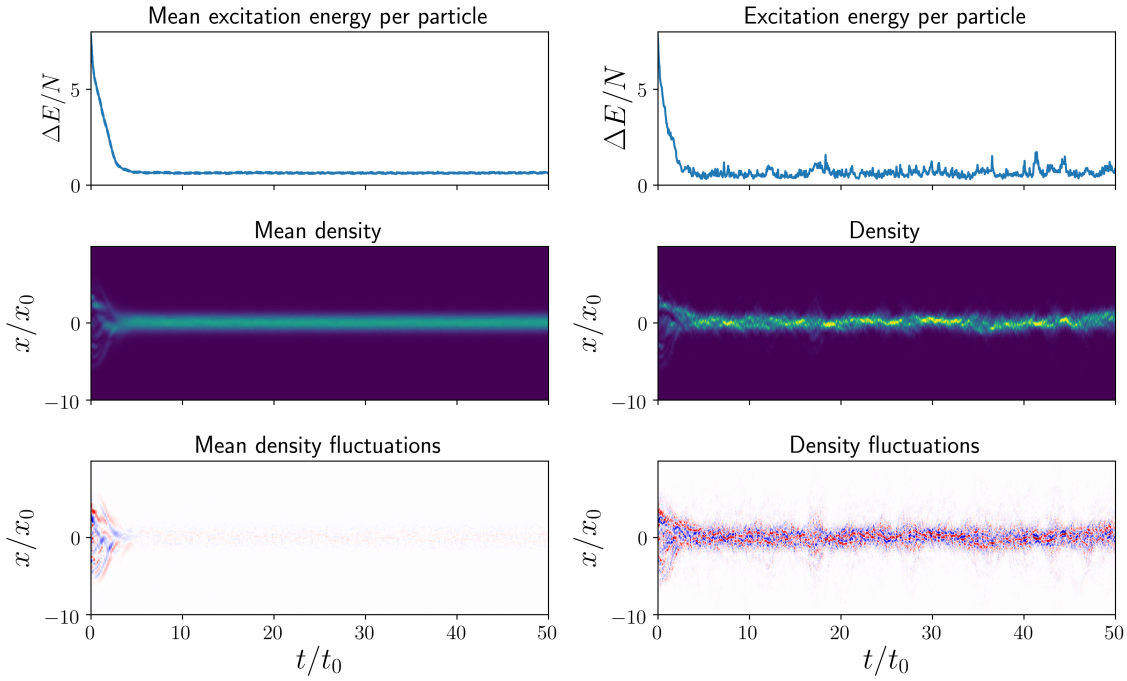

(a) The mean dynamics of 300 trajectories.

(b) The dynamics of a single trajectory.

Figure 6.3: A comparison of the mean dynamics of a single particle across 300 stochastic trajectories and the dynamics of a single trajectory. The average energy quickly decreases, reaching an equilibrium between heating and feedback cooling rates and an equilibrium energy above the ground state. For a single trajectory, fluctuations about this mean continue due to random measurement noise. Similarly, the mean density profile quickly approaches a Gaussian distribution close to the ground state, but density fluctuations about this mean continue on average. In the long-term limit, these density fluctuations mostly average out, but are non-negligible for a given trajectory.

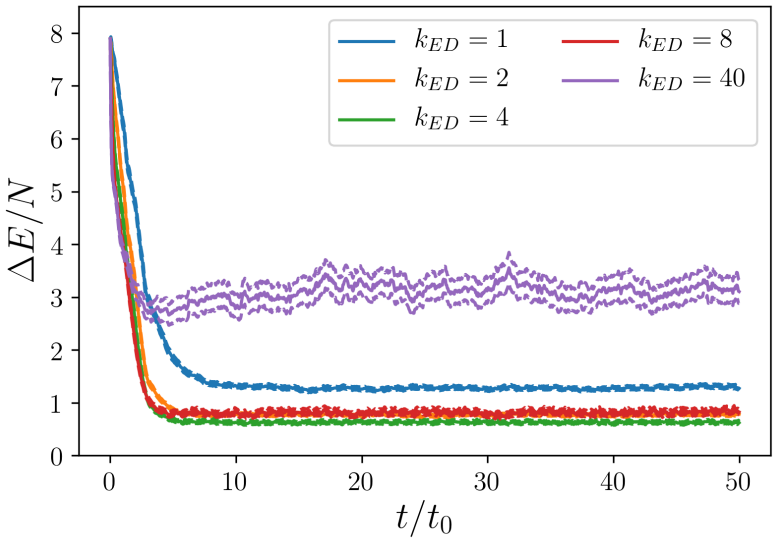

Figure 6.4: Feedback cooling with the energy-damping control across a range of values of k_{ED}, for $\alpha = 0.2$ and $r = 0.1$. Solid lines depict the mean of 300 trajectories, and coloured dashed lines indicate twice the standard error in the mean (95% confidence interval). The near-optimal value of $k_{\mathrm{ED}} = 4$ produces the lowest equilibrium energy of those simulated.

6.1.4 Control optimisation

Much like the no-measurement limit (Chapter 4), the control strength k_{ED} must be chosen judiciously to achieve the best results. Fortunately, the equilibrium behaviour is robust to variations in initial state, and so the dependence on initial state seen in Chapter 4 only has a strong effect on transient behaviour irrelevant to the equilibrium energy. For the reasons outlined in Section 4.5.2, it is still highly dependent on particle number. The optimal control can be chosen by varying k_{ED} and selecting the value that results in the lowest equilibrium energy, as depicted in Figure 6.4.

6.1.5 Effect of measurement parameters α and r

The measurement strength α and measurement resolution r have a strong effect on the equilibrium energy, shown by Szigeti *et al.* for both a single atom [3] and a many-atom BEC [4].

Recall that the measurement strength (5.29) is defined as:

$$\alpha \equiv \frac{3\Gamma(5/4)}{16\sqrt{2}\pi^4}\left(\frac{\lambda}{R_\perp}\right)^{3/2}\frac{\Gamma_{sp}}{\omega_x}\frac{\Omega^2}{\Delta^2}, \tag{6.7}$$

where Γ_{sp} is the rate at which a single atom spontaneously emits into the environment, Ω is the Rabi frequency and Δ is the detuning of the laser. It depends on the laser intensity via Ω, and so can easily be controlled; a more intense laser will lead to a higher α. A large α gathers more information about the system state, but also results in greater heating via measurement backaction. As demonstrated in Figure 6.5, the equilibrium excitation energy per particle increases approximately linearly with α, and so it follows that we should measure the system as weakly as possible for the best cooling.

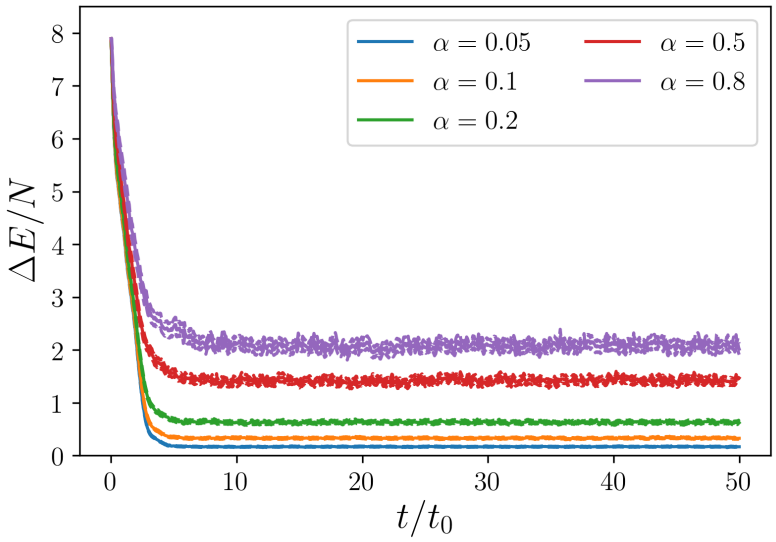

Figure 6.5: Feedback cooling with a near-optimal energy-damping control ($k_{\mathrm{ED}} = 4$) and $r = 0.1$ across a range of values of measurement strength α. Solid lines depict the mean of 300 trajectories, and coloured dashed lines indicate twice the standard error in the mean (95% confidence interval). The equilibrium excitation energy increases approximately linearly with α.

Recall that the measurement resolution r (5.28) is defined as:

$$r \equiv \frac{\sqrt{R_\perp \lambda/\pi}}{2x_0}, \tag{6.8}$$

where $R_\perp$ is the transverse width of the atomic wavefunction, λ is the wavelength of the laser, and x_0 is the longitudinal length scale $x_0 = \sqrt{\frac{\hbar}{m\omega_x}}$.

Szigeti *et al.* found that a smaller measurement resolution[2] led to a larger equilibrium energy [3, 4], but as mentioned in Section 5.3, their kernel normalisation meant that r could not be varied without inadvertently changing the measurement strength as a result. Consequently, their conclusions must be verified using our normalisation, which allows independent variation of r and α.

Since r is bounded below by the diffraction limit (6.8), it is important to consider experimentally realistic values. ^{6}Li is a fermionic species commonly used for cold atom experiments, and its useful properties can be found in Appendix A of Ref. [136]. We will consider the use of light detuned from the $2^2S_{1/2} \leftrightarrow 2^2P_{3/2}$ resonance, and thus $\lambda \sim 671$nm. For an effective 1D or 2D system, typical trapping frequencies are on the order of ∼20Hz in the longitudinal direction(s), with an aspect ratio of 1:200 being experimentally feasible [92]. Therefore, we choose a longitudinal length scale of $x_0 \sim 2$ microns. To estimate the perpendicular width $R_\perp$, we consider the width of a non-interacting Fermi gas with N_σ particles per spin component. The contribution from the nth level in the Fermi sea is:

$$\langle \phi_n | \hat{x}^2 | \phi_n \rangle = \frac{\hbar}{2m\omega_\perp} \langle \phi_n | (\hat{a}^\dagger + \hat{a})^2 | \phi_n \rangle = \frac{\hbar}{m\omega_\perp} \left(n + \frac{1}{2} \right). \tag{6.9}$$

[2] Szigeti *et al.* actually parameterised measurement resolution in terms of the Lamb-Dicke parameter $\eta = k_0 x_0$, but a large η is equivalent to a small r.

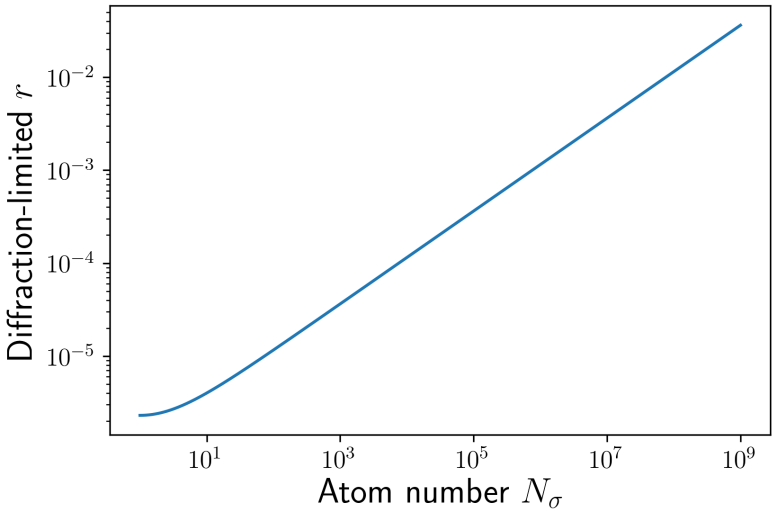

Figure 6.6: The diffraction-limited measurement resolution r as a function of atom number N_σ.

and thus an estimate of the width of the Fermi gas is given by:

$$R_\perp \approxeq \sum_{n=0}^{N_\sigma} \sqrt{\frac{1}{N_\sigma}\frac{\hbar}{m\omega_\perp}\left(n+\frac{1}{2}\right)} = \sqrt{\frac{\hbar}{m\omega_\perp}}\left(\frac{1+N_\sigma}{\sqrt{2N_\sigma}}\right). \tag{6.10}$$

A plot of the diffraction-limited r with respect to N_σ is provided in Figure 6.6. Even for an extremely large Fermi gas of $N_\sigma = 10^9$ we have $r \sim 0.036$, which is below the limit of what we can represent accurately in our simulation ($r \sim 0.05$) anyway, since small r leads to a very narrow kernel that requires a large number of grid points to resolve. Current experimental technology can achieve a resolution of ∼5 microns, which corresponds to $r \sim 0.1$ in a typical trap. Thus, we will use this value in most of our simulations, and it is realistic to vary it to the lowest representable limit.

In Figure 6.7, we vary r, showing that a smaller measurement resolution *does* actually result in a higher equilibrium energy. This intuitively makes sense: a more precise measurement places tighter limits on the localisation of the atom, resulting in greater wavefunction narrowing in position space and thus a greater increase in kinetic energy. In the limit $r \to 0$, the kernel (5.27) becomes a delta function, and so the measurement approaches a perfect one, which we know to be impossible. The heating increases without bound in this limit as a result. Consequently, the conclusions made about measurement resolution by Szigeti *et al.* [3, 4] were indeed correct. We have confirmed that a less precise measurement leads to the lowest heating and thus lowest equilibrium energy.

Although it is physically reasonable to expect weaker measurement to result in a colder system, we should be cautious in extrapolating these results to extremely small α or extremely large r. Our results suggest that we should measure as weakly and imprecisely as possible in order to obtain the best cooling. Yet, we need information about the system's state in order to apply an effective control, and a very weak and/or imprecise measurement will gather almost no information about the system. What have we missed in our model?

The answer lies in the assumptions discussed in Section 5.2.2. In keeping with previous

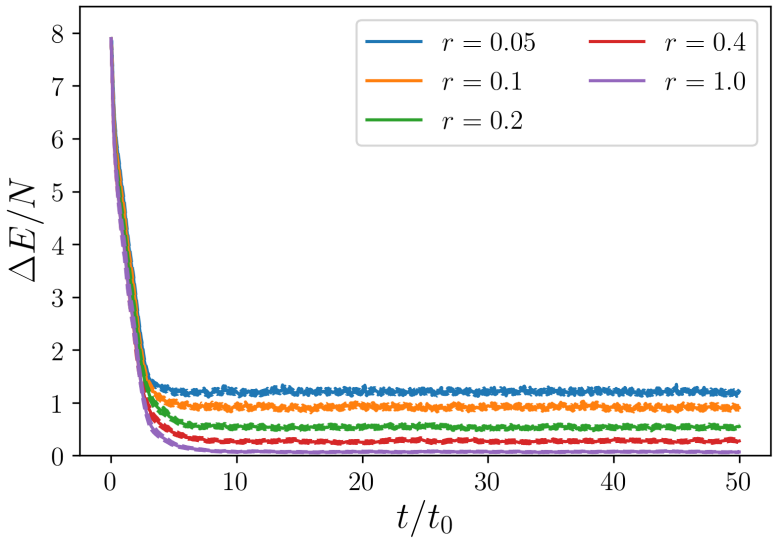

Figure 6.7: Feedback cooling with a near-optimal energy-damping control ($k_{\mathrm{ED}} = 4$) and measurement strength $\alpha = 0.3$ across a range of values of measurement resolution r. Solid lines depict the mean of 300 trajectories, and coloured dashed lines indicate twice the standard error in the mean (95% confidence interval). A smaller measurement resolution results in a higher equilibrium energy.

works for BECs [3, 4, 77], we treated the system and filter interchangeably, and did not include a system-filter separation nor a classical corrupting noise channel in the measurement. That is, we assumed that the experimenter's best estimate perfectly corresponds to the underlying system state. This will not be true if the measurement is arbitrarily weak and/or imprecise. Although eventual system-filter convergence is typically a safe assumption [132], the convergence takes time, on a time scale determined by α and r. Thus, gathering a small amount of information about the system will result in a longer convergence time. If the experimenter's best estimate of the state is inaccurate for too long, then the control may be ineffective (and even cause heating). There may therefore be some threshold beyond which the measurement signal is overpowered by corrupting classical noise and poorly-applied feedback, and convergence cannot be maintained.

It is certainly true that to minimise equilibrium energy, we should choose the system parameters that result in the weakest measurement for which the system and filter converge. However, without a system-filter separation, we cannot place lower bounds on how weakly we can measure and preserve convergence. In Section 7.1.3, we will discuss how this can be rectified, and propose a method by which one could cool to the limit of the corrupting noise channel.

6.2 Feedback control of many fermions with measurement effects

Although the single-atom limit is an excellent testbed to understand the parameter dependence and qualitative behaviour of feedback-controlled quantum gases undergoing continuous measurement, it does not capture the unique behaviour of fermions. In particular, we saw in Chapter 4 that the effectiveness of feedback cooling with the energy-damping control

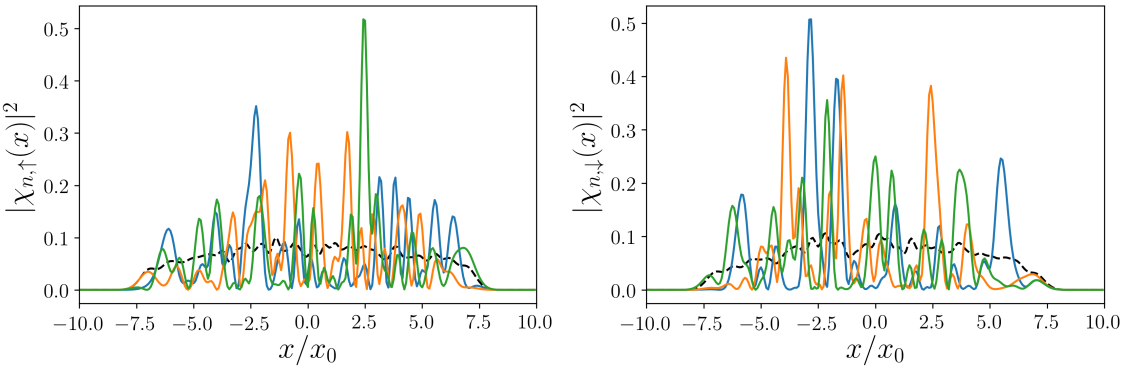

(a) The spin-up initial state.

(b) The spin-down initial state.

Figure 6.8: The probability densities of a selection of initial wavefunctions (solid coloured lines) and the spin-component averages (black dashed lines) for both spin components of the initial state.

depended on the number of particles and the presence of nonlinear scattering interactions. Recall that multiple fermionic atoms undergoing continuous density measurements in the Hartree-Fock approximation are described by the SFGPE (5.52):

$$d\chi_{n,\sigma}(x) = \Bigg[-i\tilde{H}(x)\chi_{n,\sigma}(x)+2\alpha\sqrt{\frac{\pi r}{2^{1/4}\Gamma(5/4)}}\Big(\sum_{a\in S}\int dz K_{2^{1/4}r}(x-z)\chi^*_{a,\sigma}(z)\chi_{a,\sigma}(x)\chi_{n,\sigma}(z)$$
$$-\sum_{a,b\in S}\int dz_1\int dz_2 K_{2^{1/4}r}(z_1-z_2)\chi^*_{a,\sigma}(z_1)\chi^*_{b,\sigma}(z_2)\chi_{b,\sigma}(x)\chi_{a,\sigma}(z_2)\chi_{n,\sigma}(z_1)\Big)\Bigg]dt$$
$$+\sqrt{\alpha}\int dy\left(K_r(y-x)\chi_{n,\sigma}(x)-\sum_{a\in S}\int dz K_r(y-z)\chi^*_{a,\sigma}(z)\chi_{a,\sigma}(x)\chi_{n,\sigma}(z)\right)\circ dW(y,t). \tag{6.11}$$

In this section, we simulate the SFGPE, with the aim of determining how the effectiveness of feedback cooling varies with N when measurement effects are accounted for, and what effect the nonlinearity has. With regard to the initial states for simulations in this section, we constructed two sets (corresponding to spin up and down) of 20 orthogonal wavefunctions of similar energies from superpositions of the first 30 Hermite-Gauss modes. Each initial state consisted of N single-particle wavefunctions selected from these sets. The initial states are depicted in Figure 6.8 - however, once again the results are robust to variations in initial state. Much like the single-particle initial state of Section 6.1, these wavefunctions have significant initial energy and are chosen by a random procedure, avoiding any symmetries that would hide important effects. Notably, the initial state is also spin-asymmetric.

6.2.1 Efficient simulation of the SFGPE

Although stochastic simulations of a single atom are demanding due to the need to average over hundreds of trajectories, the situation is much more dire for multiple fermions. A time-evolution step of the SFGPE (6.11) is much more expensive to calculate than that of its bosonic equivalent (Equation 25, Ref. [4]) or the stochastic Schrödinger equation (6.1).

For example, the second deterministic measurement term has a double sum over particle index and two spatial integrals, leading to a complexity[3] of $\mathcal{O}(N^3D^3)$. Representing more particles will require more grid points, since the wavefunctions $\chi_{n,\sigma}(x)$ must be orthogonal, and this scaling is superlinear. Thus, for a naive approach, the scaling of each time step is worse than $\mathcal{O}(N^6)$ - we have no hope of ever scaling such an approach to a large number of particles! Fortunately, we may follow the approach of Section 6.1.1 and simplify this using convolutions. The first deterministic measurement term of the SFGPE (6.11) is a sum over a convolution:

$$\sum_{a\in S}\int dz K_{2^{1/4}r}(x-z)\chi^*_{a,\sigma}(z)\chi_{a,\sigma}(x)\chi_{n,\sigma}(z)$$
$$=\sqrt{2\pi}\sum_{a\in S}\mathcal{F}^{-1}\left\{\mathcal{F}\left\{K_{2^{1/4}r}(x)\right\}(k)\cdot\mathcal{F}\left\{\chi^*_{a,\sigma}(z)\chi_{a,\sigma}(x)\chi_{n,\sigma}(x)\right\}(k)\right\}(x), \quad (6.12)$$

and thus we have reduced this from $\mathcal{O}(N^2D^2)$ to $\mathcal{O}(N^2D\log D)$. The second deterministic measurement term may similarly be written:

$$\sum_{a,b\in S}\int dz_1\int dz_2 K_{2^{1/4}r}(z_1-z_2)\chi^*_{a,\sigma}(z_1)\chi^*_{b,\sigma}(z_2)\chi_{b,\sigma}(x)\chi_{a,\sigma}(z_2)\chi_{n,\sigma}(z_1)$$
$$=\sqrt{2\pi}\sum_{a,b\in S}\int dz_1\chi^*_{a,\sigma}(z_1)\chi_{b,\sigma}(x)\chi_{n,\sigma}(z_1)\mathcal{F}^{-1}\left\{\mathcal{F}\left\{K_{2^{1/4}r}(x)\right\}(k)\cdot\mathcal{F}\left\{\chi^*_{b,\sigma}(z_2)\chi_{a,\sigma}(x)\right\}(k)\right\}(z_1), \quad (6.13)$$

reducing this from $\mathcal{O}(N^3D^3)$ to $\mathcal{O}(N^3D^2\log D)$. The first noise term is a simple convolution:

$$\int dy K_r(y-x)\chi_{n,\sigma}(x)\circ dW(y,t)$$
$$=\sqrt{2\pi}\chi_{n,\sigma}(x)\mathcal{F}^{-1}\left\{\mathcal{F}\left\{K_r(x)\right\}(k)\cdot\mathcal{F}\left\{\circ\, dW(x,t)\right\}(k)\right\}(x), \quad (6.14)$$

where we compute $\mathcal{F}\left\{\circ\, dW(x,t)\right\}(k)$ directly in Fourier space using Equation 6.6. This reduces from $\mathcal{O}(ND^2)$ to $\mathcal{O}(ND\log D)$. Finally, the second noise term is computed as:

$$\sum_{a\in S}\int dy\int dz K_r(y-z)\chi^*_{a,\sigma}(z)\chi_{a,\sigma}(x)\chi_{n,\sigma}(z)\circ dW(y,t)$$
$$=\sqrt{2\pi}\sum_{a\in S}\chi_{a,\sigma}(x)\int dz\chi^*_{a,\sigma}(z)\chi_{n,\sigma}(z)\mathcal{F}^{-1}\left\{\mathcal{F}\left\{K_r(x)\right\}(k)\cdot\mathcal{F}\left\{\circ\, dW(x,t)\right\}(k)\right\}(z), \quad (6.15)$$

reducing the calculation from $\mathcal{O}(N^2D^3)$ to $\mathcal{O}(N^2D^2\log D)$. The unitary terms are once again calculated using spectral methods (Section 2.3.2), which are $\mathcal{O}(ND\log D)$. Overall, this is still computationally cheaper than the naive method, but still scales poorly; it is

[3]We must compute $d\chi_{n,\sigma}(x)$ for every particle and every grid point, and thus we must perform ND computations of complexity $\mathcal{O}(N^2D^2)$.

$\mathcal{O}(N^3D^2 \log D)$, and the required D for an accurate representation of N particles scales linearly or superlinearly with N. In practice, we will fix $D = 256$ (which is sufficient for 40 atoms) and vary N, leading to a scaling of $\mathcal{O}(N^3)$.

Although the computational time is $\mathcal{O}(N^3D^2 \log D)$, optimisations can be made such that the memory requirements only scale with $ND \log D$. For example, one may construct the integrand in Equation 6.13 sequentially for each combination of a, b and z_1, adding them to a 'running total' such that we need only have one object in memory rather than all N^2D terms of the sum.

6.2.2 Scaling with atom number

In Section 4.5, we found that the cooling rate in the long-term limit was slower for larger N since multiple fermions occupy different spatial modes and thus may counter-oscillate and 'hide' density fluctuations of each spatial mode from the experimenter. Nonetheless, we were unable to draw strong conclusions about whether this effect was prohibitive, since the model did not include the competing heating rate from measurement. Now that we have the tools to include measurement backaction, we can resolve this.

We simulated non-interacting fermionic atoms subjected to continuous density measurements and the energy-damping control, for near-optimal control ($k_{\mathrm{ED}} = 4/N$) and a range of atom numbers N (4, 8, 16, 32, 40). The results are depicted in Figure 6.9. As expected, the equilibrium excitation energy per particle $\Delta E/N$ increases with N, since the cooling rate is decreased and equilibrates with measurement-induced heating at a higher energy per particle. An initial analysis suggests that the N-dependence of $\Delta E/N$ at equilbrium is linear or slightly superlinear. If this scaling continues at higher N, then direct cooling of fermions with the energy-damping control is unviable.

However, our data is limited, and we are unable to simulate more particles. With $N = 40$ we are pushing the limits of the number of orthogonal spatial modes that can be accurately represented at $D = 256$. Since the numerical simulation scales as $\mathcal{O}(N^2D \log D)$, even a modest increase to N would be costly due to dependence on N^2 and the need to increase D, and we are already pushing the limits of what we can reasonably achieve even with supercomputer help.

There is no clear reason why this scaling should be any better at larger N - a large number of spatial modes will still oscillate in different ways that may cancel out the total density fluctuations. Thus, we cautiously suggest that the energy-damping control scales poorly at large N, motivating different approaches in future.

6.2.3 Effect of interatomic scattering interactions

In Sections 4.5 and 4.6, we saw that in the absence of measurement, non-interacting two-component Fermi gases sometimes entered a dark state of total counter-oscillation, but nonlinear scattering interactions were able to perturb the system from such a state and continue cooling close to the ground state. Thus, in the no-measurement limit, we were able to achieve much better cooling of a Fermi gas for an interacting system.

One might therefore be tempted to suggest that the poor scaling with N when measurement effects are included (Section 6.2.2) is a consequence of this, since all of these simulations were non-interacting. Unfortunately, this is not the case. We fixed $N = 16$

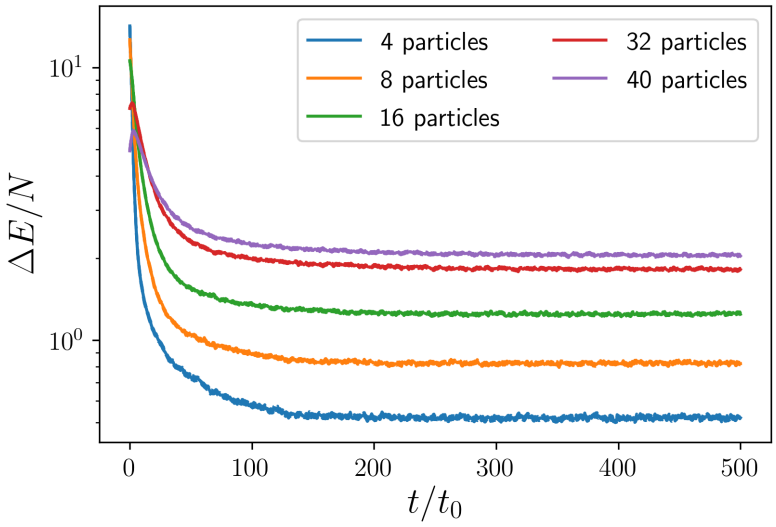

Figure 6.9: Feedback cooling with a near-optimal energy-damping control ($k_{\mathrm{ED}} = 4/N$) with measurement strength $\alpha = 0.1$ and resolution $r = 0.1$, across a range of atom numbers N. A larger number of atoms results in a larger equilibrium excitation energy per particle $\Delta E/N$, and thus the feedback cooling is less successful for large N. Solid lines depict the mean of 300 trajectories, and coloured dashed lines indicate twice the standard error in the mean (95% confidence interval). The energy-damping control does not scale well to large N for fermions, since $\Delta E/N$ scales superlinearly with N.

and varied Υ_0 up to the point of phase separation, depicted in Figure 6.10. The cooling does not significantly differ for an interacting Fermi gas, and the equilibrium excitation energy per particle increases with U_0.[4] We hypothesise that since interatomic scattering effects are only important at energies smaller than the equilibrium energy for moderate α, the nonlinearity does little to change the equilibrium excitation energy, and thus has minimal effect on the success of cooling. Consequently, this does not significantly change the long-term behaviour, and other effects of the scattering interactions dominate. Nonlinear scattering interactions are insufficient to overcome the scaling limitations of the energy-damping control for Fermi gases.

6.3 Conclusions from simulations with measurement backaction

Although the simulations of Chapter 4 gave important insight into the control-specific aspects of feedback cooling, they ignored the extremely important effect of measurement backaction. In this chapter, we have simulated the extended models developed in Chapter 5 to study feedback control under measurement. In Section 6.1, we simulated the stochastic Schrödinger equation for a single atom, gaining a qualitative understanding of the dynamics of continuous-measurement feedback control and the effect of system parameters. We found that measurement parameters for which less information about the

[4] How we interpret this result depends heavily on the energy scale and our metric for success. We have plotted this in units of $\hbar\omega$, the natural energy scale for the harmonic oscillator, but interactions introduce another energy scale to the system. The trend is reversed if we plot our energies relative to the ground state energy E_g, but is still a comparatively small effect that cannot overcome the poor scaling with N.

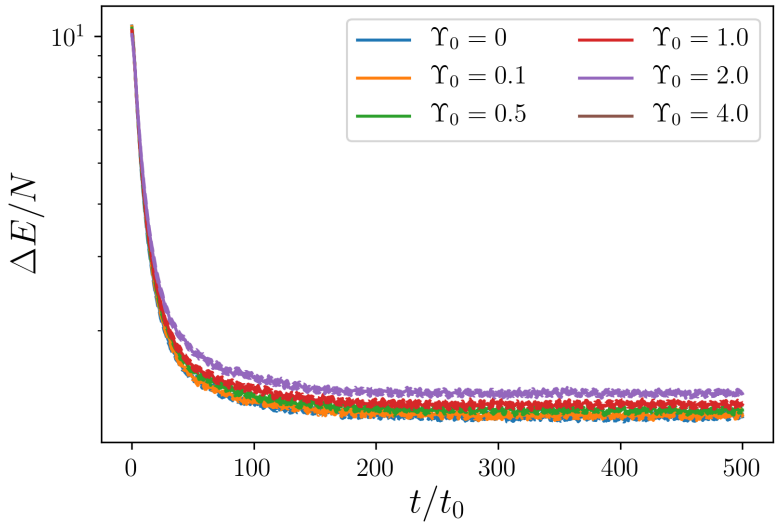

Figure 6.10: Feedback cooling with a near-optimal energy damping control $k_{\mathrm{ED}} = 4/N$ with measurement strength $\alpha = 0.1$ and resolution $r = 0.1$, for fixed $N = 16$ and a range of values of Υ_0 up to the phase-separation threshold. Solid lines depict the mean of 300 trajectories, and coloured dashed lines indicate twice the standard error in the mean (95% confidence interval). The scattering interactions do not have a significant effect on the equilibrium energy, and are thus insufficient to overcome the scaling limitations when measurement is accounted for.

system is collected (large r and small α) lead to lower equilibrium excitation energies, suggesting that one should measure an atomic gas as weakly as possible. However, we were not able to place lower bounds on *how* weakly due to the lack of a system-filter separation. In Section 6.2, we extended this to many fermions by simulating the SFGPE (6.11). We showed that the energy-damping control scales poorly with atom number N, and that the effect of scattering interactions had minimal effect. Ultimately, this more realistic model confirms our suspicions from Chapter 4; although the energy-damping control is extremely effective for bosons, it is ineffective at controlling multiple spatial modes in the same trap (corresponding to multiple fermions). This motivates the development of alternative strategies and/or controls, prospects which we discuss in Chapter 7.

Chapter 7

Conclusions and outlook

In this thesis, we investigated the prospect of using continuous-measurement feedback control to cool an atomic Fermi gas. Specifically, we developed and studied theoretical models for driving a Fermi gas towards its ground state. Drawing on previous work in feedback control of BECs, we developed two models for feedback control of an atomic Fermi gas: one ignoring the effect of measurement backaction, and one including it.

In Chapter 3, we discussed mean-field theory; we reviewed the Gross-Pitaevskii equation (3.1), which describes the dynamics of a single-mode BEC in the absence of quantum correlations, developed the FGPE (3.33) as a multimode fermionic equivalent, and described methods to find the ground states of both. In Chapter 4, we used this to simulate feedback control of a Fermi gas in the absence of measurement backaction, successfully generalising the model of Haine *et al.* [2] to fermions. We used this to rapidly prototype control schemes, and tractably understand the control-specific aspects of the model. We compared the moment control, which damps a limited number of moments of atomic density (typically $\langle\hat{x}\rangle$ and $\langle\hat{x}^2\rangle$), to the energy-damping control, which damps *all* density fluctuations directly. We found that the moment control was extremely ineffective - even more so for fermions than bosons due to their poorer scattering properties. We showed that the energy-damping control was extremely effective for a single spatial mode (such as a BEC), but it is less effective for multiple spatial modes (such as a Fermi gas, since the Hartree-Fock wavefunctions must be orthogonal to preserve Pauli exclusion) since individual atoms can counter-oscillate in such a way that total density fluctuations cancel out, even when there are non-negligible oscillations in the individual atomic wavefunctions themselves. In the non-interacting case, the Fermi gas even entered dark states due to total counter-oscillation. We showed that scattering interactions can slowly perturb the system from a counter-oscillating state, but this effect is very slow.

In Chapter 5 we introduced conditional quantum measurement theory. We used this to add measurement effects to our model of feedback cooling of fermions. Beginning with a fermionic version of the full-field stochastic master equation derived by Szigeti *et al.* [3], we derived a mean-field equation of motion for fermions undergoing continuous measurement, which we dubbed the SFGPE (5.52) - essentially a multimode fermionic version of the mean-field model of Szigeti *et al.* [4]. We took the single-fermion limit of the SFGPE, referred to as the stochastic Schrödinger equation (5.53), and showed that it agrees with the single-boson limit of Szigeti *et al.*. We then performed stochastic simulations in Chapter 6. Using the stochastic Schrödinger equation, we gained qualitative understanding of the dynamics of a measured, feedback-controlled system, and saw that measurement backaction prevents the control from bringing the system to the ground

state, instead equilibrating at an excitation energy above the ground state. Once again, the energy-damping control vastly outperformed the moment control. We investigated ways to minimise this equlibrium energy, and found that it was lower for parameters corresponding to weak measurement (low strength α and large resolution r). However, due to the lack of a system-filter separation, we were unable to quantify exactly *how* weakly one can measure the system before the control scheme fails. We then investigated how the cooling scales with atom number N by simulating the SFGPE, and found that the equilibrium energy per particle increased superlinearly with N, suggesting that although the energy-damping control works extremely well for a single spatial mode (such as a BEC), it is ineffective in controlling many overlapping spatial modes (such as a Fermi gas). Nonlinear scattering interactions did little to help, having no significant effect on the competition between feedback cooling and measurement-induced heating. Ultimately, although we have developed and applied theoretical tools that can model a measured, feedback-controlled atomic Fermi gas, our results suggest that methods which work well for bosons are unlikely to be effective for fermions, motivating alternative future approaches.

7.1 Limitations and future work

It is crucial to consider the limitations of our methods. In this section, we discuss the limitations of our approach and outline future avenues of investigation to overcome each of these limitations.

7.1.1 Failure of the control scheme for large N

A key finding of this thesis is that the energy-damping control is significantly less effective for multiple spatial modes, such as the orthogonal wavefunctions of a Hartree-Fock Fermi gas. This is an obvious limitation - we have not yet demonstrated a control scheme for Fermi gases that scales well with N. This certainly does not spell the end for feedback control of Fermi gases, since we have only shown that the methods which are effective for bosons are less effective for many fermions.

To overcome this limitation, we could attempt to devise a control that works more effectively for fermions. We have seen in this thesis that total density fluctuations are not particularly useful for driving a Fermi gas towards its ground state at low energy scales, due to counter-oscillation of the different single-particle wavefunctions. We propose that inspiration for better controls could come from the area of optimal control theory. In particular, in the absence of interatomic scattering, the model of Chapter 4 is a linear coupled system. In similar systems, there provably exists a control that will bring the system exactly to any state in a finite amount of time [137, 138], and so we believe it is possible to devise an optimal control to drive a Fermi gas towards its ground state in this limit. Many open questions in this area remain:

- Is the optimal control extremely sensitive to initial state?[1]
- Can this control be experimentally realised, or is it unrealistic?
- Is it possible to develop the optimal control into something that is robust to nonlinear

[1] This could be problematic in the initial stages of an experiment when the system and filter have not converged.

scattering interactions[2] and imperfect knowledge of the system state?

If developing an effective and realistic control for direct cooling of fermions proves to be difficult, an alternative is *sympathetic feedback cooling*. Presently, atomic Fermi gases are often produced by sympathetic evaporation (e.g. Ref. [67]). As discussed in Section 1.4, direct evaporative cooling of fermions is much harder due to their poor scattering and thermalisation properties. Thus, it is commonplace to produce a Bose-Fermi mixture, couple energy from the fermions to the bosons via scattering, and evaporate the bosons to cool the system - since bosons are much easier to cool by evaporation.

This thesis shows that it is much easier to cool a BEC than a near-degenerate Fermi gas when measuring with phase-contrast imaging and applying feedback via the energy-damping control. Consequently, we propose a new cooling strategy: trap bosons and fermions at the same spatial location, couple them by scattering interactions (which will not have the limitations of fermion-fermion scattering since it is not unfavourable for them to overlap spatially), and apply measurement and feedback cooling only to the bosons.[3] Thus, we treat the bosons as a channel through which energy can be continuously pumped out of the fermions and out of the system as a whole. This has the potential to be much more effective than sympathetic evaporation. Bose gases experience a dramatic reduction in heat capacity below T_c, which limits the thermal energy they can carry away from the fermions evaporatively. In contrast, sympathetic feedback cooling allows one to continuously cool the BEC, overcoming this barrier.

Deriving the model for this scheme is only a trivial modification to existing work. Our Hamiltonian consists of the individual dynamics of the bosons and fermions (with masses m_B and m_F, respectively), plus a quartic s-wave interspecies scattering interaction:

$$\hat{H} = \hat{H}_{\text{boson}} + \hat{H}_{\text{fermion}} + \underbrace{\frac{U_c}{2}\sum_\sigma \int d\boldsymbol{x}\hat{\psi}_\sigma^\dagger(\boldsymbol{x})\hat{\phi}^\dagger(\boldsymbol{x})\hat{\phi}(\boldsymbol{x})\hat{\psi}_\sigma(\boldsymbol{x})}_{\text{Boson-fermion scattering}}, \tag{7.1}$$

where we have the usual cold boson and fermion Hamiltonians, given by:

$$\begin{aligned}\hat{H}_{\text{boson}} &= \int d\boldsymbol{x}\hat{\phi}^\dagger(\boldsymbol{x})\left(-\frac{\hbar^2}{2m_B}\boldsymbol{\nabla}_{\boldsymbol{x}}^2 + V(\boldsymbol{x},t)\right)\hat{\phi}(\boldsymbol{x}) + \frac{U_{BB}}{2}\int d\boldsymbol{x}\hat{\phi}^\dagger(\boldsymbol{x})\hat{\phi}^\dagger(\boldsymbol{x})\hat{\phi}(\boldsymbol{x})\hat{\phi}(\boldsymbol{x}),\\ \hat{H}_{\text{fermion}} &= \sum_\sigma \int d\boldsymbol{x}\hat{\psi}_\sigma^\dagger(\boldsymbol{x})\left(-\frac{\hbar^2}{2m_F}\boldsymbol{\nabla}_{\boldsymbol{x}}^2 + V(\boldsymbol{x})\right)\hat{\psi}_\sigma(\boldsymbol{x}) + \frac{U_{FF}}{2}\sum_{\sigma\sigma'}\int d\boldsymbol{x}\hat{\psi}_\sigma^\dagger(\boldsymbol{x})\hat{\psi}_{\sigma'}^\dagger(\boldsymbol{x})\hat{\psi}_{\sigma'}(\boldsymbol{x})\hat{\psi}_\sigma(\boldsymbol{x}).\end{aligned} \tag{7.2}$$

If we consider an effective 1D system and neglect entanglement of different atomic species,[4] then deriving a stochastic master equation for the boson field is almost exactly the same as the original derivation of Szigeti *et al.* [3], since the fermionic and bosonic field operators commute. The only difference is an extra term in the unitary evolution due to the boson-

[2] This is important, since the optimal control only provably exists in the linear case.

[3] Different atomic species have different resonances, so it is certainly feasible to subject them to different trapping potentials, and to measure only one species.

[4] That is, $\hat{\rho}(t) = \hat{\rho}_B(t) \otimes \hat{\rho}_F(t)$, where $\hat{\rho}(t)$ is the state of the coupled system, $\hat{\rho}_B(t)$ the state of the boson field, and $\hat{\rho}_F(t)$ the state of the fermion field.

fermion scattering, and so the boson evolution may be written:

$$d\hat{\rho}_B = -\frac{i}{\hbar}\left[\hat{H}_{\text{boson}} + \hat{H}_{\text{coupling}}, \hat{\rho}_B\right] dt + \alpha \int dx \mathcal{D}\left[\hat{M}(x)\right]\hat{\rho}_B dt + \sqrt{\alpha}\int dx \mathcal{H}\left[\hat{M}(x)\right]\hat{\rho}_B dW(x,t) \tag{7.3}$$

where $\hat{\rho}_B$ is the conditional state of the bosons, $\hat{H}_{\text{coupling}}$ is the boson-fermion scattering term of Equation 7.1, and all other terms are as defined[5] in Section 5.4.1. Since the fermions are not being measured, they evolve unitarily:

$$d\hat{\rho}_F = -\frac{i}{\hbar}\left[\hat{H}_{\text{fermion}} + \hat{H}_{\text{coupling}}, \hat{\rho}_F\right] dt. \tag{7.4}$$

We can obtain tractable equations of motion via the usual uncorrelated mean-field approximations. For the boson field, the derivation of *Szigeti et al.* [4] mostly carries over, with the addition of one extra unitary term for the boson-fermion scattering. For the fermion field, our derivation in Section 3.2 also carries over with the addition of such an interspecies scattering term. By following the usual processes,[6] we find:

$$\begin{aligned} d\varphi(x,t) = &\left[-\frac{i}{\hbar}\tilde{H}_B(x,t)\varphi(x,t) + 2\alpha\Big(m(x,t) - \bar{m}(t)\Big)\varphi(x,t)\right] dt \\ &+ \sqrt{\alpha}\left[\vartheta(x,t) - \bar{\vartheta}(t)\right]\varphi(x,t), \end{aligned} \tag{7.5}$$

$$\begin{aligned} d\chi_{n,\sigma}(x,t) = &-\frac{i}{\hbar}\left(-\frac{\hbar^2}{2m_F}\frac{\partial^2}{\partial^2 x} + V_F(x)\right)\chi_{n,\sigma}(x,t)dt - \overbrace{\frac{iU_{FF}}{\hbar}\sum_m |\chi_{m,!\sigma}(x,t)|^2 \chi_{n,\sigma}(x,t)dt}^{\text{Fermion-fermion scattering}} \\ &\underbrace{-\frac{iU_{BF}}{\hbar}|\varphi(x,t)|^2\chi_{n,\sigma}(x,t)dt}_{\text{Boson-fermion scattering}}, \end{aligned} \tag{7.6}$$

where all measurement terms are as defined[7] in Equation 5.54, and the boson Hamiltonian on $L^2(\mathbb{R})$ is given by:

$$\tilde{H}_B(x,t) = -\frac{\hbar^2}{2m_B}\frac{\partial^2}{\partial x^2} + V_B(x) + V_C(x,t) + \overbrace{U_{BB}(N-1)|\varphi(x)|^2}^{\text{Boson-boson scattering}} + \overbrace{U_{BF}\sum_{n,\sigma}|\chi_{n,\sigma}(x)|^2}^{\text{Boson-fermion scattering}}. \tag{7.7}$$

There is much to unpack here. Equation 7.5 is a mean-field description of a trapped BEC undergoing measurement via phase-contrast imaging, feedback control via a time-dependent control potential $V_C(x,t)$, scattering between its own atoms, and coupling to a Fermi gas via boson-fermion scattering. Equation 7.6 is a mean-field description of a trapped Fermi gas with scattering between its own atoms and coupling to the BEC, but no measurement or feedback control. The fermions and bosons may be trapped with different time-independent trapping potentials $V_F(x)$ and $V_B(x)$, respectively. The fermions interact with each other with strength U_{FF} and the bosons with strength U_{BB}, but there

[5] We would use the definition of the kernel introduced in this thesis, and assume a single-component Bose gas.

[6] We use Fock state approximations on the bosons and fermions, find the equation of motion for $\langle\hat{\phi}^\dagger(x_1)\hat{\phi}(x_2)\rangle$ using Equation 7.3 and the equation of motion for $\langle\hat{\psi}^\dagger_\sigma(x_1)\hat{\psi}_\sigma(x_2)\rangle$ from Equation 7.4, and then find equations of motion for the wavefunctions $\varphi(x)$ and $\chi_{n,\sigma}(x)$ such that $\langle\hat{\phi}^\dagger(x_1)\hat{\phi}(x_2)\rangle = \varphi^*(x_1)\varphi(x_2)$ and $\langle\hat{\psi}^\dagger_\sigma(x_1)\hat{\psi}_\sigma(x_2) = \sum_n \chi^*_{n,\sigma}(x_1)\chi_{n,\sigma}(x_2)$.

[7] Under the substitution $\chi(x,t) \to \varphi(x,t)$, due to the different notation here used to distinguish bosonic and fermionic wavefunctions. We have used the new kernel definition in Equation 5.27.

is also an interspecies coupling strength U_{BF}. We have tractable equations of motion, but many open questions remain:

- Qualitatively, how effective is sympathetic cooling?
- How do the trapping potentials $V_F(x)$ and $V_B(x)$, the interaction strengths U_{FF}, U_{BB} and U_{BF}, and the number of atoms of each species affect the success of the cooling?
- How can we compute ground states for the Bose-Fermi mixture? We propose that adding imaginary-time GPE evolution to the iterative step of the Roothan algorithm would work in principle,[8] but this remains untested.

7.1.2 Neglect of quantum correlations

All models in this thesis completely ignore the effect of quantum correlations, due to the use of Fock state approximations. We expect this to be a reasonably good approximation for weakly repulsive interactions in the same regimes where the GPE provides an accurate description of a BEC, and also because density-like measurements project the system toward a state of well-defined number. However, when the interactions of a Fermi gas are attractive, there are always non-negligible correlations, and so we were not able to model attractive interactions. It is quite possible that cooling attractive Fermi gases is more favourable, and we would like to investigate this. Furthermore, Hush *et al.* showed that quantum fluctuations are more important for stronger measurements in the bosonic case [77], and we expect this to also be true for fermions. An accurate model of strongly-measured fermions will thus require the inclusion of higher-order quantum field effects.

Tools to include higher-order quantum field effects of feedback-controlled bosons already exist. The number-phase Wigner (NPW) representation developed by Hush *et al.* [78, 79] allows efficient stochastic simulation of bosons including these correlation effects, and has previously been applied to continuous-measurement feedback control of a BEC [77]. The correlation effects were non-negligible, and an additional control channel was required for effective control. Although the sympathetic cooling model outlined in Section 7.1.1 ignores fermion-boson entanglement, we could still include correlation effects in the boson field by using NPW instead of a mean field.

Including the quantum field effects of fermions would be a more substantial task. We suggest generalizing the phase-space methods of Hush *et al.* [77–79] to fermions as one possible avenue. There is some existing work in phase-space methods for fermions [139], which may provide helpful inspiration. We also note that weakly attractive atomic Fermi gases are dominated by pairing effects - in certain regimes they are described by BCS theory [31, 115], but they pair to form bosonic 'molecules' which may form a BEC [140, 141] (the transition is known as the BEC-BCS crossover, and has been the subject of much investigation [142]). There exists an extension of Hartree-Fock theory based on the BCS framework which consists of a mean-field description plus first-order pairing correlations, known as the Hartree-Fock-Bogoliubov method [143]. We speculate that this may provide inspiration for new methods to include pairing correlations in our models of feedback control of atomic Fermi gases.

[8] In principle, this should be convergent by the Banach fixed-point theorem [120, 121] for a sufficiently good initial guess - the exact same argument presented for the 'vanilla' Roothan algorithm in Section 3.3.2.

7.1.3 Additional experimental considerations

In Section 6.1.5, we found that weaker measurement parameters resulted in a lower equilibrium excitation energy - low α and large r were thus deemed favourable. Taken to the extreme, however, these results are absurd. It appeared that the system would exactly reach its ground state in the limits $\alpha \to 0$ or $r \to \infty$, but these result in *no* knowledge about the state being gained, and $\alpha = 0$ recovers exactly the model of Chapter 4. We concluded that this was an anomalous result of us assuming perfect system-filter convergence, and thus our approach was limited in that it could not quantify the weakest viable measurement.

This can be overcome by individually simulating coupled equations for the system and filter and monitoring their convergence, as was done in simpler cases by Szigeti *et al.* [132, 133]. To achieve this, we would write separate stochastic master equations for the system and filter in the form of Equations 5.12 and 5.18, respectively. Following the Hartree-Fock mean-field procedure of Section 5.4.2, we could then derive equations of motion for the system wavefunctions $\chi_{n,\sigma}(x,t)$ and filter wavefunctions $\varphi_{n,\sigma}(x,t)$. As the system evolves, we update the filter $\varphi_{n,\sigma}(x,t)$ with measurement innovations from the system $\chi_{n,\sigma}(x,t)$ (possibly corrupted by classical noise in the measurement channel), and use the filter $\varphi_{n,\sigma}(x,t)$ to compute feedback terms applied to the system $\chi_{n,\sigma}(x,t)$, forming the system-filter feedback-measurement loop depicted in Figure 5.1. This enables us to determine the threshold at which the measurement is too weak to preserve system-filter convergence, providing a lower bound on the necessary measurement strength.

We anticipate that a lower measurement strength α will result in slower system-filter convergence. It seems likely that low values of α would lead to lower equilibrium energies, but result in a system-filter convergence time that is too long to be practically achievable. Therefore, we speculate that it may be effective to begin the control process with a large α to converge the system and filter quickly, then adiabatically ramp down α such that the system and filter remain converged, and the steady-state energy drops. Therefore, one could possibly reach the optimal information-backaction tradeoff within a reasonable amount of time. A system-filter separation is necessary to investigate this, and thus it is an important direction to pursue for future work.

It is important to assess the validity of neglecting other experimental imperfections. We have assumed the experimenter is able to instantaneously calculate expectation values of the filter and apply the resulting feedback to the system. In reality, there will be a small delay, although this is typically extremely small compared to the natural timescale of the system $t_0 = \omega_x^{-1}$ [47]. Similarly, we assumed that the control potential could be controlled with arbitrary precision, but it will actually have a limited resolution. However, the resolution of configurable optical potentials based on digital-micromirror devices can be brought to within 5% of the diffraction limit [47], and is thus actually on the order of our simulation grid spacing. Consequently, our assumptions were quite reasonable. Nonetheless, it could be useful to qualitatively study the effect of such imperfections by adding a delay between calculating and applying the potential in our simulations, and 'blurring' the control $V_C(x,t)$ by convolving it with a point-spread function every time step.

7.1.4 Pure ensembles and zero temperature

All models and simulations in this thesis and much[9] previous work for bosons [2–4] assume pure ensembles, and thus are systems at zero temperature. Realistic systems might be thermal states that interact weakly with their environment beyond the decoherence induced by the measurement laser. Throughout this thesis, we equated driving the system towards its ground state, and cooling the system. Although this is reasonable in zero-temperature formalism, it is important to generalise our models to finite temperature. Ultracold Bose gases at finite temperature have previously been modelled by *c-field techniques* (see Ref. [144] for a review), and so these methods may be a useful starting point for modelling feedback control of finite-temperature Fermi gases.

7.1.5 Intractability of large-N and multidimensional simulations

Many of the proposals in this section have involved models more complicated than those studied in this thesis. However, the models of this thesis are already quite computationally taxing, since fermions cannot occupy the same mode and thus any description of multiple fermions must be multimode - the no-measurement model of Chapter 4 is $\mathcal{O}(ND^2)$, and the stochastic measurement model simulated in Chapter 6 is $\mathcal{O}(N^3D^2 \log D)$.[10] A significant limitation of this thesis is that we were therefore only able to obtain results up to moderate N. Due to computational limits, for the no-measurement model of Chapter 4, we were only able to run simulations up to $N = 400$, and in Chapter 6 we were only able to simulate the model including measurement up to $N = 40$. Recall that our mean-field theories were derived by finding equations of motion for the two-point correlation function $m_\sigma(x_1, x_2) = \langle \hat{\psi}^\dagger_\sigma(x_1)\hat{\psi}_\sigma(x_2)\rangle$. Since it is computationally favourable to evolve a moderate number of 1D PDEs over a single 2D PDE, we expanded this into the single-particle Hartree-Fock wavefunctions:

$$m_\sigma(x_1, x_2) = \sum_{n\in S} \chi^*_\sigma(x_1)\chi_\sigma(x_2). \tag{7.8}$$

However, there is nothing stopping us from simply simulating the equation of motion for $m_\sigma(x_1, x_2)$ (e.g. Equation 5.42). Notably, the complexity of its evolution does not scale explicitly with N, and the increase in complexity for larger N originates purely from the fact that we require a larger D to accurately represent more modes. In the case of the FGPE (3.33) and SFGPE (5.52), there was a complexity increase from *both*. There is thus a threshold at which it is favourable to simulate the equation of motion for $m_\sigma(x_1, x_2)$ (5.42). In Chapter 6, we were limited to tens of particles due to this scaling - we suggest that direct simulation of $m_\sigma(x_1, x_2)$ may bring the measurement model closer to the several hundred particles achieved without measurement in Chapter 4. We would do this in the Hermite-Gauss basis due to its favourable scaling properties to a large number of Hermite-Gauss modes.

Although using the Hermite-Gauss basis is necessary to scale to hundreds of fermions, it will be difficult to go beyond this, since exact Hermite-Gaussian quadrature (Section 2.3.3) does not converge beyond $D = 371$ for double-precision arithmetic. It seems likely

[9] A notable exception is the NPW filter derived and simulated by Hush *et al.* [77–79], which can be used to evolve any density matrix and thus can describe finite-temperature states.

[10] Assuming use of the Hermite-Gauss basis (Section 2.3.3) for the no-measurement model, which provides the best scaling at large N, and use of the spectral method (Section 2.3.2) for the measurement model.

that our current approach will always be limited to a moderate number of atoms, so we are in need of methods that can reliable extrapolate results to the very-large-N limit. Furthermore, we investigated only effective 1D systems since they are computationally easier to simulate. A more tractable model would be needed to extend our results to effective 2D or 3D Fermi gases.

We propose the use of a mean-field-hydrodynamic description of fermions to achieve these goals, using a modified version of the model of Adhikari [145–147]. We first consider a hydrodynamic model of sympathetic feedback cooling. Much like in Chapter 4, we consider only the control dynamics and neglect measurement backaction. Suppose we have N_F fermions of mass m_F, and N_B bosons of mass m_B. The bosons and fermions are trapped by time-independent trapping potentials $V_B(\boldsymbol{x})$ and $V_F(\boldsymbol{x})$, respectively, and the bosons are feedback-controlled by a time-dependent control potential $V_C(\boldsymbol{x},t)$. We will model the bosons by a GPE order parameter $\phi_B(\boldsymbol{x},t)$ and the fermions by a hydrodynamic density $n_F(\boldsymbol{x},t)$, normalised as $\int d\boldsymbol{x}|\phi_B(x)|^2 = N_B$ and $\int d\boldsymbol{x} n_F(\boldsymbol{x}) = N_F$. The system has Lagrangian density:

$$\begin{aligned}\mathcal{L} =& \frac{i\hbar}{2}\left[\phi_B\frac{\partial\phi_B^*}{\partial t} - \phi_B^*\frac{\partial\phi_B}{\partial t}\right] + \frac{i\hbar}{2}\left[\sqrt{n_F}\frac{\partial\sqrt{n_F^*}}{\partial t} - \sqrt{n_F^*}\frac{\partial\sqrt{n_F}}{\partial t}\right] \\ &+ \left(\frac{\hbar^2\left|\boldsymbol{\nabla}_{\boldsymbol{x}}\phi_B\right|^2}{2m_B} + (V_B+V_C)|\phi_B|^2 + \frac{1}{2}U_{BB}|\phi_B|^4\right) \\ &+ \left(\frac{\hbar^2\left|\boldsymbol{\nabla}_{\boldsymbol{x}}\sqrt{n_F}\right|^2}{6m_F} + V_F|n_F| + \frac{3}{5}A|n_F|^{5/3}\right) + U_{BF}n_F\left|\phi_B\right|^2,\end{aligned} \tag{7.9}$$

where U_{BB} and U_{BF} are the interaction strengths of boson-boson and boson-fermion scattering respectively (fermion-fermion scattering is neglected as it has a comparatively small effect), and $A = \hbar^2(6\pi^2)^{2/3}/(2m_F)$. Applying the Euler-Lagrange equations to the Lagrangian density (7.9) yields equations of motion for the bosons and fermions:

$$\left[-i\hbar\frac{\partial}{\partial t} - \frac{\hbar^2\boldsymbol{\nabla}_{\boldsymbol{x}}^2}{2m_B} + V_B(\boldsymbol{x}) + V_C(\boldsymbol{x},t) + U_{BB}|\phi_B(\boldsymbol{x})|^2 + U_{BF}n_F\right]\phi_B(\boldsymbol{x},t) = 0, \tag{7.10}$$

$$\left[-i\hbar\frac{\partial}{\partial t} - \frac{\hbar^2\boldsymbol{\nabla}_{\boldsymbol{x}}^2}{6m_F} + V_F(\boldsymbol{x}) + A|n_F|^{2/3} + U_{BF}|\phi_B|^2\right]\sqrt{n_F(\boldsymbol{x},t)} = 0. \tag{7.11}$$

This description is on the order of the complexity of a single-particle Schrödinger equation (in fact, Equation 7.10 is just the GPE coupled to the fermion density field), with N_F and N_B being mere parameters of the model and thus easily scalable to a large number. This is also tractable in 2D and 3D, allowing us to rapidly prototype the behaviour of feedback control in higher-dimensional systems. If one wishes to instead simulate direct cooling of fermions, we would similarly have the equation of motion:

$$\left[-i\hbar\frac{\partial}{\partial t} - \frac{\hbar^2\boldsymbol{\nabla}_{\boldsymbol{x}}^2}{6m_F} + V_F(\boldsymbol{x}) + V_C(\boldsymbol{x},t) + A|n_F|^{2/3}\right]\sqrt{n_F(\boldsymbol{x},t)} = 0. \tag{7.12}$$

Since this is computationally cheap, it is likely the best way to prototype new control schemes before investing in more complicated models. However, it remains to be seen whether it is possible to integrate quantum measurement effects into these hydrodynamic models, so this may at best be a no-measurement model in the vein of Chapter 4 and Haine

et al. [2]. The accuracy of the model can be benchmarked at moderate N by comparing it with the results of Chapter 4.

7.2 Outlook

In this thesis, we have generalised existing theoretical models for feedback control of BECs to multimode fermionic equivalents. Our simulations suggested that methods which work well for BECs would not work well for large-N Fermi gases, necessitating alternative future approaches. Unfortunately, we have not yet designed an effective cooling strategy for fermions.

Nonetheless, the future of feedback-controlled atomic Fermi gases is far from bleak. We have merely shown that two control schemes based on density fluctuations are ineffective for Fermi gases at large N. It is likely possible to devise a better control - in the non-interacting Hartree-Fock model without measurement backaction, an optimal control that can bring the system exactly to its ground state in a finite amount of time most likely exists [137, 138], and we may well be able to propose a simple feedback law based on something other than total spatial density fluctuations. We have developed all the theory required to test further control schemes. Additionally, the energy-damping control is extremely effective for bosons, and we have described a method by which one would be able to simulate sympathetic feedback cooling with measurement effects in the Hartree-Fock approximation using similar methods to those of Chapter 6. We have discussed ways to include the effects of quantum correlations and experimental imperfections in our system, which can be used to provide a realistic assessment of the real-world performance once an effective control scheme is devised. Furthermore, we have outlined a highly tractable mean-field-hydrodynamic model by which we can rapidly prototype such control schemes without significant computational effort.

Additional working

A.1 The Fermi-Hubbard model in atomic Fermi gases

It was first demonstrated by Jaksch *et al.* [55] that low-energy bosonic atoms in an optical lattice realise the Bose-Hubbard model. The proof is easily adapted to show that fermionic atoms in an optical lattice realise the Fermi-Hubbard model. Consider an interacting Fermi gas with an arbitrary number of spin components in a time-independent potential. We take the usual Hamiltonian (2.19) and expand out the potential into two components: a periodic lattice $V_0(\boldsymbol{x})$, and a trapping potential $V_T(\boldsymbol{x})$. This may be written as:

$$\hat{H} = \sum_{\sigma} \int d\boldsymbol{x} \hat{\psi}^{\dagger}_{\sigma}(\boldsymbol{x}) \left(-\frac{\hbar^2}{2m} \boldsymbol{\nabla}^2_{\boldsymbol{x}} + V_L(\boldsymbol{x}) + V_T(\boldsymbol{x}) \right) \hat{\psi}_{\sigma}(\boldsymbol{x}) + \frac{U_0}{2} \sum_{\sigma\sigma'} \int d\boldsymbol{x} \hat{\psi}^{\dagger}_{\sigma}(\boldsymbol{x}) \hat{\psi}^{\dagger}_{\sigma'}(\boldsymbol{x}) \hat{\psi}_{\sigma'}(\boldsymbol{x}) \hat{\psi}_{\sigma}(\boldsymbol{x}). \quad \text{(A.1)}$$

We expand the field operators into a Wannier basis (see Refs. [148, 149]) and assume that the energy scale of the system is low compared to the first excitation energy at each lattice site, such that we may discard all but the lowest vibrational states, and write:

$$\hat{\psi}_{\sigma}(\boldsymbol{x}) = \sum_{\boldsymbol{j}} w(\boldsymbol{x} - \boldsymbol{x_j}) \hat{b}_{\boldsymbol{j}\sigma}. \quad \text{(A.2)}$$

It should be noted that the Wannier functions $w(\boldsymbol{x} - \boldsymbol{x_j})$ are highly localised around the lattice site centred at $\boldsymbol{x_j}$, and thus overlaps of Wannier functions at different sites can be neglected. Substituting Equation A.2 into Equation A.1, discarding such negligible terms, noting that $\int d\boldsymbol{x} V_L(\boldsymbol{x}) |w(\boldsymbol{x} - \boldsymbol{x_j})|^2 = 0$,[1] and defining:

$$\begin{aligned} J &= -\int d\boldsymbol{x} w^*(\boldsymbol{x} - \boldsymbol{x_j}) \left(-\frac{\hbar^2}{2m} \boldsymbol{\nabla}^2_{\boldsymbol{x}} + V_L(\boldsymbol{x}) \right) w(\boldsymbol{x} - \boldsymbol{x_k}), \\ \epsilon_j &= \int d\boldsymbol{x} V_T(\boldsymbol{x}) |w(\boldsymbol{x} - \boldsymbol{x_j})|^2, \\ U &= \frac{U_0}{2} \int d\boldsymbol{x} |w(\boldsymbol{x} - \boldsymbol{x_j})|^4 = \frac{U_0}{2} \int d\boldsymbol{x} |w(\boldsymbol{x})|^4, \end{aligned} \quad \text{(A.3)}$$

[1] Up to a gauge transformation (the addition of a constant), which does not change the dynamics.

we obtain:

$$\hat{H} = -J \sum_{\langle \boldsymbol{j},\boldsymbol{k}\rangle\sigma} \left(\hat{c}^\dagger_{\boldsymbol{j}\sigma} \hat{c}_{\boldsymbol{k}\sigma} + \hat{c}^\dagger_{\boldsymbol{k}\sigma} \hat{c}_{\boldsymbol{j}\sigma} \right) + U \sum_{\boldsymbol{j}} \hat{n}_{\boldsymbol{j}\uparrow} \hat{n}_{\boldsymbol{j}\downarrow} + \sum_{\boldsymbol{j}\sigma} \epsilon_{\boldsymbol{j}\sigma} \hat{n}_{\boldsymbol{j}\sigma}, \tag{A.4}$$

which is the Fermi-Hubbard Hamiltonian (c.f. Equation 1.3).

A.2 Coherent states

In Section 3.1.1, we claimed that a coherent state of a single mode is a tensor product of coherent states in the spatial basis, a claim which we will prove here. Consider some single-particle basis $\{|\phi_j\rangle\}$, with corresponding bosonic creation and annihilation operators $\hat{c}^\dagger_j$, $\hat{c}_j$. Select a single-particle mode $|\phi_k\rangle$. A *coherent state* $|\alpha\rangle$ of that mode is an eigenstate of the corresponding annihilation operator:

$$\hat{c}_k |\alpha\rangle = \alpha |\alpha\rangle , \tag{A.5}$$

where the state is characterised by the complex eigenvalue α, and the average occupancy is given by $|\alpha|^2$. This property and many others are described in detail in Section 4.3 of Gardiner and Zoller [102]: we will only describe the essentials and prove the basis change property, which is not discussed or proven therein. All properties invoked in this section may be found there.

Define the *displacement operator* for a mode with annihilation operator $\hat{c}_k$ as:

$$\hat{D}(\hat{c}_k, \alpha) = \exp\left(\alpha \hat{c}^\dagger_k - \alpha^* \hat{c}_k \right). \tag{A.6}$$

A coherent state in the mode $|\phi_k\rangle$ can be written as a displacement of the vacuum:

$$|\alpha\rangle = \hat{D}(\hat{c}_k, \alpha) |0\rangle . \tag{A.7}$$

Taking Equation A.7, expanding the definition of the displacement operator (A.6) and expanding into a field operator basis (2.15), we obtain:

$$|\alpha\rangle = \exp\left(\alpha \int d\boldsymbol{x} \phi_j(\boldsymbol{x}) \hat{\psi}^\dagger(\boldsymbol{x}) - \alpha^* \int d\boldsymbol{x} \phi^*_j(\boldsymbol{x}) \hat{\psi}(\boldsymbol{x}) \right) |0\rangle . \tag{A.8}$$

Applying the Baker-Campbell-Hausdorff formula and commutation properties, this becomes:

$$|\alpha\rangle = \left(\prod_{\boldsymbol{x}} \exp\left(\alpha \phi_j(\boldsymbol{x}) \hat{\psi}^\dagger(\boldsymbol{x}) - \alpha^* \phi^*_j(\boldsymbol{x}) \hat{\psi}(\boldsymbol{x}) \right) \right) |0\rangle \tag{A.9}$$

$$= \bigotimes_{\boldsymbol{x}} \left(\hat{D}(\hat{\psi}(\boldsymbol{x}), \alpha\phi_j(\boldsymbol{x})) |0\rangle \right). \tag{A.10}$$

We will define $\phi(\boldsymbol{x}) = \alpha\phi_j(\boldsymbol{x})$, and write this as $|\alpha\rangle = \bigotimes_{\boldsymbol{x}} |\phi(\boldsymbol{x})\rangle$. This indicates that a coherent state of a single mode is a tensor product of coherent states at each position. The mean occupancy is now $\int d\boldsymbol{x} |\phi(\boldsymbol{x})|^2$ as a result of this definition.

A.3 Vanishing first-order correction to the interacting Fermi gas ground state

We wish to calculate the ground state of the interacting, two-component atomic Fermi gas: that is, the ground state of the usual cold-atom Hamiltonian (2.22) with fermionic field operators and $\sigma \in \{\uparrow, \downarrow\}$. We will follow the methods outlined in Chapter 5 of Nolting [82]. Let us denote the non-interacting ground state as $|\eta_0\rangle$. We will use Feynman-diagrammatic perturbation theory, such that the ground state energy may be written as $E_g^{(0)} + E_g^{(1)} + \ldots$, where $E_g^{(n)}$ is the n-th order correction to the ground state energy. We will show that the first-order correction is zero. Expanding the first-order correction into Feynman diagrams, we have:

$E_g^{(1)} =$ 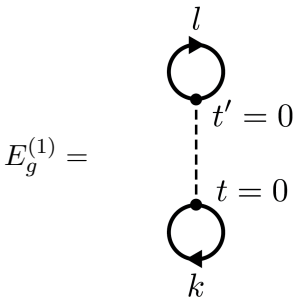

. (A.11)

Applying the $T = 0$ Feynman rules to the first diagram, we have:

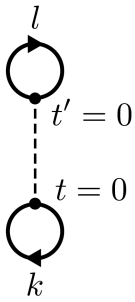

$$= \frac{1}{2} \sum_{\alpha\beta\gamma\delta} \int d\boldsymbol{x}_1 \int d\boldsymbol{x}_2 \int d\boldsymbol{x}_3 \int d\boldsymbol{x}_4 \frac{U_0}{2} \delta(\boldsymbol{x}_1 - \boldsymbol{x}_2) \langle \eta_0 | \hat{\psi}_\alpha^\dagger(\boldsymbol{x}_1) \hat{\psi}_\alpha(\boldsymbol{x}_1) | \eta_0 \rangle \cdot \langle \eta_0 | \hat{\psi}_\beta^\dagger(\boldsymbol{x}_2) \hat{\psi}_\beta(\boldsymbol{x}_2) | \eta_0 \rangle \delta_{\alpha\delta} \delta_{\beta\gamma} \delta(\boldsymbol{x}_1 - \boldsymbol{x}_4) \delta(\boldsymbol{x}_2 - \boldsymbol{x}_3)$$

$$= \frac{U_0}{4} \sum_{\alpha\beta} \int d\boldsymbol{x} \langle \eta_0 | \hat{\psi}_\alpha^\dagger(\boldsymbol{x}) \hat{\psi}_\alpha(\boldsymbol{x}) | \eta_0 \rangle \langle \eta_0 | \hat{\psi}_\beta^\dagger(\boldsymbol{x}) \hat{\psi}_\beta(\boldsymbol{x}) | \eta_0 \rangle , \tag{A.12}$$

and similarly for the second diagram, we find that:

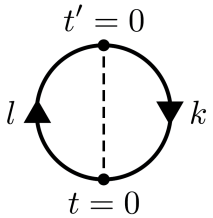

$$= -\frac{1}{2} \sum_{\alpha\beta\gamma\delta} \int d\boldsymbol{x}_1 \int d\boldsymbol{x}_2 \int d\boldsymbol{x}_3 \int d\boldsymbol{x}_4 \frac{U_0}{2} \delta(\boldsymbol{x}_1 - \boldsymbol{x}_2) \langle \eta_0 | \hat{\psi}_\alpha^\dagger(\boldsymbol{x}_1) \hat{\psi}_\alpha(\boldsymbol{x}_1) | \eta_0 \rangle \cdot \langle \eta_0 | \hat{\psi}_\beta^\dagger(\boldsymbol{x}_2) \hat{\psi}_\beta(\boldsymbol{x}_2) | \eta_0 \rangle \delta_{\alpha\beta} \delta_{\gamma\delta} \delta(\boldsymbol{x}_1 - \boldsymbol{x}_3) \delta(\boldsymbol{x}_2 - \boldsymbol{x}_4)$$

$$= -\frac{U_0}{4} \sum_{\alpha\beta} \int d\boldsymbol{x} \langle \eta_0 | \hat{\psi}_\alpha^\dagger(\boldsymbol{x}) \hat{\psi}_\alpha(\boldsymbol{x}) | \eta_0 \rangle \langle \eta_0 | \hat{\psi}_\beta^\dagger(\boldsymbol{x}) \hat{\psi}_\beta(\boldsymbol{x}) | \eta_0 \rangle . \tag{A.13}$$

Substituting Equations A.12 and A.13 into Equation A.11, we find that the first-order Feynman diagrams cancel exactly, and thus the first-order perturbative correction to the ground state energy is zero:

$$E_g^{(1)} = 0. \tag{A.14}$$

To find a nonzero perturbative correction, we would in principle need to go to second order, which is a highly non-trivial task. Further details may be found in Refs. [29, 82].

A.4 Non-interacting ground states of the harmonic oscillator

The ground state energy of a harmonically-trapped atomic gas can be calculated analytically in the non-interacting limit. We will solve this in 1D for N atoms and n_s spin components, assuming that N is divisible by n_s to avoid ground state degeneracy, per the assumptions applied throughout this thesis. We seek the ground state of the Hamiltonian:

$$\hat{H} = \sum_\sigma \int dx \hat{\psi}_\sigma^\dagger(x) \left(-\frac{\hbar^2}{2m}\frac{\partial^2}{\partial x^2} + \frac{1}{2}m\omega^2 x^2 \right) \hat{\psi}_\sigma(x). \tag{A.15}$$

The single-particle case has a well-known analytic solution [93] with eigenenergies:

$$E_n = \left(n + \frac{1}{2} \right) \hbar\omega. \tag{A.16}$$

As noted in Section 2.1, the ground state of a system of N non-interacting identical bosons simply consists of all N bosons occupying the single-particle ground state, which may be written as $|N, 0, 0, \ldots\rangle$ in occupation number notation in the energy eigenbasis. Thus, the bosonic case is trivial - we have:

$$E_g = NE_0 = \frac{N\hbar\omega}{2}. \tag{A.17}$$

In the fermionic case, the ground state is a 'Fermi sea' in which states are successively filled up, which we may write as $|1, 1, \ldots, 1, 0, \ldots\rangle$. Noting that fermions with a different internal component may have the same energy, the ground state energy in the fermionic case is given by:

$$E_g = n_s \sum_{n=0}^{N/n_s - 1} \left(n + \frac{1}{2} \right) \hbar\omega = \frac{N^2\hbar\omega}{2n_s}. \tag{A.18}$$

Therefore, the ground state energy of a non-interacting Bose gas scales with N, while the ground state energy of a non-interacting Fermi gas scales with N^2.

A.5 Effectiveness of the energy-damping control for a single spatial mode

In Section 4.2, we claimed that for a single non-interacting spatial mode (mathematically equivalent to a single particle) in a 1D harmonic trap, the only states with no density fluctuations are eigenstates. This proof is rather difficult with the wavefunction or Hilbert space formalisms, but is trivial in phase-space.

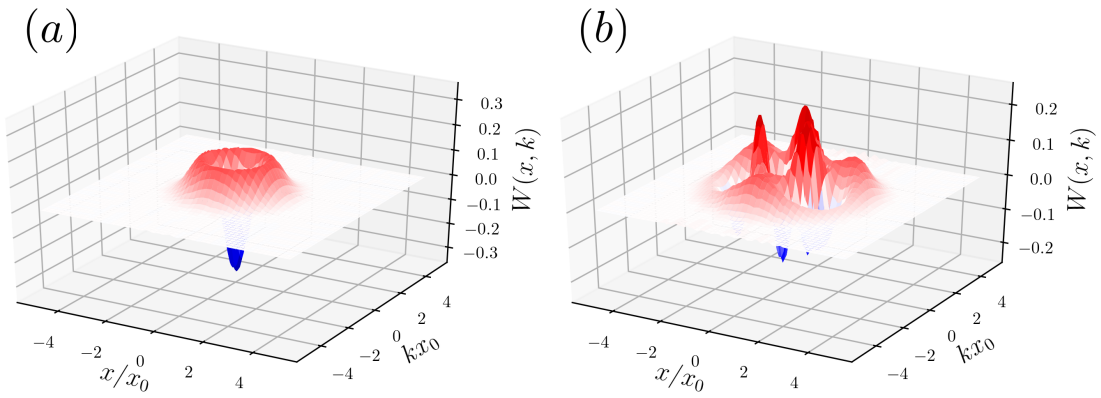

Figure A.1: Plots of the Wigner functions for (a) the eigenstate $\phi_1(x)$ and (b) the superposition $(\phi_1(x) + i\phi_4(x))/\sqrt{2}$. Note that the eigenstate has an axially symmetric Wigner function, while the Wigner function of the superposition is not axially symmetric.

Recall that a quantum state may be written as a *Wigner function*, which for a pure state in 1D with wavefunction $\psi(x)$ may be written:

$$W(x,p) = \frac{1}{\pi\hbar}\int dy \psi^*(x+y)\psi(x-y)e^{2ipy/\hbar}, \tag{A.19}$$

where the density may be calculated as $|\psi(x)|^2 = \int dp W(x,p)$. It is well known that for a pure state in the 1D harmonic oscillator, the evolution of $W(x,p)$ is just a rigid rotation in the x-p plane [150]. Thus, the only states which do not have any density fluctuations are those with axial symmetry about the W-axis. However, it is also well-known that the only pure states with this symmetry for the 1D harmonic oscillator are eigenstates of the Hamiltonian [150] (see Figure A.1 for examples), proving the claim that only eigenstates have no density oscillations.

A.6 Decoherence

In Section 5.1, we described a simple decoherence process governed by the observable $\hat{O}$, and claimed without proof that it projected the system onto the eigenbasis of $\hat{O}$ according to the Born rule. We will now prove this claim.

Suppose that $\hat{O}$ has eigenbasis $\{|n\rangle\}$, such that $\hat{O}|O_n\rangle = O_n|O_n\rangle$, where we assume a nondegenerate spectrum ($O_n \neq O_m$ for $n \neq m$). Suppose our system (described by density matrix $\hat{\rho}$) is dominated by decoherence in this observable, leading to the master equation:

$$\frac{d\hat{\rho}}{dt} = \mathcal{D}\left[\hat{O}\right]\hat{\rho}. \tag{A.20}$$

We consider the system to be initially in a pure state $\hat{\rho}$ of some superposition in the eigenbasis of $\hat{O}$:

$$\begin{aligned} \hat{\rho} &= |\Psi\rangle\langle\Psi| \\ |\Psi\rangle &= \sum_n, c_n |O_n\rangle . \end{aligned} \tag{A.21}$$

We may compute matrix elements in this basis as:

$$\rho_{nm}(t) = \langle O_n | \, \hat{\rho} \, | O_m \rangle \, . \tag{A.22}$$

Computing the matrix elements of Equation A.20, we find by simple operator algebra[2] that:

$$\frac{d\rho_{nm}(t)}{dt} = \langle O_n | \left(\frac{d\hat{\rho}}{dt} \right) | O_m \rangle = \left(nm - \frac{1}{2}n^2 - \frac{1}{2}m^2 \right) \rho_{nm}(t). \tag{A.23}$$

Equation A.23 has the simple analytic solution:

$$\rho_{nm}(t) = \rho_{nm}(t=0) \exp\left(\left(nm - \frac{1}{2}n^2 - \frac{1}{2}m^2 \right) t \right), \tag{A.24}$$

where we may easily show that $\rho_{nm}(t=0) = c_n c_m^*$ by computing the matrix elements of Equation A.21. Since the spectrum is nondegenerate, taking the long-term limit $t \to \infty$ in Equation A.24 yields:

$$\rho_{nm}(t \to \infty) = \begin{cases} |c_n|^2 & n = m, \\ 0 & n \neq m. \end{cases} \tag{A.25}$$

Thus, the density matrix in the long-term limit is diagonal in the eigenbasis of $\hat{O}$, with diagonal components $|c_n|^2$: the classical probability for a state $|O_n\rangle$ is given by $|c_n|^2$, which is exactly the Born rule [151]. In operator notation, we may write:

$$\hat{\rho}(t \to \infty) = \sum_n |c_n|^2 |O_n\rangle \langle O_n| \, . \tag{A.26}$$

We have shown that the decoherence process projects the pure state onto the eigenbasis of $\hat{O}$ according to the Born rule, as required.

[2] We use linearity, Hermiticity of the observable $\hat{O}$, and the diagonality of $\hat{O}$ in its own eigenbasis.

Appendix B

Wick's Theorem

B.1 Motivation

In deriving the mean-field dynamics of a fermionic system, we must be able to write the equation of motion for our order parameter entirely in terms of the order parameter itself. Hence, we must factorise expectation values of quartic products of field operators into expectation values of quadratic products:

$$\left\langle \hat{c}_j^\dagger \hat{c}_k^\dagger \hat{c}_l \hat{c}_m \right\rangle = \left\langle \hat{c}_j^\dagger \hat{c}_m \right\rangle \left\langle \hat{c}_k^\dagger \hat{c}_l \right\rangle \pm \left\langle \hat{c}_j^\dagger \hat{c}_l \right\rangle \left\langle \hat{c}_k^\dagger \hat{c}_m \right\rangle, \tag{B.1}$$

where the sign of the second term is positive for bosonic fields and negative for fermionic fields. In doing so, we reduce the many-body interactions to single-particle-like behaviour in a mean field. This is known as the Hartree-Fock factorisation, and is equivalent to the conventional approach to Hartree-Fock theory [29, 152]. This approximation underpins all of the fermionic simulations in this thesis, and thus it is crucial that we understand its origin. When combined with the assumption of a Fock state, this factorisation can be proven as a corollary of Wick's Theorem, the details of which follow.

B.2 Wick's Theorem

B.2.1 Misconceptions

Wick's Theorem (originally proposed by Wick [153]) is often stated as a theorem for calculating vacuum expectation values [84] or factorising higher-order Green's functions [29]. When introduced to the subject, it can be unclear how these are equivalent, and furthermore, why the theorem appears in both particle physics and condensed matter physics if it is somehow related to the vacuum state. These statements are actually corollaries of a more general theorem: in its purest form, Wick's Theorem provides an exact expression for an arbitrary product of field operators. One may then derive the special cases used in applications of quantum field theory by considering expectation values in special states.

B.2.2 Definitions

Our definitions and theorem statement follow the treatment of Ref. [152]. We will consider only the fermionic case - the bosonic case differs only in sign changes.

Normal ordering

Let $\hat{A}, \hat{B}, \hat{C}, \ldots$ denote some arbitrary field operators on some fermionic Fock space. Suppose we have some product of field operators $\hat{A}\hat{B}\hat{C}\ldots$. Suppose we have *any* rearrangement[1] of the product which places *all creation operators to the left of annihilation operators*, which we write for notational purposes as $\hat{B}\hat{C}\hat{D}\ldots$. We define the *normal-ordering* of $\hat{A}\hat{B}\hat{C}\ldots$ to be:

$$:\hat{A}\hat{B}\hat{C}\ldots: = (-1)^P \hat{B}\hat{C}\hat{D}\ldots, \tag{B.2}$$

where P is the number of operator interchanges needed to go from the ordering $\hat{A}\hat{B}\hat{C}\ldots$ to $\hat{B}\hat{C}\hat{D}\ldots$. The definition may naively seem ambiguous, since there are usually multiple rearrangements that place all creation operators to the left of annihilation operators. However, one may show any two normal orderings to be the same by applying fermion anticommutation relations, since these will just result in sign changes. For example, we have:

$$:\hat{a}_2^\dagger \hat{a}_3 \hat{a}_4^\dagger \hat{a}_2 \hat{a}_1^\dagger: = -\hat{a}_2^\dagger \hat{a}_4^\dagger \hat{a}_1^\dagger \hat{a}_3 \hat{a}_2 = \hat{a}_1^\dagger \hat{a}_2^\dagger \hat{a}_4^\dagger \hat{a}_2 \hat{a}_3, \tag{B.3}$$

where the first expression can be equated to the second or third expression by Equation B.2, and the second and third expressions can be equated by three applications of fermionic anticommutation relations. This definition is completely unambiguous, and different normal orderings can always be shown to be equivalent using anticommutation relations.

Contractions

We will begin with a special case. In a product of field operators, the *contraction* of two adjacent field operators $\hat{A}$ and $\hat{B}$ is defined as:

$$\overbracket{\hat{A}\hat{B}} = \hat{A}\hat{B} - :\hat{A}\hat{B}: \tag{B.4}$$

Clearly, $:\hat{A}\hat{B}:$ is equal to either $\hat{A}\hat{B}$ or $-\hat{B}\hat{A}$, and thus the contraction itself is equal to either $\hat{A}\hat{B} - \hat{A}\hat{B} = 0$ or $\hat{A}\hat{B} + \hat{B}\hat{A} = \left\{\hat{A}, \hat{B}\right\}$. respectively. Since the commutator of any two field operators is a c-number, it follows that the contraction of adjacent operators is also a c-number. The expectation value of a c-number is just the c-number itself, so it follows that:

$$\overbracket{\hat{A}\hat{B}} = \langle 0|\, \hat{A}\hat{B}\, |0\rangle\,, \tag{B.5}$$

where $|0\rangle$ is the vacuum state.

The generalisation to non-adjacent operators is simple: when contracting any two operators in a product, we rearrange the order of the product to make them adjacent, multiplying by -1 for each interchange of operators. Then, we apply the usual contraction to adjacent operators. Since exchanging pairs of fermionic operators under these rules results in no sign change, this definition is also completely unambiguous.

B.2.3 Statement of the theorem

We are now ready to present a statement of Wick's Theorem. The theorem states that a product of field operators is equal to its normal ordering plus the normal orderings of all

[1] By this, we mean that we just change the order of the operators in the product without any consideration of commutation operations.

possible contractions. That is, we may write:

$$\hat{A}\hat{B}\hat{C}\hat{D}\hat{E}\cdots =: \hat{A}\hat{B}\hat{C}\hat{D}\hat{E}\ldots: + \sum_{\text{singles}} :\overbrace{\hat{A}\hat{B}}CDE\ldots: + \sum_{\text{doubles}} :\overbrace{\hat{A}\hat{B}}\overbrace{\hat{C}\hat{D}}E\ldots: + \ldots \quad \text{(B.6)}$$

where the first sum is over all possible single-pair contractions, the second is over all double-pair contractions, and so forth.

The theorem is trivial for $N = 1$ and $N = 2$, and may be proven by induction for higher orders. A full proof is presented in Ref. [152].

B.3 Corollary: the Hartree-Fock factorisation

We will now derive a corollary: that the Hartree-Fock factorisation (3.28) holds for any Fock state.[2] We may write our state as:

$$|\Psi\rangle = \prod_{j\in S} \hat{c}_j^\dagger |0\rangle , \quad \text{(B.7)}$$

where S is some set of distinct indices in the chosen basis.[3] This is a vacuum-like state, where the excitations can be thought of as 'particles' and 'holes' akin to particle-hole excitations in a Fermi sea. For a given Fock state, we thus define a *generalised annihilation operator* as a nonzero field operator which annihilates the state, and a *generalised creation operator* as the adjoint of a generalised annihilation operator. In the preferred basis of $|\Psi\rangle$, all field operators are either a generalised annihilation or creation operator: for an index $j \in S$, $\hat{c}_j^\dagger$ is a generalised annihilation operator, and for $j \notin S$, it is a generalised creation operator (and vice versa for the adjoints). Hence, this is fully specified, and we may redefine contractions and normal ordering to be with respect to generalised field operators instead. For example, in the state $|\Psi\rangle = \frac{1}{\sqrt{3!}}\hat{c}_3^\dagger\hat{c}_2^\dagger\hat{c}_1^\dagger |0\rangle$, since ${\hat{c}_1}^\dagger$ and $\hat{c}_2^\dagger$ would annihilate the state, and $\hat{c}_4^\dagger$ and $\hat{c}_2$ are adjoints of operators that would annihilate the state, we have:

$$:\hat{c}_2^\dagger\hat{c}_4^\dagger\hat{c}_2\hat{c}_1^\dagger:_\Psi = \hat{c}_4^\dagger\hat{c}_2\hat{c}_2^\dagger\hat{c}_1^\dagger, \quad \text{(B.8)}$$

where the subscript Ψ indicates that this normal ordering is with respect to the generalised creation and annihilation operators of $|\Psi\rangle$. This ensures that all generalised normal-ordered products vanish when we compute expectation values with respect to $|\Psi\rangle$:

$$\langle\Psi| :\hat{A}\hat{B}\ldots:_\Psi |\Psi\rangle = 0. \quad \text{(B.9)}$$

Thus, $|\Psi\rangle$ is a vacuum state with respect to this normal-ordering convention. All the formal steps in the proof of Wick's Theorem carry over to generalised field operators [152]. The contraction of two generalised annihilation operators or two generalised field operators is zero,[4] so applying Wick's Theorem for generalised field operators to the quartic interaction

[2] A fermionic Fock state can be written as a single Slater determinant - this is the way that Hartree-Fock theory is presented in many treatments, such as that of Ref. [114].

[3] If these are not distinct, then trivially $|\Psi\rangle = 0$.

[4] $\left\{\hat{c}_j, \hat{c}_k^\dagger\right\} = 0$ unless $j = k$, which is never true if both these operators are generalised creation operators or generalised annihilation operators.

term in the preferred basis yields:

$$\hat{c}_j^\dagger \hat{c}_k^\dagger \hat{c}_l \hat{c}_m =: \hat{c}_j^\dagger \hat{c}_k^\dagger \hat{c}_l \hat{c}_m :_\Psi - \langle\Psi|\, \hat{c}_j^\dagger \hat{c}_l \,|\Psi\rangle : \hat{c}_k^\dagger \hat{c}_m :_\Psi + \langle\Psi|\, \hat{c}_j^\dagger \hat{c}_m \,|\Psi\rangle : \hat{c}_k^\dagger \hat{c}_l :_\Psi + \langle\Psi|\, \hat{c}_k^\dagger \hat{c}_l \,|\Psi\rangle : \hat{c}_j^\dagger \hat{c}_m :_\Psi$$
$$- \langle\Psi|\, \hat{c}_k^\dagger \hat{c}_m \,|\Psi\rangle : \hat{c}_j^\dagger \hat{c}_l :_\Psi + \langle\Psi|\, \hat{c}_j^\dagger \hat{c}_m \,|\Psi\rangle \langle\Psi|\, \hat{c}_k^\dagger \hat{c}_l \,|\Psi\rangle - \langle\Psi|\, \hat{c}_j^\dagger \hat{c}_l \,|\Psi\rangle \langle\Psi|\, \hat{c}_k^\dagger \hat{c}_m \,|\Psi\rangle\,, \quad \text{(B.10)}$$

Since the normal orderings are with respect to the generalised creation and annihilation operators of $|\Psi\rangle$, we have $\langle\Psi| : \hat{A}\hat{B}\cdots :_\Psi |\Psi\rangle = 0$ for all normally-ordered terms. Computing the expectation value of both sides with respect to $|\Psi\rangle$ therefore eliminates all terms with a normally-ordered string of operators as a factor, yielding:

$$\langle\Psi|\, \hat{c}_j^\dagger \hat{c}_k^\dagger \hat{c}_l \hat{c}_m \,|\Psi\rangle = \langle\Psi|\, \hat{c}_j^\dagger \hat{c}_m \,|\Psi\rangle \langle\Psi|\, \hat{c}_k^\dagger \hat{c}_l \,|\Psi\rangle - \langle\Psi|\, \hat{c}_j^\dagger \hat{c}_l \,|\Psi\rangle \langle\Psi|\, \hat{c}_k^\dagger \hat{c}_m \,|\Psi\rangle\,. \quad \text{(B.11)}$$

Although this resembles the desired result, this assumes a product in the preferred basis (the basis in which our Fock state $|\Psi\rangle$ is constructed). For a product in an arbitrary basis, we may expand into the preferred basis:

$$\langle\Psi|\, \hat{d}_a^\dagger \hat{d}_b^\dagger \hat{d}_c \hat{d}_d \,|\Psi\rangle = \sum_{jklm} A_{ja}^* A_{kb}^* A_{lc} A_{md} \langle\Psi|\, \hat{c}_j^\dagger \hat{c}_k^\dagger \hat{c}_l \hat{c}_m \,|\Psi\rangle\,. \quad \text{(B.12)}$$

Substituting Equation B.11 and using linearity:

$$\langle\Psi|\, \hat{d}_a^\dagger \hat{d}_b^\dagger \hat{d}_c \hat{d}_d \,|\Psi\rangle = \langle\Psi|\left(\sum_j A_{ja}^* \hat{c}_j^\dagger\right)\left(\sum_m A_{md} \hat{c}_m\right)|\Psi\rangle \langle\Psi|\left(\sum_k A_{kb}^* \hat{c}_k^\dagger\right)\left(\sum_l A_{lc} \hat{c}_l\right)|\Psi\rangle$$
$$- \langle\Psi|\left(\sum_j A_{ja}^* \hat{c}_j^\dagger\right)\left(\sum_l A_{lc} \hat{c}_l\right)|\Psi\rangle \langle\Psi|\left(\sum_k A_{kb}^* \hat{c}_k^\dagger\right)\left(\sum_m A_{md} \hat{c}_m\right)|\Psi\rangle\,. \quad \text{(B.13)}$$

Noting the bracketed terms are just transformations back into the original basis, we have:

$$\langle\Psi|\, \hat{d}_a^\dagger \hat{d}_b^\dagger \hat{d}_c \hat{d}_d \,|\Psi\rangle = \langle\Psi|\, \hat{d}_a^\dagger \hat{d}_d \,|\Psi\rangle \langle\Psi|\, \hat{d}_b^\dagger \hat{d}_c \,|\Psi\rangle - \langle\Psi|\, \hat{d}_a^\dagger \hat{d}_c \,|\Psi\rangle \langle\Psi|\, \hat{d}_b^\dagger \hat{d}_d \,|\Psi\rangle\,, \quad \text{(B.14)}$$

which is the desired result (c.f. Equation 3.28), since the field operators are in an arbitrary basis.

B.3.1 Time-ordered products

Wick's Theorem can be extended to time-ordered products of field operators, and is thus commonly used to factorise higher-order Green's functions in quantum field theory. A statement and proof of the time-ordered version can be found in Ref. [83].

This forms the backbone of perturbation theory in particle physics and condensed matter physics: interacting Green's functions can be expressed perturbatively in terms of non-interacting Green's functions at all orders, which may then be reduced to products of non-interacting single-particle Green's functions by means of Wick's Theorem. Feynman diagrams and their associated rules are a way of keeping track of Wick contractions. The Feynman-diagrammatic perturbation theory discussed in Section 3.3.2 and applied in Appendix A.3 is essentially a diagrammatic representation of the time-ordered version of Wick's Theorem.

Bibliography

[1] Joe Hope. *Feral*. Hope Publishing, 2019. ISBN: 978-0648562207.

[2] S. A. Haine et al. "Control of an atom laser using feedback". In: *Phys. Rev. A* 69 (1 Jan. 2004), p. 013605. DOI: 10.1103/PhysRevA.69.013605. URL: https://link.aps.org/doi/10.1103/PhysRevA.69.013605.

[3] S. S. Szigeti et al. "Continuous measurement feedback control of a Bose-Einstein condensate using phase-contrast imaging". In: *Physical Review A* 80.1 (July 2009), p. 013614. ISSN: 1050-2947. DOI: 10.1103/PhysRevA.80.013614. URL: https://link.aps.org/doi/10.1103/PhysRevA.80.013614.

[4] S. S. Szigeti et al. "Feedback control of an interacting Bose-Einstein condensate using phase-contrast imaging". In: *Phys. Rev. A* 82 (4 Oct. 2010), p. 043632. DOI: 10.1103/PhysRevA.82.043632. URL: https://link.aps.org/doi/10.1103/PhysRevA.82.043632.

[5] M. H. Anderson et al. "Observation of Bose-Einstein Condensation in a Dilute Atomic Vapor". In: *Science* 269.5221 (1995), pp. 198–201. ISSN: 0036-8075. DOI: 10.1126/science.269.5221.198. eprint: https://science.sciencemag.org/content/269/5221/198.full.pdf. URL: https://science.sciencemag.org/content/269/5221/198.

[6] C. C. Bradley et al. "Evidence of Bose-Einstein Condensation in an Atomic Gas with Attractive Interactions". In: *Phys. Rev. Lett.* 75 (9 Aug. 1995), pp. 1687–1690. DOI: 10.1103/PhysRevLett.75.1687. URL: https://link.aps.org/doi/10.1103/PhysRevLett.75.1687.

[7] K. B. Davis et al. "Bose-Einstein Condensation in a Gas of Sodium Atoms". In: *Phys. Rev. Lett.* 75 (22 Nov. 1995), pp. 3969–3973. DOI: 10.1103/PhysRevLett.75.3969. URL: https://link.aps.org/doi/10.1103/PhysRevLett.75.3969.

[8] N.P. Robins et al. "Atom lasers: Production, properties and prospects for precision inertial measurement". In: *Physics Reports* 529.3 (2013). Atom lasers: production, properties and prospects for precision inertial measurement, pp. 265–296. ISSN: 0370-1573. DOI: https://doi.org/10.1016/j.physrep.2013.03.006. URL: http://www.sciencedirect.com/science/article/pii/S037015731300118X.

[9] K. S. Hardman et al. "Simultaneous Precision Gravimetry and Magnetic Gradiometry with a Bose-Einstein Condensate: A High Precision, Quantum Sensor". In: *Phys. Rev. Lett.* 117 (13 Sept. 2016), p. 138501. DOI: 10.1103/PhysRevLett.117.138501. URL: https://link.aps.org/doi/10.1103/PhysRevLett.117.138501.

[10] Immanuel Bloch, Jean Dalibard, and Sylvain Nascimbène. "Quantum simulations with ultracold quantum gases". In: *Nature Physics* 8.4 (2012), pp. 267–276. ISSN: 1745-2481. DOI: 10.1038/nphys2259. URL: https://doi.org/10.1038/nphys2259.

[11] Christian Gross and Immanuel Bloch. "Quantum simulations with ultracold atoms in optical lattices". In: *Science* 357.6355 (2017), pp. 995–1001. ISSN: 0036-8075. DOI: 10.1126/science.aal3837. eprint: https://science.sciencemag.org/

content/357/6355/995.full.pdf. URL: https://science.sciencemag.org/content/357/6355/995.

[12] Immanuel Bloch. "Quantum simulations come of age". In: *Nature Physics* 14.12 (2018), pp. 1159–1161. ISSN: 1745-2481. DOI: 10.1038/s41567-018-0371-x. URL: https://doi.org/10.1038/s41567-018-0371-x.

[13] D C McKay and B DeMarco. "Cooling in strongly correlated optical lattices: prospects and challenges". In: *Reports on Progress in Physics* 74.5 (Apr. 2011), p. 054401. DOI: 10.1088/0034-4885/74/5/054401. URL: https://doi.org/10.1088%2F0034-4885%2F74%2F5%2F054401.

[14] Peter Ring and Peter Schuck. *The Nuclear Many-Body Problem (Theoretical and Mathematical Physics)*. Springer, 2005. ISBN: 354021206X.

[15] E. Y. Loh et al. "Sign problem in the numerical simulation of many-electron systems". In: *Phys. Rev. B* 41 (13 May 1990), pp. 9301–9307. DOI: 10.1103/PhysRevB.41.9301. URL: https://link.aps.org/doi/10.1103/PhysRevB.41.9301.

[16] S. R. White et al. "Numerical study of the two-dimensional Hubbard model". In: *Phys. Rev. B* 40 (1 July 1989), pp. 506–516. DOI: 10.1103/PhysRevB.40.506. URL: https://link.aps.org/doi/10.1103/PhysRevB.40.506.

[17] Fakher F. Assaad and Diethelm Würtz. "Reinvestigation of the sign problem in the two-dimensional Hubbard model". In: *Zeitschrift für Physik B Condensed Matter* 80.3 (Oct. 1990), pp. 325–329. ISSN: 1431-584X. DOI: 10.1007/BF01323512. URL: https://doi.org/10.1007/BF01323512.

[18] J. Carlson et al. "Quantum Monte Carlo methods for nuclear physics". In: *Rev. Mod. Phys.* 87 (3 Sept. 2015), pp. 1067–1118. DOI: 10.1103/RevModPhys.87.1067. URL: https://link.aps.org/doi/10.1103/RevModPhys.87.1067.

[19] Owe Philipsen. "Lattice calculations at non-zero chemical potential: The QCD phase diagram". In: *PoS* CONFINEMENT8 (2008), p. 011. DOI: 10.22323/1.077.0011.

[20] Philippe de Forcrand. "Simulating QCD at finite density". In: *PoS* LAT2009 (2009), p. 010. DOI: 10.22323/1.091.0010. arXiv: 1005.0539 [hep-lat].

[21] Tom Lancaster and Stephen J. Blundell. *Quantum Field Theory for the Gifted Amateur*. Oxford University Press, 2014. ISBN: 9780199699339.

[22] Martin C. Gutzwiller. "Effect of Correlation on the Ferromagnetism of Transition Metals". In: *Phys. Rev. Lett.* 10 (5 Mar. 1963), pp. 159–162. DOI: 10.1103/PhysRevLett.10.159. URL: https://link.aps.org/doi/10.1103/PhysRevLett.10.159.

[23] Junjiro Kanamori. "Electron Correlation and Ferromagnetism of Transition Metals". In: *Progress of Theoretical Physics* 30.3 (Sept. 1963), pp. 275–289. ISSN: 0033-068X. DOI: 10.1143/PTP.30.275. eprint: http://oup.prod.sis.lan/ptp/article-pdf/30/3/275/5278869/30-3-275.pdf. URL: https://doi.org/10.1143/PTP.30.275.

[24] J. Hubbard and Brian Hilton Flowers. "Electron correlations in narrow energy bands". In: *Proceedings of the Royal Society of London. Series A. Mathematical and Physical Sciences* 276.1365 (1963), pp. 238–257. DOI: 10.1098/rspa.1963.0204. eprint: https://royalsocietypublishing.org/doi/pdf/10.1098/rspa.1963.0204. URL: https://royalsocietypublishing.org/doi/abs/10.1098/rspa.1963.0204.

[25] H. A. Gersch and G. C. Knollman. "Quantum Cell Model for Bosons". In: *Phys. Rev.* 129 (2 Jan. 1963), pp. 959–967. DOI: 10.1103/PhysRev.129.959. URL: https://link.aps.org/doi/10.1103/PhysRev.129.959.

[26] F.D.M. Haldane. ""Solidification" in a soluble model of bosons on a one-dimensional lattice: The "Boson-Hubbard chain"". In: *Physics Letters A* 80.4 (1980), pp. 281–283. ISSN: 0375-9601. DOI: https://doi.org/10.1016/0375-9601(80)90022-5. URL: http://www.sciencedirect.com/science/article/pii/0375960180900225.

[27] Matthew P. A. Fisher et al. "Boson localization and the superfluid-insulator transition". In: *Phys. Rev. B* 40 (1 July 1989), pp. 546–570. DOI: 10.1103/PhysRevB.40.546. URL: https://link.aps.org/doi/10.1103/PhysRevB.40.546.

[28] J. J. Sakurai and Jim Napolitano. *Modern Quantum Mechanics*. 2nd ed. Cambridge University Press, 2017. DOI: 10.1017/9781108499996.

[29] Henrik. Bruus and Karsten. Flensberg. *Many-Body Quantum Theory in Condensed Matter Physics*. Oxford University Press, 2004. ISBN: 0198566336.

[30] J. P. F. LeBlanc et al. "Solutions of the Two-Dimensional Hubbard Model: Benchmarks and Results from a Wide Range of Numerical Algorithms". In: *Phys. Rev. X* 5 (4 Dec. 2015), p. 041041. DOI: 10.1103/PhysRevX.5.041041. URL: https://link.aps.org/doi/10.1103/PhysRevX.5.041041.

[31] J. Bardeen, L. N. Cooper, and J. R. Schrieffer. "Theory of Superconductivity". In: *Phys. Rev.* 108 (5 Dec. 1957), pp. 1175–1204. DOI: 10.1103/PhysRev.108.1175. URL: https://link.aps.org/doi/10.1103/PhysRev.108.1175.

[32] P. W. ANDERSON. "The Resonating Valence Bond State in La2CuO4 and Superconductivity". In: *Science* 235.4793 (1987), pp. 1196–1198. ISSN: 0036-8075. DOI: 10.1126/science.235.4793.1196. eprint: https://science.sciencemag.org/content/235/4793/1196.full.pdf. URL: https://science.sciencemag.org/content/235/4793/1196.

[33] P W Anderson et al. "The physics behind high-temperature superconducting cuprates: the plain vanilla version of RVB". In: *Journal of Physics: Condensed Matter* 16.24 (June 2004), R755–R769. DOI: 10.1088/0953-8984/16/24/r02. URL: https://doi.org/10.1088/0953-8984/16/24/r02.

[34] Ákos Rapp et al. "Color Superfluidity and "Baryon" Formation in Ultracold Fermions". In: *Phys. Rev. Lett.* 98 (16 Apr. 2007), p. 160405. DOI: 10.1103/PhysRevLett.98.160405. URL: https://link.aps.org/doi/10.1103/PhysRevLett.98.160405.

[35] J. A. Vergés et al. "Fit of Pariser-Parr-Pople and Hubbard model Hamiltonians to charge and spin states of polycyclic aromatic hydrocarbons". In: *Phys. Rev. B* 81 (8 Feb. 2010), p. 085120. DOI: 10.1103/PhysRevB.81.085120. URL: https://link.aps.org/doi/10.1103/PhysRevB.81.085120.

[36] M. Schüler et al. "Optimal Hubbard Models for Materials with Nonlocal Coulomb Interactions: Graphene, Silicene, and Benzene". In: *Phys. Rev. Lett.* 111 (3 July 2013), p. 036601. DOI: 10.1103/PhysRevLett.111.036601. URL: https://link.aps.org/doi/10.1103/PhysRevLett.111.036601.

[37] Z. S. Sadeq and J. E. Sipe. "A Simple Hubbard Model for the Excited States of π Conjugated -acene Molecules". In: *Frontiers in Optics 2016*. Optical Society of America, 2016, FF5H.6. DOI: 10.1364/FIO.2016.FF5H.6. URL: http://www.osapublishing.org/abstract.cfm?URI=FiO-2016-FF5H.6.

[38] Wayne W. Lukens, Nicola Magnani, and Corwin H. Booth. "Application of the Hubbard Model to Cp*2Yb(bipy), a Model System for Strong Exchange Coupling in Lanthanide Systems". In: *Inorganic Chemistry* 51.19 (2012). PMID: 22988887, pp. 10105–10110. DOI: 10.1021/ic300037q. eprint: https://doi.org/10.1021/ic300037q. URL: https://doi.org/10.1021/ic300037q.

[39] J. Hubbard. "Generalized Wigner lattices in one dimension and some applications to tetracyanoquinodimethane (TCNQ) salts". In: *Phys. Rev. B* 17 (2 Jan. 1978), pp. 494–505. DOI: 10.1103/PhysRevB.17.494. URL: https://link.aps.org/doi/10.1103/PhysRevB.17.494.

[40] Richard P. Feynman. "Simulating physics with computers". In: *International Journal of Theoretical Physics* 21.6-7 (June 1982), pp. 467–488. ISSN: 0020-7748. DOI: 10.1007/BF02650179. URL: http://link.springer.com/10.1007/BF02650179.

[41] Seth Lloyd. "Universal Quantum Simulators". In: *Science* 273.5278 (1996), pp. 1073–1078. ISSN: 0036-8075. DOI: 10.1126/science.273.5278.1073. eprint: https://science.sciencemag.org/content/273/5278/1073.full.pdf. URL: https://science.sciencemag.org/content/273/5278/1073.

[42] D. Deutsch. "Quantum Theory, the Church-Turing Principle and the Universal Quantum Computer". In: *Proceedings of the Royal Society A: Mathematical, Physical and Engineering Sciences* 400.1818 (July 1985), pp. 97–117. DOI: 10.1098/rspa.1985.0070. URL: https://doi.org/10.1098/rspa.1985.0070.

[43] T. D. Ladd et al. "Quantum computers". In: *Nature* 464.7285 (Mar. 2010), pp. 45–53. DOI: 10.1038/nature08812. URL: https://doi.org/10.1038/nature08812.

[44] Frank Arute et al. "Quantum supremacy using a programmable superconducting processor". In: *Nature* 574.7779 (Oct. 2019), pp. 505–510. DOI: 10.1038/s41586-019-1666-5. URL: https://doi.org/10.1038%2Fs41586-019-1666-5.

[45] Philipp Hauke et al. "Can one trust quantum simulators?" In: *Reports on Progress in Physics* 75.8 (July 2012), p. 082401. DOI: 10.1088/0034-4885/75/8/082401. URL: https://doi.org/10.1088/0034-4885/75/8/082401.

[46] Rudolf Grimm, Matthias Weidemüller, and Yurii B. Ovchinnikov. "Optical Dipole Traps for Neutral Atoms". In: ed. by Benjamin Bederson and Herbert Walther. Vol. 42. Advances In Atomic, Molecular, and Optical Physics. Academic Press, 2000, pp. 95–170. DOI: https://doi.org/10.1016/S1049-250X(08)60186-X. URL: http://www.sciencedirect.com/science/article/pii/S1049250X0860186X.

[47] G. Gauthier et al. "Direct imaging of a digital-micromirror device for configurable microscopic optical potentials". In: *Optica* 3.10 (Oct. 2016), pp. 1136–1143. DOI: 10.1364/OPTICA.3.001136. URL: http://www.osapublishing.org/optica/abstract.cfm?URI=optica-3-10-1136.

[48] P. A. Altin et al. "R85b tunable-interaction Bose–Einstein condensate machine". In: *Review of Scientific Instruments* 81.6 (2010), p. 063103. DOI: 10.1063/1.3430538. eprint: https://doi.org/10.1063/1.3430538. URL: https://doi.org/10.1063/1.3430538.

[49] Ketterle W., Durfee D.S., and Stamper-Kurn D.M. "Making, probing and understanding Bose-Einstein condensates". In: *Proceedings of the International School of Physics* 140.Bose-Einstein Condensation in Atomic Gases (1999), pp. 67–176. ISSN: 0074-784X. DOI: 10.3254/978-1-61499-225-7-67. URL: http://doi.org/10.3254/978-1-61499-225-7-67.

[50] Waseem S. Bakr et al. "A quantum gas microscope for detecting single atoms in a Hubbard-regime optical lattice". In: *Nature* 462.7269 (2009), pp. 74–77. ISSN:

1476-4687. DOI: 10.1038/nature08482. URL: https://doi.org/10.1038/nature08482.

[51] Elmar Haller et al. "Single-atom imaging of fermions in a quantum-gas microscope". In: *Nature Physics* 11 (July 2015), 738 EP -. URL: https://doi.org/10.1038/nphys3403.

[52] M. R. Andrews et al. "Direct, Nondestructive Observation of a Bose Condensate". In: *Science* 273.5271 (1996), pp. 84–87. ISSN: 0036-8075. DOI: 10.1126/science.273.5271.84. eprint: https://science.sciencemag.org/content/273/5271/84.full.pdf. URL: https://science.sciencemag.org/content/273/5271/84.

[53] C. C. Bradley, C. A. Sackett, and R. G. Hulet. "Bose-Einstein Condensation of Lithium: Observation of Limited Condensate Number". In: *Phys. Rev. Lett.* 78 (6 Feb. 1997), pp. 985–989. DOI: 10.1103/PhysRevLett.78.985. URL: https://link.aps.org/doi/10.1103/PhysRevLett.78.985.

[54] P. B. Wigley et al. "Non-destructive shadowgraph imaging of ultra-cold atoms". In: *Opt. Lett.* 41.20 (Oct. 2016), pp. 4795–4798. DOI: 10.1364/OL.41.004795. URL: http://ol.osa.org/abstract.cfm?URI=ol-41-20-4795.

[55] D. Jaksch et al. "Cold Bosonic Atoms in Optical Lattices". In: *Phys. Rev. Lett.* 81 (15 Oct. 1998), pp. 3108–3111. DOI: 10.1103/PhysRevLett.81.3108. URL: https://link.aps.org/doi/10.1103/PhysRevLett.81.3108.

[56] W. Hofstetter et al. "High-Temperature Superfluidity of Fermionic Atoms in Optical Lattices". In: *Phys. Rev. Lett.* 89 (22 Nov. 2002), p. 220407. DOI: 10.1103/PhysRevLett.89.220407. URL: https://link.aps.org/doi/10.1103/PhysRevLett.89.220407.

[57] N. Goldman, J. C. Budich, and P. Zoller. "Topological quantum matter with ultracold gases in optical lattices". In: *Nature Physics* 12 (June 2016), 639 EP -. URL: https://doi.org/10.1038/nphys3803.

[58] M Saffman. "Quantum computing with atomic qubits and Rydberg interactions: progress and challenges". In: *Journal of Physics B: Atomic, Molecular and Optical Physics* 49.20 (Oct. 2016), p. 202001. DOI: 10.1088/0953-4075/49/20/202001. URL: https://doi.org/10.1088%2F0953-4075%2F49%2F20%2F202001.

[59] A. Micheli et al. "Single Atom Transistor in a 1D Optical Lattice". In: *Phys. Rev. Lett.* 93 (14 Oct. 2004), p. 140408. DOI: 10.1103/PhysRevLett.93.140408. URL: https://link.aps.org/doi/10.1103/PhysRevLett.93.140408.

[60] M.E. Mosquera et al. "Bose–Einstein condensation in helium white dwarf stars. I". In: *Physics Letters B* 683.2 (2010), pp. 119–122. ISSN: 0370-2693. DOI: https://doi.org/10.1016/j.physletb.2009.12.011. URL: http://www.sciencedirect.com/science/article/pii/S0370269309014336.

[61] Rym Bouchendira et al. "New Determination of the Fine Structure Constant and Test of the Quantum Electrodynamics". In: *Phys. Rev. Lett.* 106 (8 Feb. 2011), p. 080801. DOI: 10.1103/PhysRevLett.106.080801. URL: https://link.aps.org/doi/10.1103/PhysRevLett.106.080801.

[62] Richard H. Parker et al. "Measurement of the fine-structure constant as a test of the Standard Model". In: *Science* 360.6385 (2018), pp. 191–195. ISSN: 0036-8075. DOI: 10.1126/science.aap7706. eprint: https://science.sciencemag.org/content/360/6385/191.full.pdf. URL: https://science.sciencemag.org/content/360/6385/191.

[63] Holger Müller et al. "Atom-Interferometry Tests of the Isotropy of Post-Newtonian Gravity". In: *Phys. Rev. Lett.* 100 (3 Jan. 2008), p. 031101. DOI: 10.1103/

PhysRevLett.100.031101. URL: https://link.aps.org/doi/10.1103/PhysRevLett.100.031101.

[64] Jan Harms et al. "Low-frequency terrestrial gravitational-wave detectors". In: *Phys. Rev. D* 88 (12 Dec. 2013), p. 122003. DOI: 10.1103/PhysRevD.88.122003. URL: https://link.aps.org/doi/10.1103/PhysRevD.88.122003.

[65] Naoto Masuhara et al. "Evaporative Cooling of Spin-Polarized Atomic Hydrogen". In: *Phys. Rev. Lett.* 61 (8 Aug. 1988), pp. 935–938. DOI: 10.1103/PhysRevLett.61.935. URL: https://link.aps.org/doi/10.1103/PhysRevLett.61.935.

[66] Harold J. Metcalf and Peter van der Straten. "Laser Cooling and Trapping of Neutral Atoms". In: *The Optics Encyclopedia*. American Cancer Society, 2007. ISBN: 9783527600441. DOI: 10.1002/9783527600441.oe005. eprint: https://onlinelibrary.wiley.com/doi/pdf/10.1002/9783527600441.oe005. URL: https://onlinelibrary.wiley.com/doi/abs/10.1002/9783527600441.oe005.

[67] Andrew G. Truscott et al. "Observation of Fermi Pressure in a Gas of Trapped Atoms". In: *Science* 291.5513 (2001), pp. 2570–2572. ISSN: 0036-8075. DOI: 10.1126/science.1059318. eprint: https://science.sciencemag.org/content/291/5513/2570.full.pdf. URL: https://science.sciencemag.org/content/291/5513/2570.

[68] K. M. O'Hara et al. "Observation of a Strongly Interacting Degenerate Fermi Gas of Atoms". In: *Science* 298.5601 (2002), pp. 2179–2182. ISSN: 0036-8075. DOI: 10.1126/science.1079107. eprint: https://science.sciencemag.org/content/298/5601/2179.full.pdf. URL: https://science.sciencemag.org/content/298/5601/2179.

[69] C. J. Pethick and H. Smith. *Bose–Einstein Condensation in Dilute Gases*. 2nd ed. Cambridge University Press, 2008. DOI: 10.1017/CBO9780511802850.

[70] Wolfgang Ketterle and N.J. Van Druten. "Evaporative Cooling of Trapped Atoms". In: ed. by Benjamin Bederson and Herbert Walther. Vol. 37. Advances In Atomic, Molecular, and Optical Physics. Academic Press, 1996, pp. 181–236. DOI: https://doi.org/10.1016/S1049-250X(08)60101-9. URL: http://www.sciencedirect.com/science/article/pii/S1049250X08601019.

[71] Jing Zhang et al. "Quantum feedback: Theory, experiments, and applications". In: *Physics Reports* 679 (2017). Quantum feedback: theory, experiments, and applications, pp. 1–60. ISSN: 0370-1573. DOI: https://doi.org/10.1016/j.physrep.2017.02.003. URL: http://www.sciencedirect.com/science/article/pii/S0370157317300479.

[72] H. M. Wiseman and L. K. Thomsen. "Reducing the Linewidth of an Atom Laser by Feedback". In: *Phys. Rev. Lett.* 86 (7 Feb. 2001), pp. 1143–1147. DOI: 10.1103/PhysRevLett.86.1143. URL: https://link.aps.org/doi/10.1103/PhysRevLett.86.1143.

[73] L. K. Thomsen and H. M. Wiseman. "Atom-laser coherence and its control via feedback". In: *Phys. Rev. A* 65 (6 June 2002), p. 063607. DOI: 10.1103/PhysRevA.65.063607. URL: https://link.aps.org/doi/10.1103/PhysRevA.65.063607.

[74] Mattias Johnsson, Simon Haine, and Joseph J. Hope. "Stabilizing an atom laser using spatially selective pumping and feedback". In: *Phys. Rev. A* 72 (5 Nov. 2005), p. 053603. DOI: 10.1103/PhysRevA.72.053603. URL: https://link.aps.org/doi/10.1103/PhysRevA.72.053603.

[75] A. C. Doherty and K. Jacobs. "Feedback control of quantum systems using continuous state estimation". In: *Phys. Rev. A* 60 (4 Oct. 1999), pp. 2700–2711. DOI:

10.1103/PhysRevA.60.2700. URL: https://link.aps.org/doi/10.1103/PhysRevA.60.2700.

[76] S. D. Wilson et al. "Effects of measurement backaction in the stabilization of a Bose-Einstein condensate through feedback". In: *Phys. Rev. A* 76 (1 July 2007), p. 013610. DOI: 10.1103/PhysRevA.76.013610. URL: https://link.aps.org/doi/10.1103/PhysRevA.76.013610.

[77] M R Hush et al. "Controlling spontaneous-emission noise in measurement-based feedback cooling of a Bose–Einstein condensate". In: *New Journal of Physics* 15.11 (Nov. 2013), p. 113060. DOI: 10.1088/1367-2630/15/11/113060. URL: https://doi.org/10.1088%2F1367-2630%2F15%2F11%2F113060.

[78] M. R. Hush, A. R. R. Carvalho, and J. J. Hope. "Number-phase Wigner representation for efficient stochastic simulations". In: *Phys. Rev. A* 81 (3 Mar. 2010), p. 033852. DOI: 10.1103/PhysRevA.81.033852. URL: https://link.aps.org/doi/10.1103/PhysRevA.81.033852.

[79] M. R. Hush, A. R. R. Carvalho, and J. J. Hope. "Number-phase Wigner representation for scalable stochastic simulations of controlled quantum systems". In: *Phys. Rev. A* 85 (2 Feb. 2012), p. 023607. DOI: 10.1103/PhysRevA.85.023607. URL: https://link.aps.org/doi/10.1103/PhysRevA.85.023607.

[80] Kerson Huang. *Introduction to Statistical Physics*. Oxford University Press, 2001. ISBN: 0-7484-0942-4.

[81] A. Einstein. "Quantentheorie des einatomigen idealen Gases, 2. Abhandlung". In: *Stizunger. Kgl. Preuss. Akad. Wiss* 1:3 (1925).

[82] Wolfgang Nolting and William D. Brewer. *Fundamentals of Many-body Physics*. Springer Berlin Heidelberg, 2009. DOI: 10.1007/978-3-540-71931-1. URL: https://doi.org/10.1007/978-3-540-71931-1.

[83] Michael E. Peskin and Daniel V. Schroeder. *An Introduction to quantum field theory*. Reading, USA: Addison-Wesley, 1995. ISBN: 9780201503975, 0201503972.

[84] M. Srednicki. *Quantum field theory*. Cambridge University Press, 2007. ISBN: 9780521864497, 9780511267208.

[85] V. Fock. "Konfigurationsraum und zweite Quantelung". In: *Zeitschrift für Physik* 75.9 (Sept. 1932), pp. 622–647. ISSN: 0044-3328. DOI: 10.1007/BF01344458. URL: https://doi.org/10.1007/BF01344458.

[86] Christopher J. Foot. *Atomic Physics (Oxford Master Series in Physics)*. Oxford University Press, 2005. ISBN: 0198506961.

[87] U. Fano. "Effects of Configuration Interaction on Intensities and Phase Shifts". In: *Phys. Rev.* 124 (6 Dec. 1961), pp. 1866–1878. DOI: 10.1103/PhysRev.124.1866. URL: https://link.aps.org/doi/10.1103/PhysRev.124.1866.

[88] Herman Feshbach. "A unified theory of nuclear reactions. II". In: *Annals of Physics* 19.2 (1962), pp. 287–313. ISSN: 0003-4916. DOI: https://doi.org/10.1016/0003-4916(62)90221-X. URL: http://www.sciencedirect.com/science/article/pii/000349166290221X.

[89] Sebastian Erne et al. "Universal dynamics in an isolated one-dimensional Bose gas far from equilibrium". In: *Nature* 563.7730 (2018), pp. 225–229. ISSN: 1476-4687. DOI: 10.1038/s41586-018-0667-0. URL: https://doi.org/10.1038/s41586-018-0667-0.

[90] Guillaume Gauthier et al. "Giant vortex clusters in a two-dimensional quantum fluid". In: *Science* 364.6447 (June 2019), pp. 1264–1267. DOI: 10.1126/science.aat5718. URL: https://doi.org/10.1126/science.aat5718.

[91] Henning Moritz et al. "Confinement Induced Molecules in a 1D Fermi Gas". In: *Phys. Rev. Lett.* 94 (21 June 2005), p. 210401. DOI: 10.1103/PhysRevLett.94.210401. URL: https://link.aps.org/doi/10.1103/PhysRevLett.94.210401.

[92] K. Fenech et al. "Thermodynamics of an Attractive 2D Fermi Gas". In: *Phys. Rev. Lett.* 116 (4 Jan. 2016), p. 045302. DOI: 10.1103/PhysRevLett.116.045302. URL: https://link.aps.org/doi/10.1103/PhysRevLett.116.045302.

[93] David J. Griffiths and Darrell F. Schroeter. *Introduction to Quantum Mechanics*. 3rd ed. Cambridge University Press, 2018. DOI: 10.1017/9781316995433.

[94] Francis Begnaud Hildebrand. *Introduction to Numerical Analysis*. 2nd ed. McGraw-Hill, 1974. ISBN: 0-07-028761-9.

[95] P. Blair Blakie. "Numerical method for evolving the projected Gross-Pitaevskii equation". In: *Phys. Rev. E* 78 (2 Aug. 2008), p. 026704. DOI: 10.1103/PhysRevE.78.026704. URL: https://link.aps.org/doi/10.1103/PhysRevE.78.026704.

[96] Kurt Jacobs. *Stochastic Processes for Physicists: Understanding Noisy Systems*. Cambridge University Press, 2010. DOI: 10.1017/CBO9780511815980.

[97] C.W. Gardiner. *Handbook of Stochastic Methods: for Physics, Chemistry and the Natural Sciences*. 3rd ed. Springer-Verlag Heidelberg, 2004. ISBN: 3-540-20882-8.

[98] Graham R. Dennis, Joseph J. Hope, and Mattias T. Johnsson. "XMDS2: Fast, scalable simulation of coupled stochastic partial differential equations". In: *Computer Physics Communications* 184.1 (2013), pp. 201–208. ISSN: 0010-4655. DOI: https://doi.org/10.1016/j.cpc.2012.08.016. URL: http://www.sciencedirect.com/science/article/pii/S0010465512002822.

[99] E P Gross. "Structure of a quantized vortex in boson systems". In: *Il Nuovo Cimento* 20.3 (May 1961), pp. 454–477. ISSN: 0029-6341. DOI: 10.1007/BF02731494. URL: http://link.springer.com/10.1007/BF02731494.

[100] Eugene P Gross. "Hydrodynamics of a Superfluid Condensate". In: *Journal of Mathematical Physics* 4.2 (Feb. 1963), pp. 195–207. ISSN: 0022-2488. DOI: 10.1063/1.1703944. URL: http://aip.scitation.org/doi/10.1063/1.1703944.

[101] L. P. Pitaevskii. "Vortex lines in an imperfect Bose gas". In: *Sov. Phys. JETP* 13 (Aug. 1961), pp. 451–454.

[102] Crispin Gardiner and Peter Zoller. *Quantum Noise: A Handbook of Markovian and Non-Markovian Quantum Stochastic Methods with Applications to Quantum Optics*. Springer-Verlag Berlin Heidelberg, 2004. ISBN: 978-3-540-22301-6.

[103] M. R. Andrews et al. "Observation of Interference Between Two Bose Condensates". In: *Science* 275.5300 (1997), pp. 637–641. ISSN: 0036-8075. DOI: 10.1126/science.275.5300.637. eprint: https://science.sciencemag.org/content/275/5300/637.full.pdf. URL: https://science.sciencemag.org/content/275/5300/637.

[104] Wu-Ming Liu, Biao Wu, and Qian Niu. "Nonlinear Effects in Interference of Bose-Einstein Condensates". In: *Phys. Rev. Lett.* 84 (11 Mar. 2000), pp. 2294–2297. DOI: 10.1103/PhysRevLett.84.2294. URL: https://link.aps.org/doi/10.1103/PhysRevLett.84.2294.

[105] Immanuel Bloch et al. "Optics with an Atom Laser Beam". In: *Phys. Rev. Lett.* 87 (3 July 2001), p. 030401. DOI: 10.1103/PhysRevLett.87.030401. URL: https://link.aps.org/doi/10.1103/PhysRevLett.87.030401.

[106] A. Smerzi et al. "Quantum Coherent Atomic Tunneling between Two Trapped Bose-Einstein Condensates". In: *Phys. Rev. Lett.* 79 (25 Dec. 1997), pp. 4950–

4953. DOI: 10.1103/PhysRevLett.79.4950. URL: https://link.aps.org/doi/10.1103/PhysRevLett.79.4950.

[107] Masahito Ueda and Anthony J. Leggett. "Macroscopic Quantum Tunneling of a Bose-Einstein Condensate with Attractive Interaction". In: *Phys. Rev. Lett.* 80 (8 Feb. 1998), pp. 1576–1579. DOI: 10.1103/PhysRevLett.80.1576. URL: https://link.aps.org/doi/10.1103/PhysRevLett.80.1576.

[108] R. Dum et al. "Creation of Dark Solitons and Vortices in Bose-Einstein Condensates". In: *Phys. Rev. Lett.* 80 (14 Apr. 1998), pp. 2972–2975. DOI: 10.1103/PhysRevLett.80.2972. URL: https://link.aps.org/doi/10.1103/PhysRevLett.80.2972.

[109] S. Burger et al. "Dark Solitons in Bose-Einstein Condensates". In: *Phys. Rev. Lett.* 83 (25 Dec. 1999), pp. 5198–5201. DOI: 10.1103/PhysRevLett.83.5198. URL: https://link.aps.org/doi/10.1103/PhysRevLett.83.5198.

[110] L. Khaykovich et al. "Formation of a Matter-Wave Bright Soliton". In: *Science* 296.5571 (2002), pp. 1290–1293. ISSN: 0036-8075. DOI: 10.1126/science.1071021. eprint: https://science.sciencemag.org/content/296/5571/1290.full.pdf. URL: https://science.sciencemag.org/content/296/5571/1290.

[111] Karl-Peter Marzlin, Weiping Zhang, and Ewan M. Wright. "Vortex Coupler for Atomic Bose-Einstein Condensates". In: *Phys. Rev. Lett.* 79 (24 Dec. 1997), pp. 4728–4731. DOI: 10.1103/PhysRevLett.79.4728. URL: https://link.aps.org/doi/10.1103/PhysRevLett.79.4728.

[112] David L. Feder, Charles W. Clark, and Barry I. Schneider. "Vortex Stability of Interacting Bose-Einstein Condensates Confined in Anisotropic Harmonic Traps". In: *Phys. Rev. Lett.* 82 (25 June 1999), pp. 4956–4959. DOI: 10.1103/PhysRevLett.82.4956. URL: https://link.aps.org/doi/10.1103/PhysRevLett.82.4956.

[113] M. R. Matthews et al. "Vortices in a Bose-Einstein Condensate". In: *Phys. Rev. Lett.* 83 (13 Sept. 1999), pp. 2498–2501. DOI: 10.1103/PhysRevLett.83.2498. URL: https://link.aps.org/doi/10.1103/PhysRevLett.83.2498.

[114] Attila Szabo and Neil Ostlund. *Modern Quantum Chemistry*. 1st ed. McGraw-Hill, 1996. ISBN: 978-0-486-69186-2.

[115] Stefano Giorgini, Lev P. Pitaevskii, and Sandro Stringari. "Theory of ultracold atomic Fermi gases". In: *Rev. Mod. Phys.* 80 (4 Oct. 2008), pp. 1215–1274. DOI: 10.1103/RevModPhys.80.1215. URL: https://link.aps.org/doi/10.1103/RevModPhys.80.1215.

[116] W. Bao and Q. Du. "Computing the Ground State Solution of Bose–Einstein Condensates by a Normalized Gradient Flow". In: *SIAM Journal on Scientific Computing* 25.5 (2004), pp. 1674–1697. DOI: 10.1137/S1064827503422956. eprint: https://doi.org/10.1137/S1064827503422956. URL: https://doi.org/10.1137/S1064827503422956.

[117] D. Lunney, J. M. Pearson, and C. Thibault. "Recent trends in the determination of nuclear masses". In: *Rev. Mod. Phys.* 75 (3 Aug. 2003), pp. 1021–1082. DOI: 10.1103/RevModPhys.75.1021. URL: https://link.aps.org/doi/10.1103/RevModPhys.75.1021.

[118] Alejandro J Garza and Gustavo E. Scuseria. "Comparison of self-consistent field convergence acceleration techniques." In: *The Journal of chemical physics* 137 5 (2012), p. 054110.

[119] C. C. J. Roothaan. "New Developments in Molecular Orbital Theory". In: *Reviews of Modern Physics* 23.2 (Apr. 1951), pp. 69–89. ISSN: 0034-6861. DOI: 10.1103/

RevModPhys.23.69. URL: https://link.aps.org/doi/10.1103/RevModPhys.23.69.

[120] Stefan Banach. "Sur les opérations dans les ensembles abstraits et leur application aux équations intégrales". In: *Fundamenta Mathematicae* 3 (1922), pp. 133–181. DOI: 10.4064/fm-3-1-133-181. URL: https://doi.org/10.4064/fm-3-1-133-181.

[121] John K. Hunter and Bruno Nachtergaele. *Applied Analysis*. World Scientific, 2001, pp. 61–63. ISBN: 9789812705433.

[122] Felix Plasser et al. "Efficient and Flexible Computation of Many-Electron Wave Function Overlaps". In: *Journal of Chemical Theory and Computation* 12.3 (Mar. 2016), pp. 1207–1219. ISSN: 1549-9618. DOI: 10.1021/acs.jctc.5b01148. URL: http://pubs.acs.org/doi/10.1021/acs.jctc.5b01148.

[123] Eric Cancès and Claude Le Bris. "On the convergence of SCF algorithms for the Hartree-Fock equations". In: *ESAIM: Mathematical Modelling and Numerical Analysis* 34.4 (July 2000), pp. 749–774. ISSN: 0764-583X. DOI: 10.1051/m2an:2000102. URL: http://www.esaim-m2an.org/10.1051/m2an:2000102.

[124] Sadhan K. Adhikari. "Mixing-demixing in a trapped degenerate fermion-fermion mixture". In: *Phys. Rev. A* 73 (4 Apr. 2006), p. 043619. DOI: 10.1103/PhysRevA.73.043619. URL: https://link.aps.org/doi/10.1103/PhysRevA.73.043619.

[125] B. DeMarco and D. S. Jin. "Onset of Fermi Degeneracy in a Trapped Atomic Gas". In: *Science* 285.5434 (1999), pp. 1703–1706. ISSN: 0036-8075. DOI: 10.1126/science.285.5434.1703. eprint: https://science.sciencemag.org/content/285/5434/1703.full.pdf. URL: https://science.sciencemag.org/content/285/5434/1703.

[126] Yousuke Takeuchi and Hiroyuki Mori. "Mixing-demixing transition in one-dimensional boson-fermion mixtures". In: *Phys. Rev. A* 72 (6 Dec. 2005), p. 063617. DOI: 10.1103/PhysRevA.72.063617. URL: https://link.aps.org/doi/10.1103/PhysRevA.72.063617.

[127] A. S. Bradley, S. J. Rooney, and R. G. McDonald. "Low-dimensional stochastic projected Gross-Pitaevskii equation". In: *Phys. Rev. A* 92 (3 Sept. 2015), p. 033631. DOI: 10.1103/PhysRevA.92.033631. URL: https://link.aps.org/doi/10.1103/PhysRevA.92.033631.

[128] Nouredine Zettili. *Quantum Mechanics*. 2nd ed. John Wiley & Sons, 2009. ISBN: 978-0-470-02679-3.

[129] Howard M. Wiseman and Gerard J. Milburn. *Quantum Measurement and Control*. Cambridge University Press, 2009. DOI: 10.1017/CBO9780511813948.

[130] Kurt Jacobs. *Quantum Measurement Theory and its Applications*. Cambridge University Press, 2014. DOI: 10.1017/CBO9781139179027.

[131] B. Misra and E. C. G. Sudarshan. "The Zeno's paradox in quantum theory". In: *Journal of Mathematical Physics* 18.4 (Apr. 1977), pp. 756–763. DOI: 10.1063/1.523304. URL: https://doi.org/10.1063/1.523304.

[132] S. S. Szigeti et al. "Robustness of system-filter separation for the feedback control of a quantum harmonic oscillator undergoing continuous position measurement". In: *Phys. Rev. A* 87 (1 Jan. 2013), p. 013626. DOI: 10.1103/PhysRevA.87.013626. URL: https://link.aps.org/doi/10.1103/PhysRevA.87.013626.

[133] Stuart S. Szigeti et al. "Ignorance Is Bliss: General and Robust Cancellation of Decoherence via No-Knowledge Quantum Feedback". In: *Phys. Rev. Lett.* 113 (2

July 2014), p. 020407. DOI: 10.1103/PhysRevLett.113.020407. URL: https://link.aps.org/doi/10.1103/PhysRevLett.113.020407.

[134] Stuart Szigeti. Private communication. 13 August 2019.

[135] Stuart Szigeti. Private communication. 20 October 2019.

[136] M. E. Gehm. "Preparation of an Optically-Trapped Degenerate Fermi Gas of 6Li: Finding the Route to Degeneracy". PhD thesis. Duke University, 2003.

[137] Jr-Shin Li and Navin Khaneja. "Control of inhomogeneous quantum ensembles". In: *Phys. Rev. A* 73 (3 Mar. 2006), p. 030302. DOI: 10.1103/PhysRevA.73.030302. URL: https://link.aps.org/doi/10.1103/PhysRevA.73.030302.

[138] J. Li. "Ensemble Control of Finite-Dimensional Time-Varying Linear Systems". In: *IEEE Transactions on Automatic Control* 56.2 (Feb. 2011), pp. 345–357. DOI: 10.1109/TAC.2010.2060259.

[139] Nick Proukakis et al. *Quantum Gases*. IMPERIAL COLLEGE PRESS, 2013. Chap. 27. DOI: 10.1142/p817. eprint: https://www.worldscientific.com/doi/pdf/10.1142/p817. URL: https://www.worldscientific.com/doi/abs/10.1142/p817.

[140] C. A. Regal, M. Greiner, and D. S. Jin. "Observation of Resonance Condensation of Fermionic Atom Pairs". In: *Phys. Rev. Lett.* 92 (4 Jan. 2004), p. 040403. DOI: 10.1103/PhysRevLett.92.040403. URL: https://link.aps.org/doi/10.1103/PhysRevLett.92.040403.

[141] M. W. Zwierlein et al. "Condensation of Pairs of Fermionic Atoms near a Feshbach Resonance". In: *Phys. Rev. Lett.* 92 (12 Mar. 2004), p. 120403. DOI: 10.1103/PhysRevLett.92.120403. URL: https://link.aps.org/doi/10.1103/PhysRevLett.92.120403.

[142] Giancarlo Calvanese Strinati et al. "The BCS–BEC crossover: From ultra-cold Fermi gases to nuclear systems". In: *Physics Reports* 738 (2018). The BCS–BEC crossover: From ultra-cold Fermi gases to nuclear systems, pp. 1–76. ISSN: 0370-1573. DOI: https://doi.org/10.1016/j.physrep.2018.02.004. URL: http://www.sciencedirect.com/science/article/pii/S0370157318300267.

[143] Walid Younes, Daniel Marc Gogny, and Jean-François Berger. "Hartree-Fock-Bogoliubov Theory". In: *A Microscopic Theory of Fission Dynamics Based on the Generator Coordinate Method*. Cham: Springer International Publishing, 2019, pp. 3–40. ISBN: 978-3-030-04424-4. DOI: 10.1007/978-3-030-04424-4_1. URL: https://doi.org/10.1007/978-3-030-04424-4_1.

[144] P.B. Blakie et al. "Dynamics and statistical mechanics of ultra-cold Bose gases using c-field techniques". In: *Advances in Physics* 57.5 (2008), pp. 363–455. DOI: 10.1080/00018730802564254. eprint: https://doi.org/10.1080/00018730802564254. URL: https://doi.org/10.1080/00018730802564254.

[145] Sadhan K. Adhikari. "Mean-field description of a dynamical collapse of a fermionic condensate in a trapped boson-fermion mixture". In: *Phys. Rev. A* 70 (4 Oct. 2004), p. 043617. DOI: 10.1103/PhysRevA.70.043617. URL: https://link.aps.org/doi/10.1103/PhysRevA.70.043617.

[146] Sadhan K Adhikari. "Free expansion of fermionic dark solitons in a boson–fermion mixture". In: *Journal of Physics B: Atomic, Molecular and Optical Physics* 38.19 (Sept. 2005), pp. 3607–3617. DOI: 10.1088/0953-4075/38/19/013. URL: https://doi.org/10.1088%2F0953-4075%2F38%2F19%2F013.

[147] Sadhan K. Adhikari. "Fermionic bright soliton in a boson-fermion mixture". In: *Phys. Rev. A* 72 (5 Nov. 2005), p. 053608. DOI: 10.1103/PhysRevA.72.053608. URL: https://link.aps.org/doi/10.1103/PhysRevA.72.053608.

[148] Gregory H. Wannier. "The Structure of Electronic Excitation Levels in Insulating Crystals". In: *Phys. Rev.* 52 (3 Aug. 1937), pp. 191–197. DOI: 10.1103/PhysRev.52.191. URL: https://link.aps.org/doi/10.1103/PhysRev.52.191.

[149] Gregory H. Wannier. "Dynamics of Band Electrons in Electric and Magnetic Fields". In: *Rev. Mod. Phys.* 34 (4 Oct. 1962), pp. 645–655. DOI: 10.1103/RevModPhys.34.645. URL: https://link.aps.org/doi/10.1103/RevModPhys.34.645.

[150] T.L. Curtright, D.B. Fairlie, and C.K. Zachos. *A Concise Treatise on Quantum Mechanics in Phase Space*. World Scientific Pub Co Inc, 2014. ISBN: 9814520438.

[151] Max Born. "Zur Quantenmechanik der Stoßvorgänge". In: *Zeitschrift für Physik* 37.12 (Dec. 1926), pp. 863–867. ISSN: 0044-3328. DOI: 10.1007/BF01397477. URL: https://doi.org/10.1007/BF01397477.

[152] Gabriele Giuliani and Giovanni Vignale. *Quantum theory of the electron liquid*. Vol. 9780521821. Cambridge: Cambridge University Press, 2005, pp. 1–777. ISBN: 9780511619915. DOI: 10.1017/CBO9780511619915. URL: http://ebooks.cambridge.org/ref/id/CBO9780511619915.

[153] G. C. Wick. "The Evaluation of the Collision Matrix". In: *Phys. Rev.* 80 (2 Oct. 1950), pp. 268–272. DOI: 10.1103/PhysRev.80.268. URL: https://link.aps.org/doi/10.1103/PhysRev.80.268.